General Disclaimer

One or more of the Following Statements may affect this Document

- This document has been reproduced from the best copy furnished by the organizational source. It is being released in the interest of making available as much information as possible.

- This document may contain data, which exceeds the sheet parameters. It was furnished in this condition by the organizational source and is the best copy available.

- This document may contain tone-on-tone or color graphs, charts and/or pictures, which have been reproduced in black and white.

- This document is paginated as submitted by the original source.

- Portions of this document are not fully legible due to the historical nature of some of the material. However, it is the best reproduction available from the original submission.

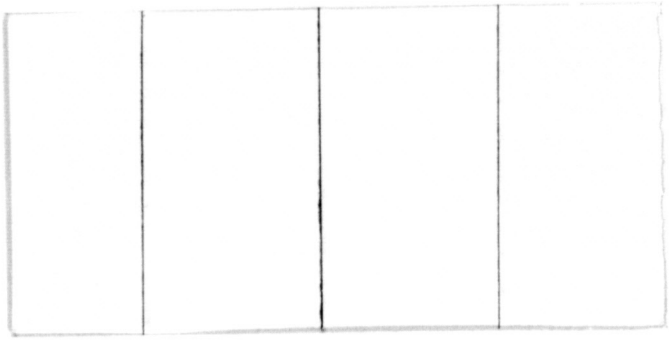

(NASA-CR-102776) THERMAL ACOUSTIC OSCILLATIONS, VOLUME 2 Final Report (Lockheed Missiles and Space Co.) 140 p HC $5.75 CSCL 20A

N75-25674

Unclas
G3/71 24753

Lockheed

HUNTSVILLE RESEARCH & ENGINEERING CENTER

LOCKHEED MISSILES & SPACE COMPANY, INC.
A SUBSIDIARY OF LOCKHEED AIRCRAFT CORPORATION

HUNTSVILLE, ALABAMA

Lockheed

Missiles & Space Company, Inc.

HUNTSVILLE RESEARCH & ENGINEERING CENTER

Cummings Research Park
4800 Bradford Drive,
Huntsville, Alabama

THERMAL ACOUSTIC OSCILLATIONS

VOLUME II
FINAL REPORT
March 1975

Contract NAS8-26642

Prepared for National Aeronautics and Space Administration
Marshall Space Flight Center, Alabama 35812

by

Lawrence W. Spradley
William H. Sims
Chien Fan

APPROVED: Juan K. Lovin

Juan K. Lovin, Supervisor
Thermal Environment Section

George D. Ramy
for J.S. Farrior
Resident Director

FOREWORD

This report is Volume II of a three-volume final report which presents results of work performed by the Lockheed-Huntsville Research & Engineering Center for the NASA-Marshall Space Flight Center under Contract NAS8-26642.

The NASA contract monitor for this study was E. Haschal Hyde of the Structures & Populsion Laboratory.

The total work performed under Contract NAS8-26642 is documented in three separate volumes. Volumes I and III are:

Volume I — Study of Multilayered Insulation Pipe Penetrations, LMSC-HREC TR D390690-I

Volume III — Long Term Cryogen Storage, LMSC-HREC TR D390690-III

The document control numbers of Volumes I and III are identical to this volume with the exception that the last digit following the basic DCN is either a -I or -III.

CONTENTS

Section		Page
	FOREWORD	ii
1	INTRODUCTION AND SUMMARY	1
	1.1 Thermal Acoustic Oscillation Phenomena	1
	1.2 Study Objectives and Approach	2
	1.3 Summary of Conclusions and Results	4
	1.4 Report Contents	5
2	TECHNICAL DISCUSSION	7
	2.1 Literature Review, Phenomena Description and Implications	7
	2.2 Analytical Model	28
	2.3 Experimental Verification Program	49
	2.4 Analytical Comparisons with Previous Investigations	78
	2.5 Comparison of LMSC Theory and Experiment	82
3	CONCLUSIONS	95
	3.1 Thermal Acoustic Oscillations Phenomena	95
	3.2 Experimental Anomalies	96
	3.3 Analytical Methods	97
4	RECOMMENDATIONS	98
	4.1 Analytical Methods	98
	4.2 Experimental Program	99
5	REFERENCES	100
Appendix		
	Mathematical Formulation of the TAO Model	A-1

LIST OF TABLES

Table		
1	Tubes Tested for Thermal Acoustic Oscillations	57
2	Oscillation Intensity Test Results	62

Table		Page
3a	Test Data of Oscillation Intensity Effect on Heat Transfer for Stainless Steel Tube	76
3b	Test Data of Oscillation Intensity Effect on Heat Transfer for Aluminum Tube	77
A-1	Finite Difference Approximations	A-14

LIST OF FIGURES

Figure		
1	Basic Apparatus Studied by Sondhauss and Rayleigh	8
2	Schematic of Basic Apparatus for Observing Thermal Acoustic Oscillation in Liquid Helium Storage Systems	10
3	Illustration of Thermal Acoustic Oscillations Phenomena	12
4	Heat Pumping Rate vs Intensity (from Bannister, Ref. 14)	17
5	Configuration Used by Bannister for Visual Observation of Thermal Acoustic Oscillations	18
6a	Results of Bannister (Ref. 14): Open End of Tube 2.54 cm Below Liquid Helium Surface (f = 20.5 Hz, A = 2.82 x 10^4 N/m^2)	19
6b	Results of Bannister (Ref. 14): Open End of Tube at Liquid Helium Surface (f = 21.2 Hz, A = 4.07 x 10^4 N/m^2	20
6c	Results of Bannister (Ref. 14): Open End of Tube 5.1 cm Above Liquid Helium Surface (f = 34.1 Hz, A = 8.0 x 10^4 N/m^2)	21
7	Work of Rott (Ref. 21)	24
8	Data of Von Hoffmann Compared with Theory of Rott (from Ref. 22)	25
9	Dimensionless Velocity and Pressure Profiles from Numerical Solution of Thermoacoustic Oscillations (from Ref. 23)	27
10	Experimental Data of Bannister (Ref. 14)	29
11	Summary of Approach for Thermal Acoustic Oscillations Study	31
12	Geometric Configuration and Coordinate System for Thermal Acoustic Oscillations Model	33
13	Stability Diagram for Helium	39
14	Pressure Amplitude vs L/D for Parametric L_c/L	41
15	Pressure Amplitude vs T_h/T_c Ratio for Parametric L/D	43

Figure		Page
16	Oscillation Frequency vs L/D for Parametric L_c/L	44
17	Oscillation Intensity (f x P_A) vs L/D for Parametric L_c/L	45
18	Ratio of Total Heat Leak (with Oscillations) to Normal Conduction Heat Leak vs L/D for Parametric L_c/L	47
19	Ratio of Total Heat Leak (with Oscillation) to Normal Conduction Heat Leak vs Pressure Amplitude	48
20	Schematic of TAO Test Hardware	50
21	Schematic of Modified Ballistic Mount for Piezotron Model 206 Pressure Transducer	52
22	Research LHe Dewar	54
23	Calibration Curve of Resistance vs Temperature for Cryoresistor	59
24	Schematic of Test Tube/Foam Plug Configuration	60
25	Experimental Measurements of Oscillation Intensity as a Function of L_c/L	70
26	Calibration Curve for Hastings-Raydist Flowmeter Used for Measurement of Boiloff Rates	73
27	Schematic of Flow System for Measuring Boiloff Due to Oscillations	74
28	Comparison of Present Analytical Calculations with Theory of Rott (Ref. 21) for Helium Stability Diagram	79
29	Comparison of Pressure Amplitude with Data of Bannister (Ref. 14)	81
30	Comparison of Present Analytical Calculations with Experimental Data of Bannister (Ref. 14) for Heat Rate vs L/D	83
31	Stability Diagram for Helium	84
32	Comparison of Analytical and Experimental Oscillation Frequencies as a Function of Tube L/D for Constant L_c/L and T_h/T_c	85
33	Comparison of Analytical and Experimental Peak-to-Peak Pressure Amplitudes for Constant L_c/L and L/D for Parametric T_h/T_c	86
34	Comparison of Analytical and Experimental Peak-to-Peak Pressure Amplitudes for Parametric Length/Inside Diameter Ratio	87
35	Comparison of Analytical and Experimental Oscillation Intensities as a Function of Tube L/D for Constant L_c/L and T_h/T_c	88

Figure		Page
36	Ratio of Total Heat Leak (with Oscillations) to Normal Conduction Heat Leak versus Oscillation Intensity	89
37	Ratio of Total Heat Leak (with oscillations) to Normal Conduction Heat Leak vs Pressure Amplitude	90
A-1	Geometric Configuration and Coordinate System	A-3
A-2	Navier-Stokes Equations for Cylinder (Dimensionless Variables)	A-6
A-3	Dimensionless Groups for Navier-Stokes Equations Used in TAO Model	A-7
A-4	Grid System for Finite Difference Equations	A-11
A-5	Block Diagram for Thermal Acoustic Oscillations Computer Program (TAO)	A-18
A-6	Pressure Profile at 0.25L from Hot End of Closed Tube (Helium, L/D = 15)	A-20
A-7	Temperature History at a Point Near the Open End of Tube (L/D = 100)	A-21
A-8	Example of Power Spectral Density for Multiple Frequency Content	A-25
A-9	General Statistical Analysis Computer Program Schematic Flow Chart	A-27

Section 1
INTRODUCTION AND SUMMARY

1.1 THERMAL ACOUSTIC OSCILLATION PHENOMENA

In 1850, Sondhaus observed that audible sound was produced from the tubes used by glass blowers. A gas flame applied to a bulb-end caused the air in the tube to oscillate and produce a clear sound which was characteristic of the dimensions of the tube. This discovery is known as the Sondhaus thermal acoustic oscillations phenomenon. Lord Rayleigh in 1878 provided an explanation for the spontaneous occurrence of these heat driven oscillations. He explains that the oscillations occur if heat is added to the air at the point of greatest compression and heat is taken out at the point of greatest-expansion. This explanation has become known as the "Rayleigh criterion."

The occurrence of thermal acoustic oscillations in low temperature apparatus was observed by investigations as early as the 1940s. The oscillations occur because the Rayleigh criterion is fulfilled for these systems. A tube which penetrates a cryogenic storage vessel can become filled with vapor due to normal boiloff of the cryogen. If the tube is closed on one end and exposed to an ambient thermal environment, then heat is added to the vapor at the closed end. Oscillations are initiated by expansion of the fluid as it is heated. The oscillations, in turn, force vapor from the tube at the open end. Cool vapor is then withdrawn into the tube to replace the mass which was ejected. This process is sufficient to sustain the oscillations for long periods of time for certain geometries and boundary values. The large temperature gradient imposed on a compressible fluid is the driving mechanism.

In addition to being annoying, these thermal acoustic oscillations can be detrimental to the storage of cryogens. The acoustic pressure waves transfer heat from the warm end of the tube into the cold liquid. Investigations have determined that the additional heat leak due to oscillations can be several

orders of magnitude larger than the normal (no oscillation) penetration heat leak. This large amount of heat pumped into a cryogenic storage vessel can cause such large boiloff to render long-term storage on space missions impossible.

The thermal acoustic oscillations phenomena has been the subject of many investigations, both analytically and experimentally. Most of the experimental work has been concerned with characterizing the oscillations rather than measuring the boiloff rate (i.e., heat leak) for different tubes and parametric values. The analytical efforts have been confined to studies of linearized hydrodynamic equations. These attempts have failed to predict sustained oscillations due to the neglect of the nonlinear driving mechanisms. No attempt has been made, until the present work, to analytically predict the heat transfer due to thermal acoustic oscillations.

1.2 STUDY OBJECTIVES AND APPROACH

The objectives of this study are to determine:

- The conditions which cause or suppress oscillations
- The frequency, amplitude and intensity of oscillations when they exist
- The additional heat leak induced by the oscillations, and
- Parametric system parameters which can be adjusted to suppress oscillations and thus heat transfer.

A general analytical tool was developed for satisfying these objectives. In addition to developing the analytical model, a major objective of the study is to obtain parametric curves which can be used by a designer in analyzing a particular system. This requires a parametric study to be done using the analytical tool. The final goal is to verify the analytical model by comparison with experimental data.

The approach used in the model development was to obtain a system of differential equations and boundary conditions which represent the physical problem.

The most general equations describing the thermal acoustic oscillations phenomena are the Navier-Stokes equations. These are very complex in their general form, and no solution for general cases have been reported. The approach taken here applies certain assumptions, which are justified, to obtain equations which can be solved. Even in their simplest form for thermal acoustic oscillations, these cannot be solved in "closed form." However, numerical methods using a digital computer have been very successful in solving problems in many aspects of fluid mechanics. The thermal acoustic oscillations (TAO) computer program is based on a numerical solution of the Navier-Stokes equations.

In addition to a model for obtaining the solution profiles, a method for determining the dominant frequency content, amplitude and intensity of the oscillations is needed. A General Statistical Analysis (GSA) computer program was utilized for this purpose. The TAO solutions are processed by a Fast Fourier Transform algorithm and the power spectral density function is computed. The TAO program and the GSA program together constitute the analytical tools used in this study.

An experimental verification program was conducted in conjunction with the analytical model development. A liquid helium research dewar was used for the experimentation. Stainless steel and aluminum tubes having length to diameter ratios from 100 to 1000 were used as the test penetrations. A Kistler Piezotron pressure transducer was used in conjunction with a dual trace oscilloscope, a McIntosh audio amplifier, and a true rms meter to record the oscillation wave characteristics. The boiloff measurements were taken from a commercial LHe dewar using a system containing vent valves, flow valves, a surge tank, flow rate measurement valve, a Hastings-Raydist flowmeter and a differential voltmeter. Measurements were made for oscillation frequency and amplitude and boiloff rate for a matrix of tubes sizes, materials, and distances of the tube in the dewar. The data were reduced and compared with results of the analytical predictions.

1.3 SUMMARY OF CONCLUSIONS AND RESULTS

The study has resulted in a number of conclusions regarding thermal acoustic oscillations in cryogenic storage systems. These conclusions are summarized below.

- A literature review has revealed that thermal acoustic oscillations are a common occurrence in liquid helium storage systems. Most investigators have discovered very large additional heat leaks due to the oscillations.
- The present study has shown by analysis and experiment that the oscillations do occur and can be sustained for long periods of time.
- Thermal acoustic oscillations can potentially occur in any cryogenic system which contains a tube penetration.
- The oscillations can be initiated purely by thermal means, i.e., expansion of gas in a tube heated on one end and having an open end exposed to a very cold environment.
- The stability of oscillations has been shown to be a function of the length-to-diameter ratio of the tube, the temperature ratio of warm end to cold end, the length of tube exposed to the cold environment, the proximity of the tube to the liquid surface and perhaps external disturbances.
- A stability diagram was devised for use in estimating the existence of oscillations.
- Thermal acoustic oscillations produce large heat leaks to stored cryogens. Analysis and experiment have shown that as much as two orders of magnitude increase in heat transfer can occur if oscillations are present.
- The frequency of the oscillations studied range from $\sim$ 2Hz to as large as 100 Hz.
- A warm-end to cold-end temperature ratio of at least 6 is required to sustain oscillations.
- Pressure amplitudes (peak-to-peak) as large as $\sim$ 0.4 atm were obtained for large length-to-diameter ratio tubes.
- The ratio of total heat transfer to pure conduction heat transfer correlates with oscillation intensity.
- Thermal acoustic oscillations can disturb the liquid cryogen itself by injecting mass causing stirring and apparent "turbulent-like" flow at the vapor/liquid interface.

- The large heat leak produced by the oscillations can have significant effects on storage of cryogens for space missions such as the Space Tug. The boiloff rates could be large enough to cut mission times short or prohibit them altogether.
- The study has identified system parameters which are at the designers disposal for possibly preventing oscillations from occurring.
- T_h/T_c ratio below about 6 should prevent sustained oscillations. This is accomplished most readily by cooling the closed end of the tube.
- The $L_c L$ ratio should be kept small, i.e., minimize the length of tube exposed to the cold environment.
- Tubes with small L/D ratios (e.g., 25) are less likely to induce oscillations.
- The open end of the tube should not be placed close to the liquid surface. This will minimize stirring if oscillations do occur.
- The oscillations can be damped by occasional venting through a valve, etc., at the "closed" end of the tube.

1.4 REPORT CONTENTS

The organization of this report is summarized below to aid the reader in quickly locating desired information.

Section	Page	Description
2.1	7	A historical survey of the literature is given, including discussions on the explanation of thermal acoustic oscillations and their potential effects.
2.2	28	This section presents a discussion of the analytical model of thermal acoustic oscillations including assumptions made, model parameters and computer programs. Section 2.2.5 presents analytical results from the computer program study.
2.3	49	The experimental verifications program is discussed. The apparatus used in conducting the tests, sample test data, and experimental anomalies are described.
2.4	78	The Lockheed analytical predictions are compared and contrasted with previously reported theory and experimental data.

Section	Page	Description
2.5	82	This section gives comparisions of Lockheed's analytical model predictions (2.2) with the experimental data (2.3). Comparisons include existence of oscillations, wave characteristics, and net heat leak.
3.0	95	The conclusions reached as a result of this study are summarized in terms of thermal acoustic oscillations phenomena, experimental anomalies, and analytical methods.
4.0	98	A summary list of recommended items for further study is given. Both analytical and experimental tasks are suggested.
5.0	100	Thermal acoustic oscillation references are listed.
Appendix	A-1	The Appendix contains details of the mathematical formulation of the thermal acoustic oscillation problem including equations, numerical methods and computer program descriptions.

Section 2
TECHNICAL DISCUSSION

2.1 LITERATURE REVIEW, PHENOMENA DESCRIPTION AND IMPLICATIONS

This section presents a review of the literature on thermal acoustic oscillations and a description of the phenomenon itself. The papers which are concerned with applications to low temperature apparatus and those dealing with computation of thermal acoustic waves are of particular interest in this study. These publications, given in Refs. 1 through 35, are reviewed in summary form. Those which present results directly applicable to the goals of the present study are reviewed in some detail.

2.1.1 Phenomenon Discovery (Sondhauss)

The discovery of the thermal acoustic oscillation phenomenon is generally credited to Sondhauss in 1850 (Ref. 1). He observed the heat-generated sound produced by glass blowers when blowing a bulb on the end of a narrow tube. This "Sondhauss tube" was open on one end and terminated in a bulb on the other. A steady gas flame applied to the bulb-end caused the air in the tube to oscillate and produce a clear sound which was characteristic of the dimensions of the tube. Larger bulbs and longer tubes produced lower frequency sounds and hotter flames produced more intense sounds. The apparatus used by Sondhauss in his early studies is shown schematically in Fig. 1. Heat was added at the bulb end and removed from the open end which was exposed to ambient air. Although Sondhauss apparently discovered the phenomenon he gave no explanations for the production of the sound.

2.1.2 First Explanation of Phenomenon (Rayleigh Criterion)

Lord Rayleigh, 1878 (Ref. 2), was the first to explain the physical mechanism for the spontaneous occurrence of thermal acoustic oscillations.

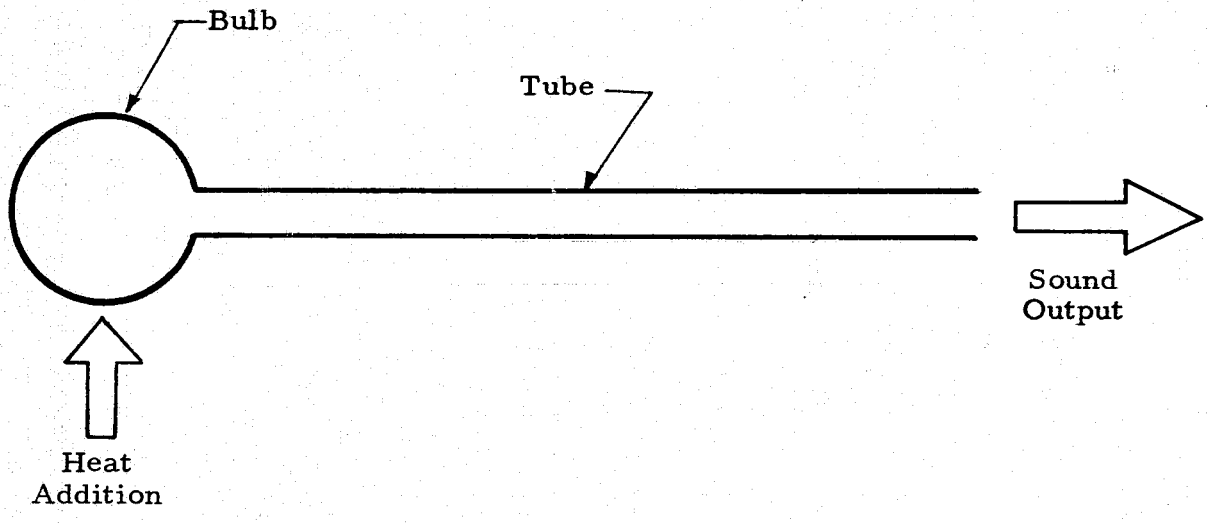

Fig. 1 - Basic Apparatus Studied by Sondhauss and Rayleigh

His explanation of the mechanism is that oscillations are encouraged if heat is added to the air at the point of greatest compression and heat is taken out at the point of greatest expansion. Rayleigh explained that this criterion is fulfilled in the Sondhauss tube because the moment of greatest compression occurs when the gas is compressed into the hot end where it becomes heated and expands, thus encouraging the oscillation; in addition, the moment of greatest rarefaction occurs when the gas expands into the cool end of the tube where heat is removed which also encourages oscillation. Under the conditions described by Rayleigh, small wave-type disturbances grow and become self-sustained oscillations due to heating and cooling effects. It is the relative temperature difference between the ends of the tube which causes this effect. Thus the oscillations can be started by either heating one end, cooling one end, or both.

2.1.3 Observation of Oscillations in Cryogenic Apparatus (Taconis)

Apparently the first observation of thermal acoustic oscillations in low temperature apparatus was made by Taconis, 1949 (Ref. 3). He observed spontaneous acoustic oscillations in a hollow tube which was used for stirring liquid helium. The upper end of the tube was closed (at room temperature) while the lower end was immersed in the liquid helium. Taconis' explanation of how the large thermal gradient along the tube caused the oscillations was essentially a restatement of the Rayleigh criterion. He noted, however, that the oscillations caused an effective "stirring" such that heat transferred to the fluid was so great that large boiling occurred. The net effect of the "stirring" was to significantly increase the heat transfer and result in the boiling.

A schematic of the apparatus in which acoustic oscillations occur in cryogenic systems is given in Fig. 2. A storage device containing the liquid is penetrated by a tube. The purpose of the tube is for filling the tank, for venting the device, for stirring the liquid, etc. The upper closed end of the tube is exposed to ambient temperature and the open end is exposed to the cold environment. As heat leaks into the storage vessel, the liquid starts to boil off, filling the tube with vapor. The gas-filled tube thus has one end at near-ambient temperature and the other end at

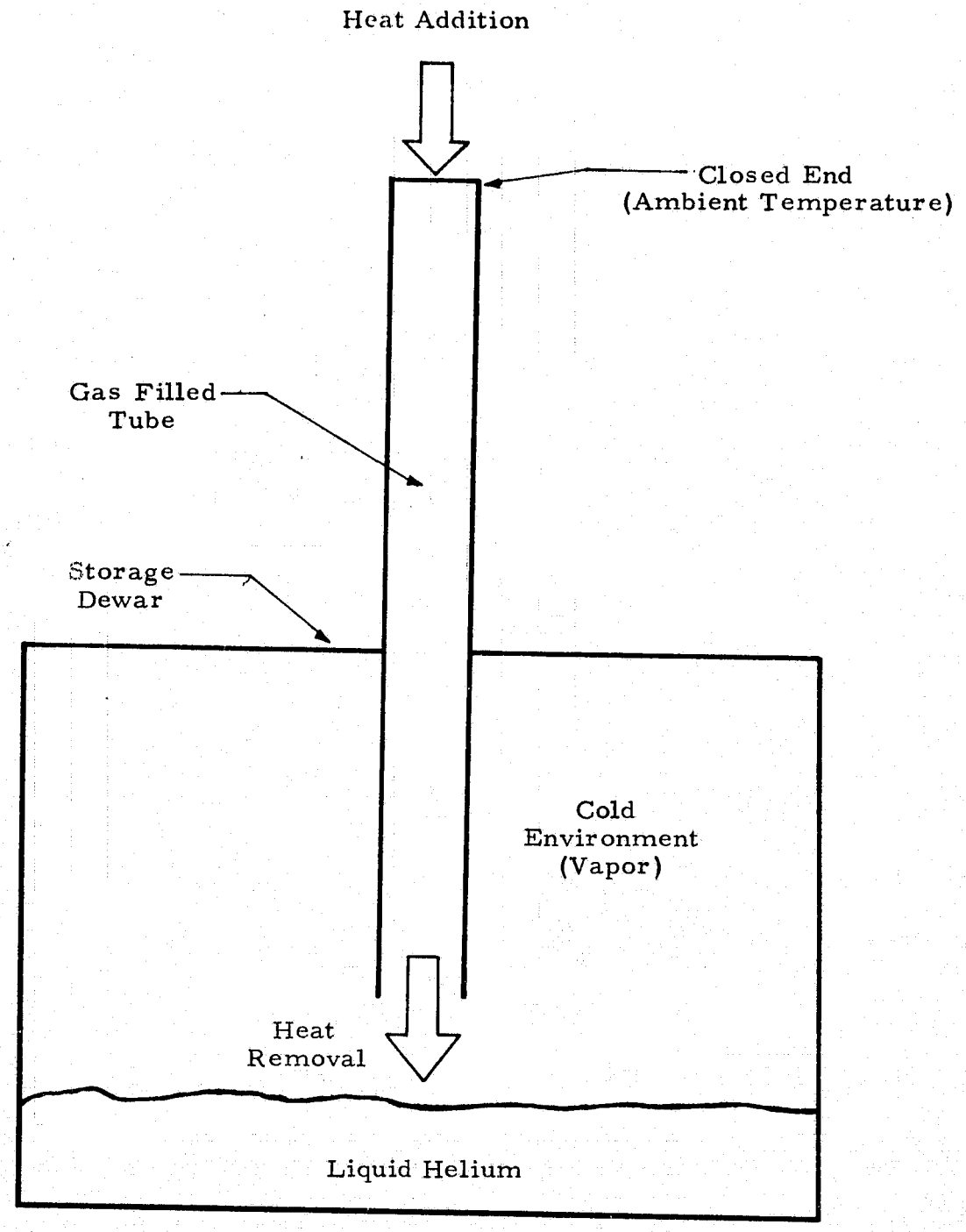

Fig. 2 - Schematic of Basic Apparatus for Observing Thermal Acoustic Oscillation in Liquid Helium Storage Systems

near-cryogenic temperature. The acoustic oscillations begin as a result of the expansion of the gas from the closed end as heat is transferred by conduction. The oscillations then are encouraged as heat is taken from the gas near the cold end. The Rayleigh criterion is thus fulfilled for the cryogenic apparatus and provides and explanation for the spontaneous occurrence of acoustic oscillations observed by Taconis.

2.1.4 Phenomena Illustration

Figure 3 is a schematic which illustrates the sequence of events for thermal acoustic oscillations in a liquid helium storage vessel. At the initial "time" t = 0, the tube is filled with helium gas at some initial uniform temperature. The upper closed end of the tube is always exposed to the hot (ambient) temperature. An instant of time later (t_1), the gas in the pipe heats up at the top and cools down at the bottom due to conduction heat transfer. The gas column has some temperature distribution at t = 2 as shown. As heat is continually added from the top, the cold gas is moved down the tube at t = 3 since the hot gas expands from the closed end. The expansion continues at t = 4 forcing the warm gas out the end of the tube. This convective heat transfer then increases to the boil-off of the liquid. At time t = 5, cold gas is drawn back into the tube since the pressure at open end is now lower than the internal gas pressure in the dewar. This "suction" continues at t = 6, but the gas which was drawn in now warms up due to continued heat addition at the top. The time t = 7 shows the process being repeated as the oscillations sustain themselves purely by thermal means.

This simple illustration was presented to clarify the mechanism by which the oscillations are started (thermal expansion), the mechanism by which heat is transferred (mass transfer), and the mechanism by which the oscillations are sustained (heat addition and removal). The illustration in Figure 3 is a simplified display of the mechanisms explained by Rayleigh in 1878.

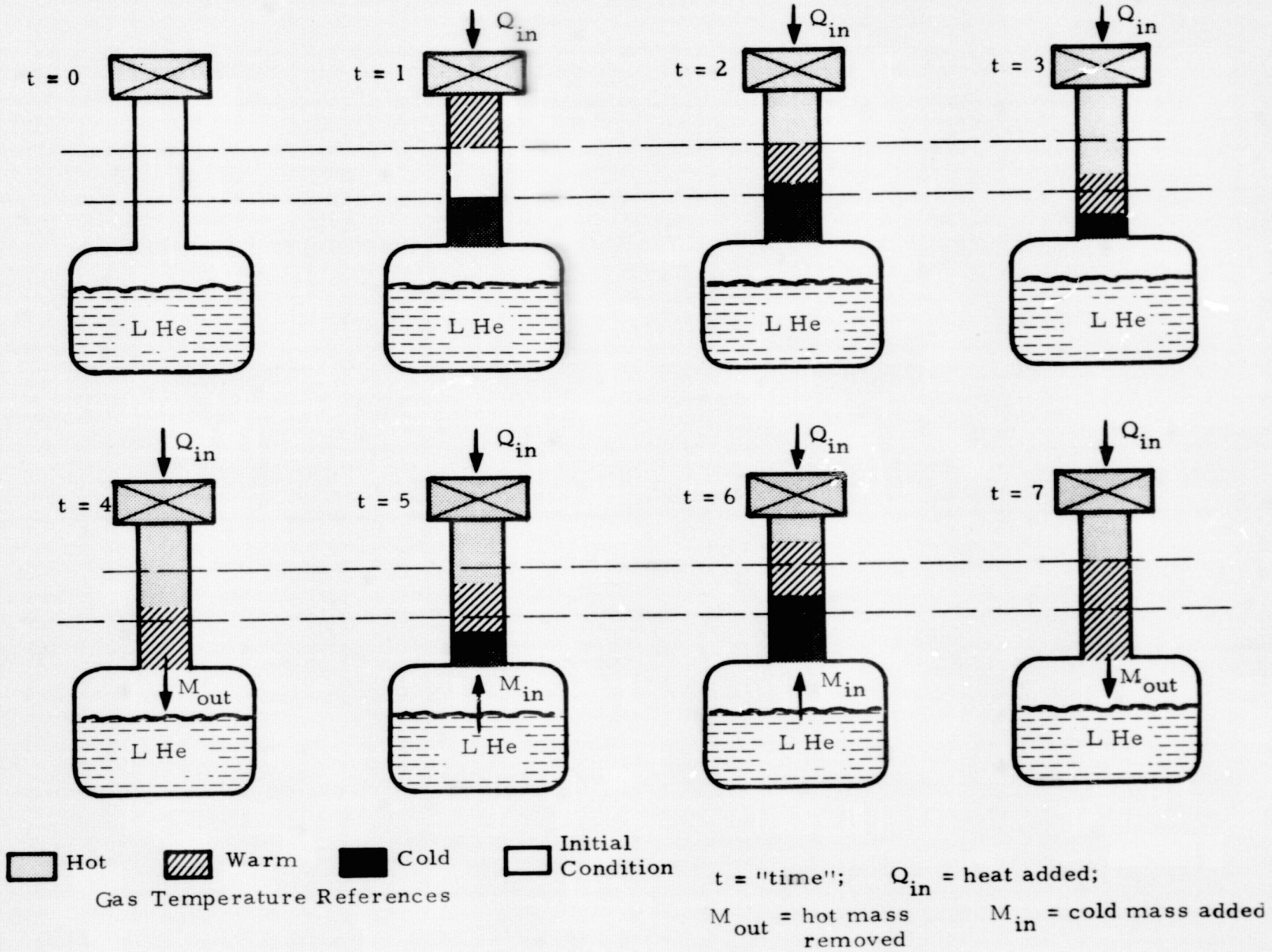

Fig. 3 - Illustration of Thermal Acoustic Oscillations Phenomena

The discussion which follows presents the historical development of the technology and understanding of this phenomenon. Analytical and experimental studies have been done on: (1) characterizing the conditions which cause oscillations; (2) determining the additional heat leaks produced by the oscillations; and (3) explaining the mechanisms whereby oscillations are sustained or damped out. The emphasis on understanding the phenomenon is coupled to the major problem of cryogen boil-off and the reduced ability for long-term storage. The significance of the large additional heat leak in cryogenic storage vessels is repeatedly shown in the numerous observations which are reviewed in the follow subsections.

2.1.5 Theoretical Analysis (Kramers)

Kramers, 1949 (Ref. 4), was the first to attempt a theoretical analysis of the Sondhauss oscillation problem, but had limited success. He attacked the problem by considering small amplitude waves which could be described by the linearized hydrodynamic equations of mass, momentum and energy. The waves were considered to have three components: a main wave, a friction wave, and a heat conduction wave. He successfully separated the wave components and solved the resulting linearized equations, but he was unable to account for the sustained oscillations which were observed in many of his experiments. Kramers attributed the failure of his theory to the fact that the terms he neglected in linearizing were probably not negligible. A nonlinear approach was thus indicated in 1949, but apparently not attempted until the present work.

2.1.6 Experiments of Wexler; Clement and Gaffney

Wexler, 1959 (Ref. 5), observed oscillations during a study to design storage containers for liquid helium. When the end of a vent tube was restricted by a rubber tube the oscillations could be felt by holding the rubber tube. He makes the statement, without supporting data, that the influx of heat due to the oscillations may be 1000 times the normal heat leak.

Clement and Gaffney, 1954 (Ref. 6), experimentally studied spontaneous thermal oscillations, which occurred in small diameter tubes having one end at room temperature and the other end at liquid helium temperature. They observed that the optimum conditions for oscillations occurred when the end at room temperature was completely closed and the end immersed in the liquid helium was open. Their experiment indicated that a tube completely open at the hot end could not be made to oscillate unless its inside diameter was less than approximately 1 mm. Tubes having the cold end completely closed could not be made to oscillate at all. They also observed oscillations in the annular space between the double wall of a liquid helium transfer-siphon tube. Oscillations in the annular space could be damped simply by placing a snug fitting brass ring in the annulus near the cold end to block the gas motion. Another important fact discovered by Clement and Gaffney was that oscillations occurred in a tube when the cold end was withdrawn above the liquid surface. In addition, they observed step-like changes in the oscillation frequency as the tube was withdrawn from the liquid. The frequency increased suddenly as the tube moved out of the liquid and continued to increase as the tube was further withdrawn. This allowed the use of a tube as an indicator to designate the location of the liquid helium surface.

2.1.7 Work of Trilling; Chu; Ditmars and Furukawa

Trilling, 1955 (Ref. 7), conducted an analytical study of heat generated pressure waves. He linearized the hydrodynamic equations and separated them into three components representing the three modes of motion. He showed that sharp increases in boundary temperature can cause pressure waves to propagate in much the same manner as pushing a piston through a gas-filled pipe. The magnitude of the pressure pulse was found to be directly proportional to the 1/4th root of the acoustic Reynolds number. This work, unlike Kramers, was not applied directly to the problem of oscillations in cryogenic apparatus.

Chu, 1963 (Ref. 8), presents a complex theoretical treatment of heat generated pressure waves. He studied self-sustained, thermally driven oscillations in a closed pipe. The pressure-time curve is given as a saw-tooth function and the velocity-time curve as a square-wave function. The frequency was found to be approximately equal to the resonance frequency of the system. Ditmars and Furukawa, 1964 (Ref. 9), have noted that in certain low temperature experiments, the presence of thermal acoustic oscillations often causes the calorimetric measurements to be difficult or even impossible due to the large additional heat leaks.

2.1.8 Analysis of Feldman

Feldman, 1966 (Ref. 10), conducted an extensive experimental and theoretical study of the Sondhauss oscillation. A physical analysis of the heat exchange mechanism driving the Sondhauss oscillation was presented. The Sondhauss oscillator was treated as a heat engine operating on a specified thermodynamic engine cycle. In order for the amplitude of the oscillation to grow to a steady state condition, energy additions had to be properly phased so that a net increase occurred in the total energy of the gas system after each cycle of oscillation. Thus, for a sustained reasonant thermoacoustic oscillation to occur, the following conditions must be met: (1) the steady heat source had to interact with the pressure fluctuations in the system so that the energy additions to the gas are phased to cause the oscillations to increase in amplitude (Rayleigh criterion); (2) the heat addition rate had to be greater than some minimum value (heat-in greater than heat-out); (3) the heated cavity had to be shaped so that a resonant gas oscillation can occur, (Feldman observed that a tube length to diameter ratio of approximately 15 was required); and (4) the heat source had to be located at a point in the pipe where both the gas velocity and pressure are sensitive to heat additions such as in the closed end of the Sondhauss pipe. He found that the gas oscillation could be initiated by some random external disturbance, or if the rate of heating is large enough a thermal expansion pressure wave could start the oscillation. Additional papers by Feldman, including a literature survey, are given in Refs. 11 through 13.

2.1.9 Experimental Program of J. D. Bannister

J. D. Bannister, 1966 (Ref. 14), conducted experiments for measuring spontaneous pressure oscillations in tubes connecting liquid helium reservoirs to room temperature environments. He measured oscillation pressure amplitudes and frequencies together with longitudinal temperature profiles and heat pumping rates for tubes ranging in length from 122 to 214 centimeters and diameters from 0.318 to 1.27 centimeters. Bannister's experimental results indicate that: (1) spontaneous pressure oscillations occurring in tubes, which connect liquid helium reservoirs to their 300°K environments, have an amplitude directly proportional to the slenderness ratio of the gas column, and (2) the heat pumped by spontaneous oscillations is proportional to the product of pressure amplitude times frequency.

Figure 4 is a plot of the heat transfer ratio versus intensity as presented by Bannister in Ref. 14. The heat transfer rate shown is that component derived only from the oscillations; it does not include any conduction heat transfer down the tubes. The significant finding represented by this curve is that the heat leak is linearly proportional to the oscillation intensity. A curve shown subsequently in subsection 2.1.16 indicates that the additional heat leak due to oscillations can be two orders of magnitude larger than the normal conduction heat leak.

In addition to the data presented in the paper, a 16 mm movie was made in connection with his work. A glass dewar was used such that the oscillations could be observed. This film was obtained from Mr. Bannister for use in the present study and has proved to be very valuable. Some excerpts from this film are given for illustrative purposes in Figures 5 and 6. Figure 5 gives the configuration used for the visual observation tests. Figures 6a, 6b, and 6c show results of the tests for a tube below, at, and above the surface. These figures show the gas (dark areas) being pumped out of the tube and also the large degree of stirring they cause. This film should dispel all doubts about the existence and magnitude of thermal acoustic oscillations in liquid helium storage devices.

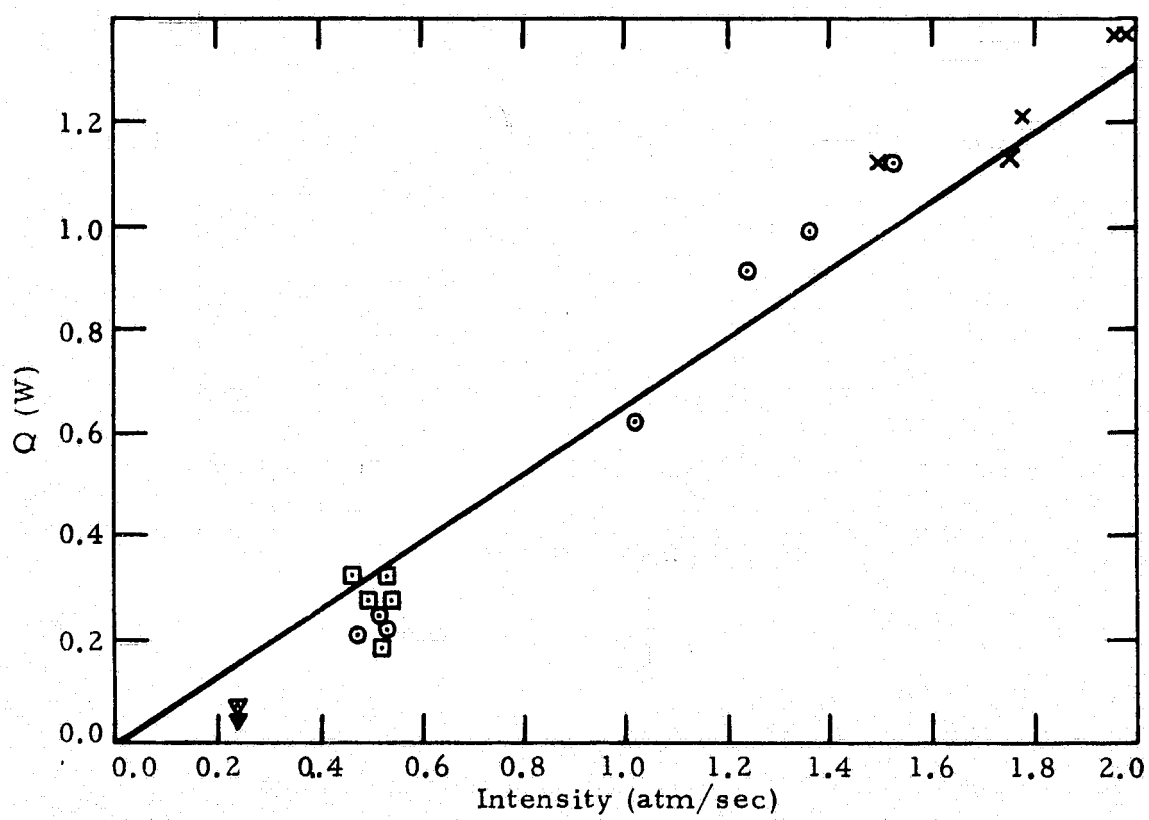

Fig. 4 - Heat Pumping Rate vs Intensity (from Bannister, Ref. 14)

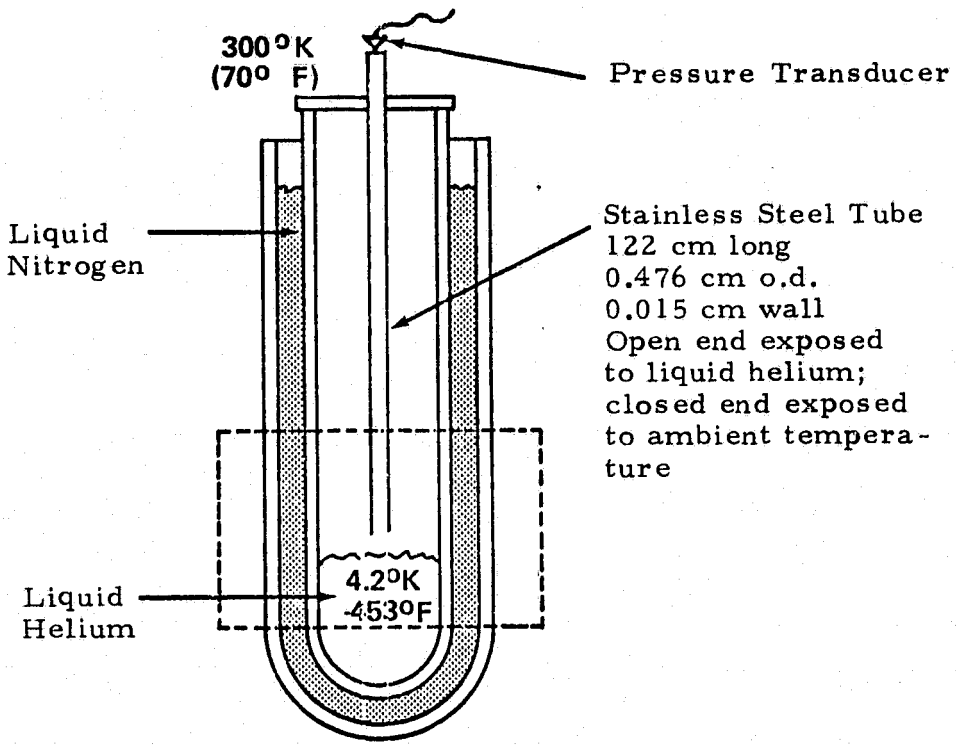

Fig. 5 - Configuration Used by Bannister for Visual Observation of Thermal Acoustic Oscillations (Region in dotted lines is shown in movie excerpts.)

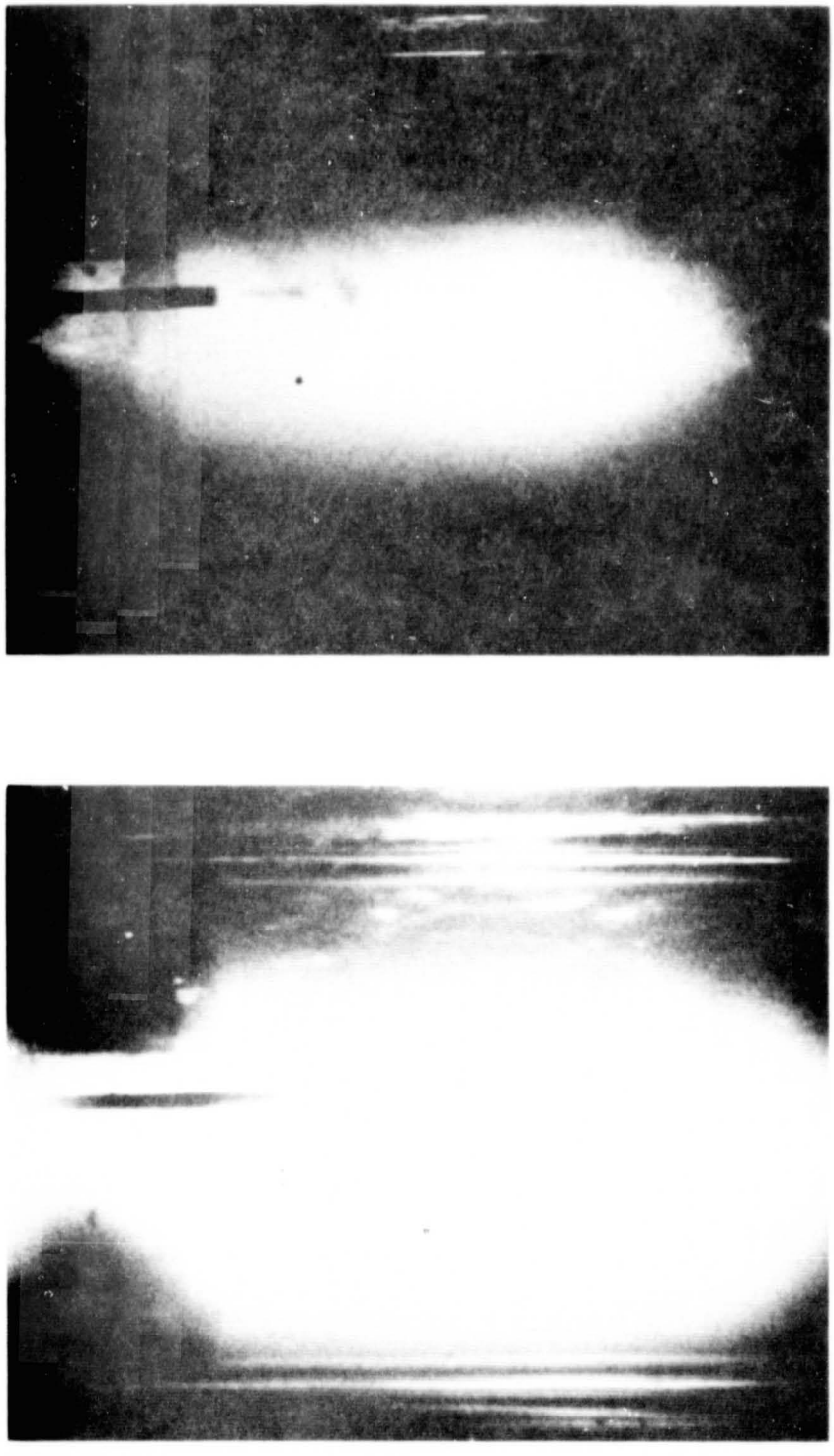

Fig. 6a - Results of Bannister (Ref. 14): Open End of Tube 2.54 cm Below Liquid Helium Surface ($f = 20.5$ Hz, $A = 2.82 \times 10^4$ N/m^2)

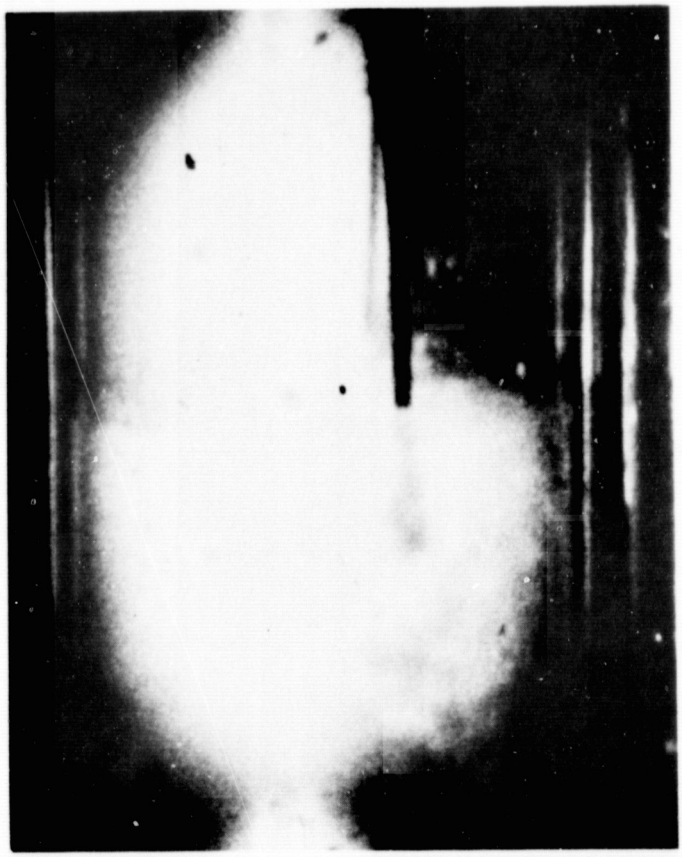

Fig. 6b - Results of Bannister (Ref. 14): Open End of Tube at Liquid Helium Surface (f = 21.2 Hz, A = 4.07×10^4 N/m^2)

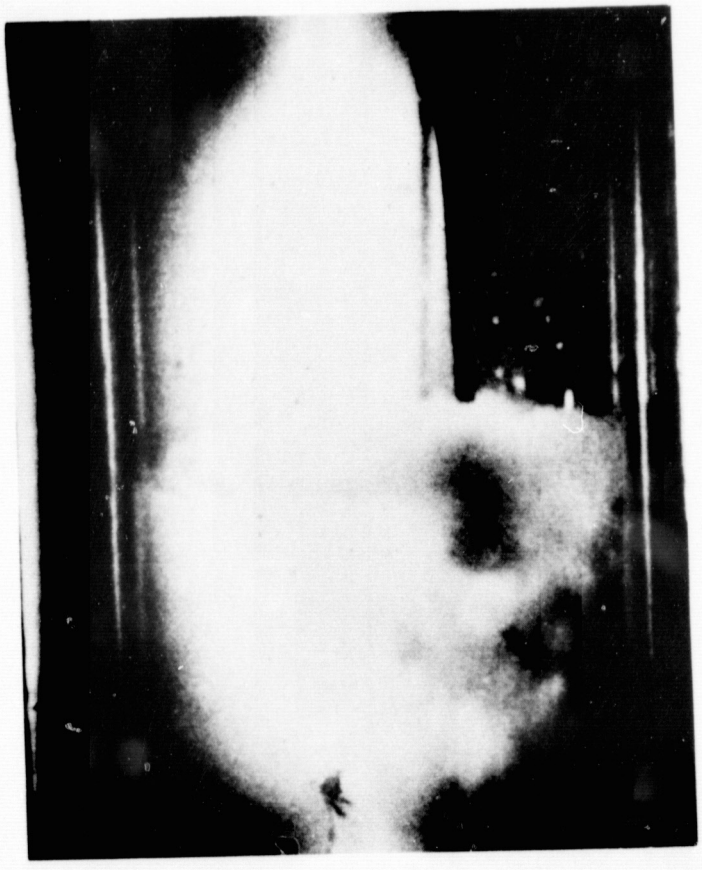

Fig. 6c - Results of Bannister (Ref. 14): Open End of Tube 5.1 cm Above Liquid Helium Surface (f = 34.1 Hz, A = 8.0×10^4 N/m^2)

2.1.10 Observations of Larkin; Thurston and Rogers

Larkin, 1967 (Ref. 15), was apparently the first to solve the nonlinear conservation equations for simulating thermally induced wave motion. He used a finite-difference method and a digital computer to generate the results. The model consists of two infinite plates with helium gas as the fluid. His analysis was concerned with the initiation of transient waves and not with sustained motion. Results of this analysis indicate that: (1) the heat transfer can be greatly increased over pure conduction due to acoustic pressure waves and (2) numerical methods can be used successfully to calculate thermal acoustic oscillations.

Thurston and Rogers, 1967 (Ref. 16), report that thermal acoustic oscillations occurred as a result of forced convection heating of dense hydrogen with film boiling. The experimental measurements of frequency and amplitude were correlated in terms of a "boiling" number and a Strouhal number. The inception of oscillations is correlated in terms of a specific volume number. The authors inferred that a dense-core superheated film mechanism was used to explain the role of heat transfer in producing the oscillations.

2.1.11 Theoretical Analysis of Stability (Thullen and Smith; Rott)

Thullen and Smith, 1968 (Ref. 17), present an analysis for determining the parameters and operating region for oscillations associated with liquid helium. They used a "lumped parameter" theoretical model and correlated the zones of growing and decaying oscillations in terms of dimensionless groups. Comparison of the results with some experimental measurements taken from a complex configuration show that the general behavior trend is correct. Accuracy of 6% is claimed by the authors when comparing their frequencies with Bannister's results.

Rott, 1969 (Ref. 18), presents a complex mathematical formulation of the linearized equations for small amplitude motion. His purpose was to

determine the stability limit for thermal acoustic oscillations. This paper presents no results, only the formulation of the problem. However, he presents some very useful results in a later paper subsequently discussed. Mortell, 1971 (Ref. 19), also gives the detailed mathematics for description of small amplitude resonant motions of a gas in a tube.

2.1.12 Experimental and Theoretical Study of Collier

Collier, 1972 (Ref. 20), investigated thermally induced oscillations in cryogenic systems. In an experimental study, he found that the surface temperature of a steadily heated cylinder oscillates with an amplitude of about 0.25°K and a frequency of about 8 Hz when immersed in slush hydrogen. The amplitude and period of oscillation were found to be relatively independent of the heat flux at the surface in the range from 0.25 to 1.5 watts/cm^2. The author claims that the experimental results were consistent with a theoretical model which was developed and which predicted oscillations in the thermal expansion of a liquid film located between the heated surface and the slush. The model was based on the assumptions of "relatively incompressible" and "slowly accelerating" fluid flow. Since the important effects of viscosity were neglected in Collier's model, his results can be considered as approximate qualitative solutions.

2.1.13 Stability Theory of Rott

Rott, 1973 (Ref. 21), presents an extension of his previous work (Ref. 18) aimed at determining the oscillation stability limit for helium. He used a "second-order" linear theory to produce, for a range of dimensionless parameters, a curve indicating the range where oscillations can be expected to occur. One of Rott's curves is reproduced in Fig. 7. The governing parameters were determined to be the ratio of the hot end temperature to cold end temperature, the aspect ratio of the tube, the length of the "cold" part of the tube and the acoustic Reynold's number. The dimensionless parameters determined by Rott are used in the present study to display a similar plot for stability analysis. This is discussed in more detail in Section 3.4.

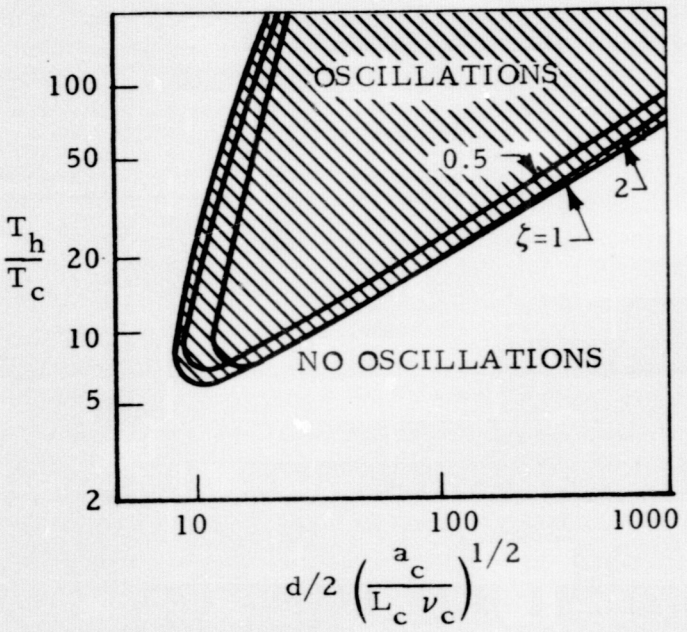

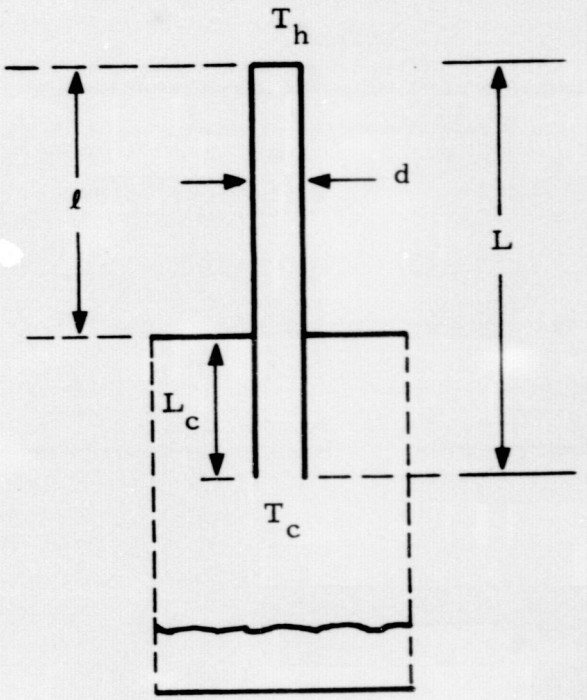

$\zeta = \frac{L-\ell}{\ell}$

Configuration of Rott

Fig. 7 - Work of Rott (Ref. 21)

2.1.14 Experiments of Von Hoffmann et al

Von Hoffmann, Lienert and Quack, 1973 (Ref. 22), present results of an experimental study to verify the stability limit of Rott. Tubes of various sizes were inserted into a double glass dewar. A brass vessel filled with liquid nitrogen was used to control the temperature of the "warm" end of the tube in order to vary the T_h/T_c ratio. A piezoelectric pressure sensor at the closed upper end of the tube was connected to an oscilloscope so that the oscillations could be observed. A plot of the results, compared to the theory of Rott, is given in Fig. 8 as reproduced from Ref. 22.

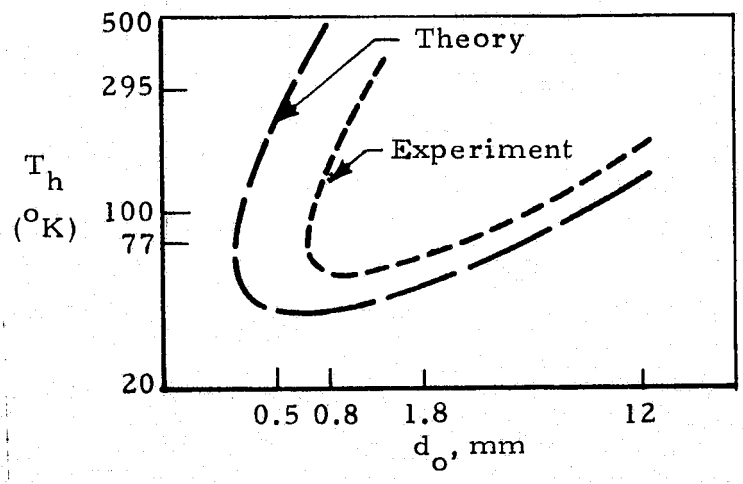

Fig. 8 - Data of Von Hoffmann Compared with Theory of Rott (from Ref. 22)

Von Hoffman claims qualitative agreement as shown by Fig. 8 and explains the lack of quantitative agreement on his experimental inaccuracies. He also notes that it was very difficult to get reproducible results for the pressure amplitude. This work appears to be the most recent effort (to 1974) on experimental studies of thermal acoustic oscillations.

2.1.15 Numerical Solution of Spradley

Spradley, 1974 (Ref. 23), at Lockheed-Huntsville developed a numerical method for the solution of a nonsteady, viscous, heat conducting, compressible flow problem by a vigorous nonlinear formulation. In this model, helium gas, initially at a uniform temperature, T_o, was confined between two parallel boundaries. At time t = 0, the temperature of the lower plate is suddenly raised to $T_w = 2\ T_o$, while the upper plate is kept at the constant value T_o. Because of heat transfer and compressibility effects, thermal acoustic waves are set up in the system. These wave phenomena greatly increase the heat transfer rate into the system. Typical results of this solution, as obtained from the computer program, are shown in Fig. 9. This figure shows the calculated dimensionless velocity and pressure profiles as a function of time at the center between the two plates. This figure also shows the oscillatory nature of the wave motion. The period of the calculated wave is 1.55 units of dimensionless time which corresponds to the acoustic wave period in this system which is $2/\sqrt{\gamma}$ or 1.55. Thus the calculated waves are acoustical. This analysis also shows that thermally induced wave motion can greatly increase the heat transfer over the pure conduction mode. A general numerical technique and computer program was developed for solving the nonlinear conservation equations governing the thermally induced waves. Complete profiles of temperature, pressure, gas velocity and heating rate can be obtained. This work forms the basis for the present study of thermal acoustic oscillation in tubes connected to low temperature apparatus.

Other work concerned with this general area of thermal acoustic oscillations is given in Refs. 24 through 35. Considerable effort was expended on this literature survey, but there always is the possibility of an important omission. The authors would appreciate learning of any such work or any other unpublished efforts in this field.

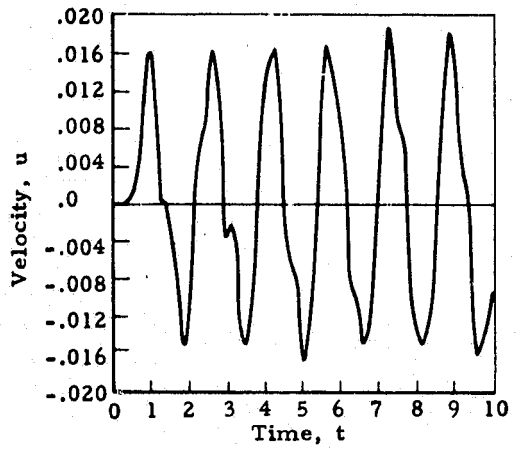

a. Velocity vs Time

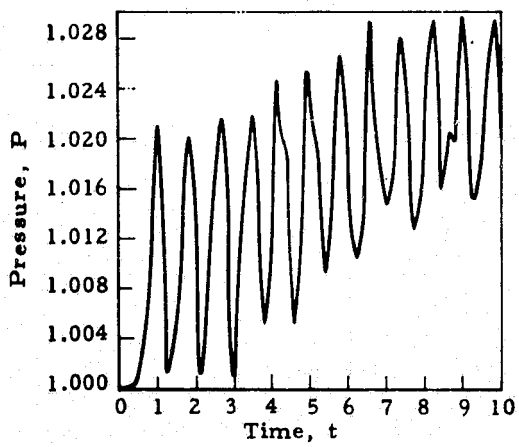

b. Pressure vs Time

Fig. 9 - Dimensionless Velocity and Pressure Profiles from Numerical Solution of Thermoacoustic Oscillations (from Ref. 23)

2.1.16 Summary and Perspective

The preceeding review of the literature has presented a historical overview of thermal acoustic oscillations complemented by a discussion of the physical mechanisms that cause them. Discovery of the phenomenon was by Sondhauss in 1850, the first explanation of the cause was by Rayleigh in 1878, and the first observation of the spontaneous occurence of oscillation in cryogenic apparatus was made by Taconis in 1949. Since Taconis' work, numerous observations of thermal acoustic oscillations have been made together with the accompaning large heat leaks they can cause. The heat addition at the closed end of a tube and the heat removal at the open end causes sustained oscillations for a long period of time. Figure 10 is a re-plot of the data of J. D. Bannister showing that the heat addition due to oscillations can be two orders of magnitude larger than the pure conduction heat leak (data spread is different experiment conditions). The large amount of heat pumped into a cryogenic storage vessel can cause such large boil-off that long term storage on space missions can be impossible unless the systems are designed to suppress oscillations. There is a possibility of these oscillations occurring in any cryogenic storage system with fill lines, vent lines or other tube penetration connected to an ambient environment.

The discussion in succeeding sections describes the analysis and experiments performed by Lockheed and presents curves showing effects of system parameters on oscillation characteristics. Analytical predictions and experimental measurements of heat transfer are shown and implications for long term storage are given in Sections 2.4 and 2.5. Conclusions resulting from this study are summarized in Section 3 and recommendations for further study are given in Section 4.

2.2 ANALYTICAL MODEL

A brief, general description of the analytical model of thermal acoustic oscillations is presented in this section. Details of the mathematics, fluid mechanics and numerical method are given in Appendix A.

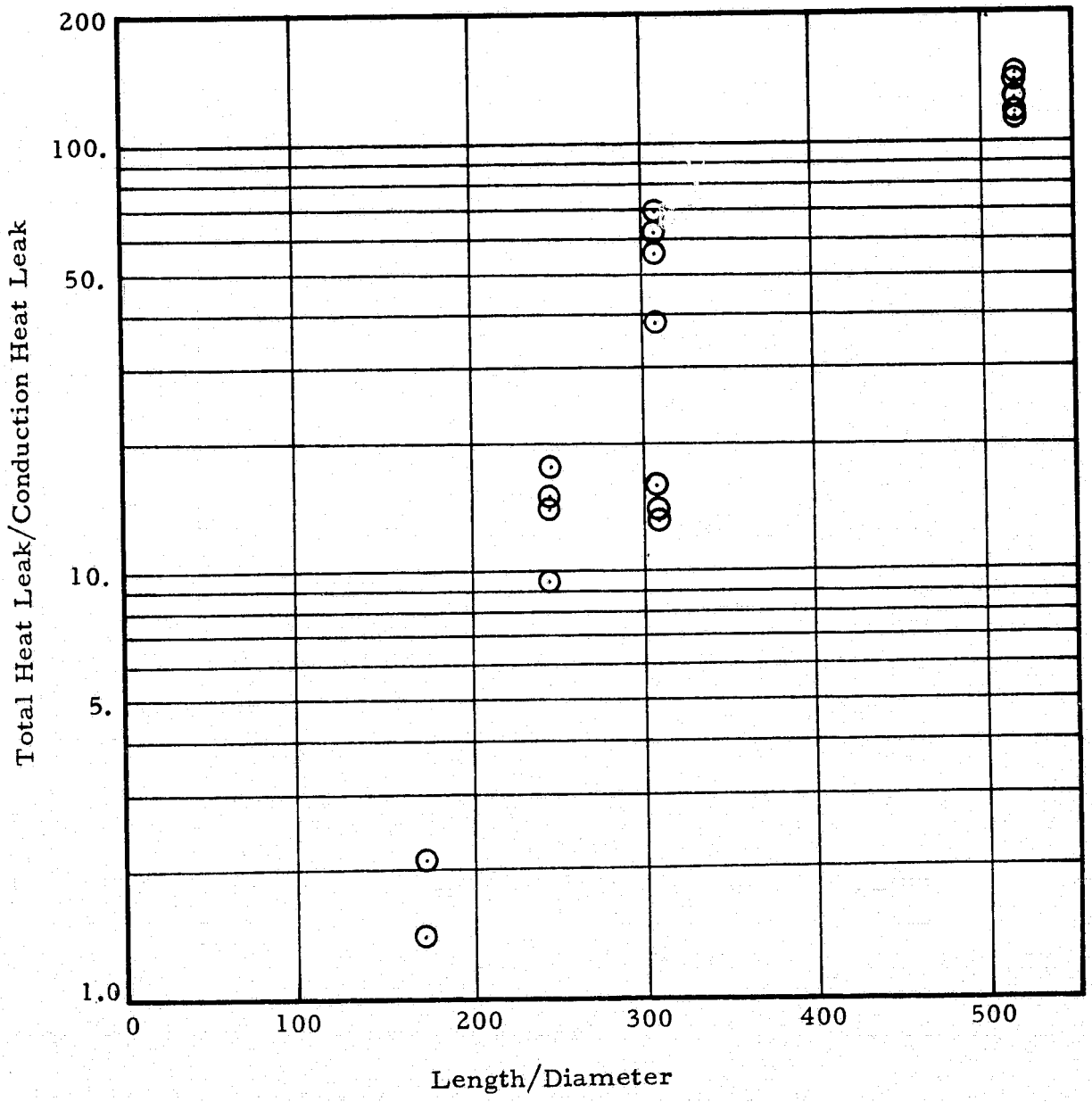

Fig. 10 - Experimental Data of Bannister (Ref. 14)

2.2.1 Model Description

Kramers, 1949 (Ref. 4), attempted to theoretically model thermal acoustic oscillations using a linearized system of equations. He could not predict the sustained oscillations and attributed his failure to the neglect of nonlinear effects. Rott (Ref. 21), in 1973 was somewhat successful in an analytical approach using a second-order linear theory. The approach taken for the present work is to use a full nonlinear model to study the various problems associated with thermal acoustic oscillations. To the authors' knowledge, this is the first work to attempt such an analysis.

The objective of this study dictated the nonlinear approach. A general analytical tool was sought for use in predicting:

- The conditions which cause or suppress oscillations
- The frequency, amplitude and intensity of oscillations when they exist
- The additional heat leak induced by the oscillations, and
- Parametric system parameters which can be adjusted to suppress oscillations and thus heat transfer.

In addition to developing the analytical model, a major objective of the study was to obtain parametric curves which can be used by a designer in analyzing a particular system. This requires a parametric study to be done using the analytical tool. The final goal was to verify the analytical model by comparison with experimental data. A summary of the approach taken is given in Fig. 11.

The first step in the model development is to obtain a system of differential equations and boundary conditions which represent the physical problem. The most general equations describing thermal acoustic oscillations phenomena are the Navier-Stokes equations. These are very complex in their general form, and no solution for general cases have been reported as of 1975. The approach taken here is to apply certain assumptions, which must be justified, in order to obtain equations which can be solved. Even in their

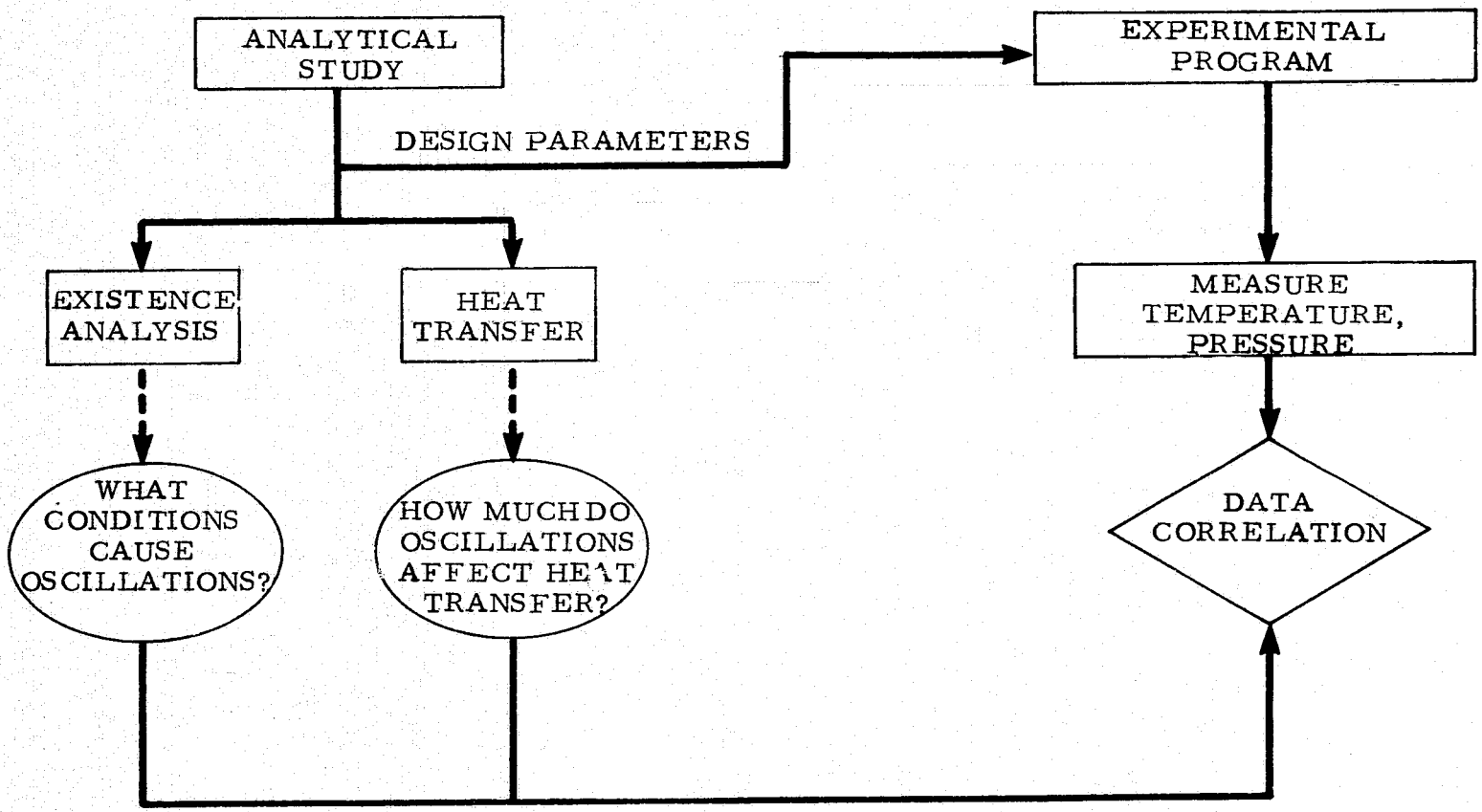

Fig. 11 - Summary of Approach for Thermal Acoustic Oscillations Study

simplest form for thermal acoustic oscillations, these cannot be solved in "closed form." However, numerical methods, using a digital computer, have been very successful in solving problems in many aspects of fluid mechanics. The thermal acoustic oscillations (TAO) computer program is based on a numerical solution of the Navier-Stokes equations. These equations and the solution technique are given in Appendix A.

In addition to a model for obtaining the solution profiles, a method for determining the dominant frequency content, amplitude and intensity of the oscillations is needed. A General Statistical Analysis (GSA) computer program (Ref. 37) was utilized for this purpose. The TAO solutions are processed by a Fast Fourier Transform algorithm and the power spectral density function is computed. The TAO program and the GSA program together constitute the analytical tools for use in this study.

The assumptions used in developing the model are of interest to the designer in determining the applicability of the model to a particular configuration. The geometric configuration used for the model is shown in Figure 12. A cylindrical tube closed on one end and open on the other is shown. A subset of the model allows the tube to be closed on both ends. The basic form of the model is developed by applying the following assumptions:

- The tube is filled with gas; no liquid region is modeled.
- Flow in the tube is laminar and axisymmetric.
- Thermal conductivity, viscosity and heat capacity are functions of temperature only.
- Radiation, internal heat sources and viscous dissipation of energy are negligible.
- The closed end of the tube is assumed to be connected to a large volume of cold gas.
- The closed end of the tube is held at a constant (room) temperature.
- The fluid is not restricted to helium, but helium was used in all calculations for this study.
- The flow is driven entirely by thermal expansion due to a large temperature gradient imposed on a compressible fluid.

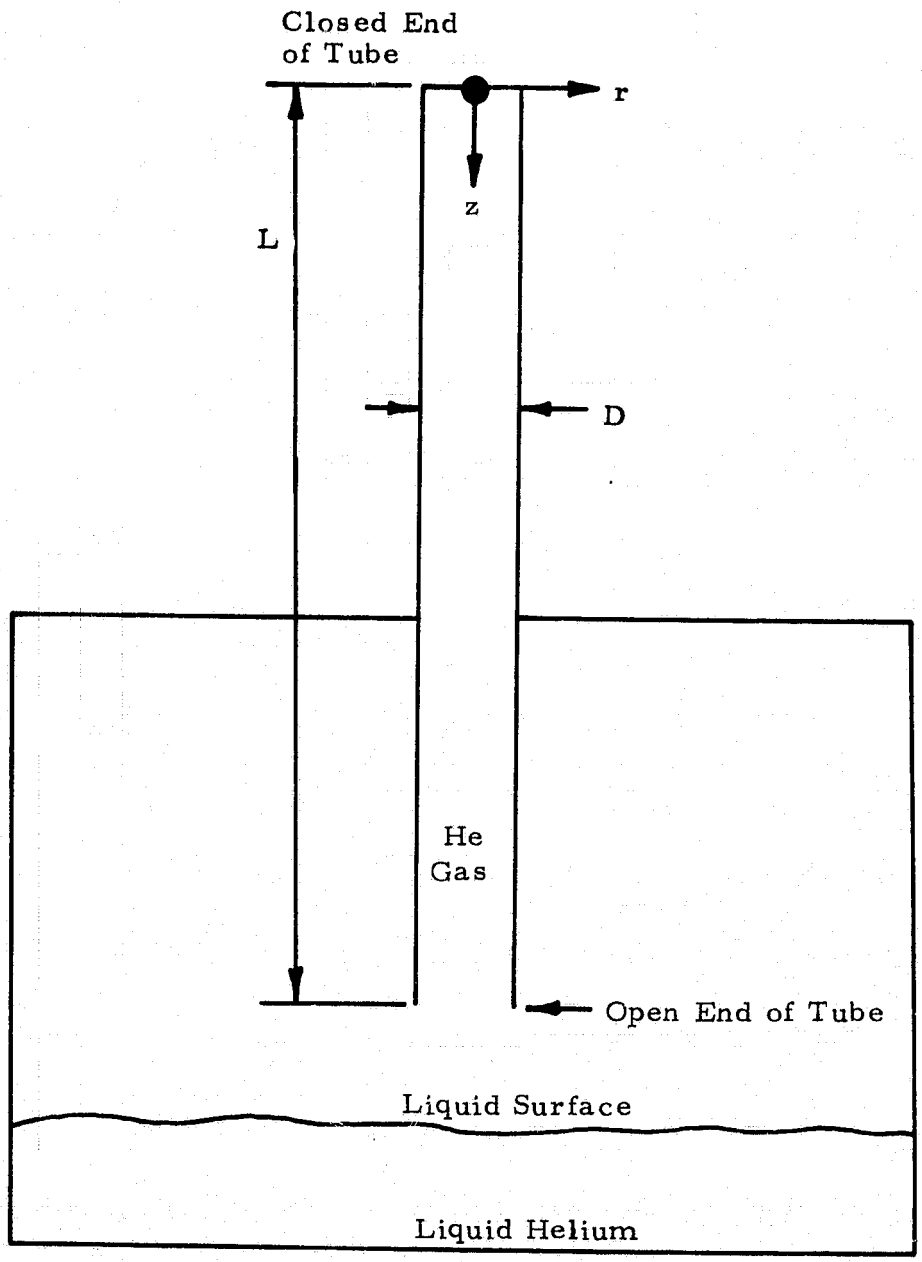

Fig. 12 - Geometric Configuration and Coordinate System for Thermal Acoustic Oscillations Model

- The stability of the system to small perturbations is governed by the pressure oscillations at the open end of the tube.

In addition to these major model assumptions, there are others used in writing the differential equations: (1) a Newtonian relation with Stokes hypothesis (see Appendix A) is assumed for the viscosity; (2) an ideal gas law with variable compressibility coefficient relates the pressure to temperature and density; (3) gravitational body forces are neglected; (4) conduction heat losses from the tube walls are supplied as boundary values; and (5) the pressure perturbations are assumed to be sine waves. Justification for these assumptions is also given in Appendix A.

2.2.2. Model Parameters

Parameters used for the analytical TAO model are based on the stated objectives of this study and on those pertinent papers which have appeared in the literature. Each of these that appear in the model is briefly discussed as to how they influence the oscillations.

- L/D - The length-to-diameter ratio of the tube determines to great extent whether or not oscillations will occur. If they do occur, the length of the tube influences the frequency and hence intensity.
- T_h/T_c - The ratio of the "hot" temperature at the closed end to the "cold" temperature at the open end is the driving mechanism for initiating and sustaining oscillations.
- L_c/L - The ratio of the length of tube exposed to the cold environment, L_c to the total length L. This parameter also strongly influences the intensity of the oscillations and, in the physical situation, the disturbance of the liquid surface.
- R_e - The acoustic Reynolds number,

$$R_e = \frac{\rho L a}{\mu}$$

where a, the local acoustic velocity (speed of sound), strongly governs the stability of the system to perturbations, i.e., whether or not the oscillations are sustained.

- k, μ, C_p, Z versus T - The temperature variation of the conductivity, k, the viscosity μ, the specific heat C_p and compressibility Z are vital to proper modeling because of the large temperature range considered.
- f, A, I - The frequency, f, amplitude, A, and intensity, I = fA, are important factors which influence the heat leak due to oscillations. In addition, these may also influence structural design since large intensity pressure oscillations can cause structural damage.
- Q/Q_t = The ratio of the total heat leak (oscillations plus conduction) to the normal heat leak in the tube walls is a measure of the effect of oscillations on boiloff rates and hence efficiency of storage of the cryogen.

The above sets of parameters were used in constructing the TAO model and in performing the parametric study. Effects which have an influence on the oscillations but which could not be included in the present scope are summarized as follows:

- The effect of the internal pressure rise in the storage dewar is not considered.
- The amount of liquid in the dewar and the distance of the tube from the liquid surface are not modeled.
- The effect of liquid being present in the tube is neglected.
- The turbulence which is apparently induced at the liquid surface due to large intensity oscillations can not be modeled with current technology.

The influence of these neglected effects is discussed in conjunction with the discussion of results in Section 2.4.

2.2.3 TAO Computer Program

The analytical model was programmed for a digital computer using FORTRAN V language. The Univac 1108 system at NASA-MSFC was used for most of the computer studies. The program consists of a main routine which calls subroutines to solve each of the governing equations. A block diagram is given in Appendix A.

The required program inputs include

- Initial conditions T_o , P_o
- L, D, L_c
- T_h, T_c, q_{loss} (boundary values for tube wall)
- Gas property tables, μ , k, C_p, z
- Perturbation parameters, f_p, A_p, and
- Program control flags.

The computation sequence is a series of loops to iterate on the open end boundary values, to solve the equations at discrete grid points, and to march the solution forward in time. The outputs include:

- Complete flowfield definition; temperature, pressure, velocity, and density in the gas column.
- Heat transfer, Q/Q_t
- A magnetic tape for use in the GSA program in computing frequency, f, amplitude, A , and intensity, I.

The program is operational on a production basis. The proper selection of grid size and time step for compatibility with the tube length/diameter ratio is essential for stability of the numerical method. The program should be used by an experienced analyst due to this stability of the numerical scheme, the peculiar nature of specific configurations and the general complexity of the TAO program.

2.2.4 Spectral Analysis

This portion of the thermal acoustic-oscillations study is directed toward determining the wave characteristics of the computed TAO solutions. A simple, yet inaccurate, method would be to plot the pressure waves versus time at numerous points and compute the frequency directly. This approach was not taken here because of: (1) the inherent inaccuracies; (2) the large numbers of cases to be processed; and (3) the calculated wave forms have multi-frequency content, i.e., a higher frequency wave super-

imposed on the main lower frequency wave. The alternate approach of using a power spectral density analysis was taken since a general purpose program for this task was already available.

The Lockheed-Huntsville General Statistical Analysis (GSA) program (Ref. 37) was utilized for performing the spectral analysis. The inputs can be any functions of time such as temperature and pressure. These are supplied via magnetic tape from the TAO solutions. The GSA program then calculates mean values, mean squared values, standard deviations and variances. The data are then detrended and tapered to give zero mean value and slope. The Fourier transform of the complex function is then computed using a Fast Fourier Transform (FFT) algorithm and the calculations are made for a number of statistical functions.

The power spectral density (PSD) function for a set of random data having oscillating properties describes the general frequency composition of the data in terms of the spectral density of its mean value. We start with a series recorded in a suitable period of time. The series may represent the calculated velocity, pressure or temperature solutions of the thermal acoustic oscillations computer program. The mean square values of the times series in a frequency range between f and $f + \Delta f$, may be obtained by filtering the series with a band-pass filter having sharp cutoff characteristics, and computing the average of the squared output from the filter. This average squared value will approach an exact mean square value as the observation time approaches infinity. Hence, the power spectral density of the series at the frequency f is the mean square value of the property at f per unit frequency. This program was utilized to obtain the dominant frequency content of the waves. Details of the mathematics, including the equations and a program flow chart are given in Appendix A.

2.2.5 Analytical Results

Typical results from the analytical model are presented in this subsection. The purpose of presenting the analytical predictions which follow is to (next page):

- Illustrate typical analytical model solutions
- Summarize the parametric study
- Provide a designer with curves to estimate when a configuration can thermally oscillate, and
- Aid in the presentation of the findings of this study

The Lockheed TAO analytical predictions and experimental data are compared in Section 2.4.

The analytical calculations are summarized in Figs. 13 through 19. These results were obtained by processing a matrix of cases using the TAO and GSA programs. Helium is the working fluid used in all calculations. Both aluminum (6061-T6) and stainless steel (304 CRES) tubes with length-to-diameter ratios ranging from 25 to 500 were analyzed.

Independent parameters used in the model were:

L/D	length to diameter ratio of the tube
T_h/T_c	ratio of hot end temperature to cold end temperature
L_c/L	ratio of length of tube exposed to cold temperature to the total length of the tube

Dependent parameters used in the model were:

f	frequency (Hz)
P_A	peak-to-peak pressure amplitude (atm)
I	oscillation intensity (atm/ sec)
Q/Q_t	heat transfer ratio (%)

The latter parameter, Q/Q_t, is the ratio of the total heat leak to the normal conduction heat leak, ie $(Q_o + Q_t) /Q_t$.

Figure 13 is a stability diagram for helium. The diagram was constructed by processing many cases with the TAO program varying T_h/T_c and the Δ parameter shown. This Δ parameter is used for the correlation

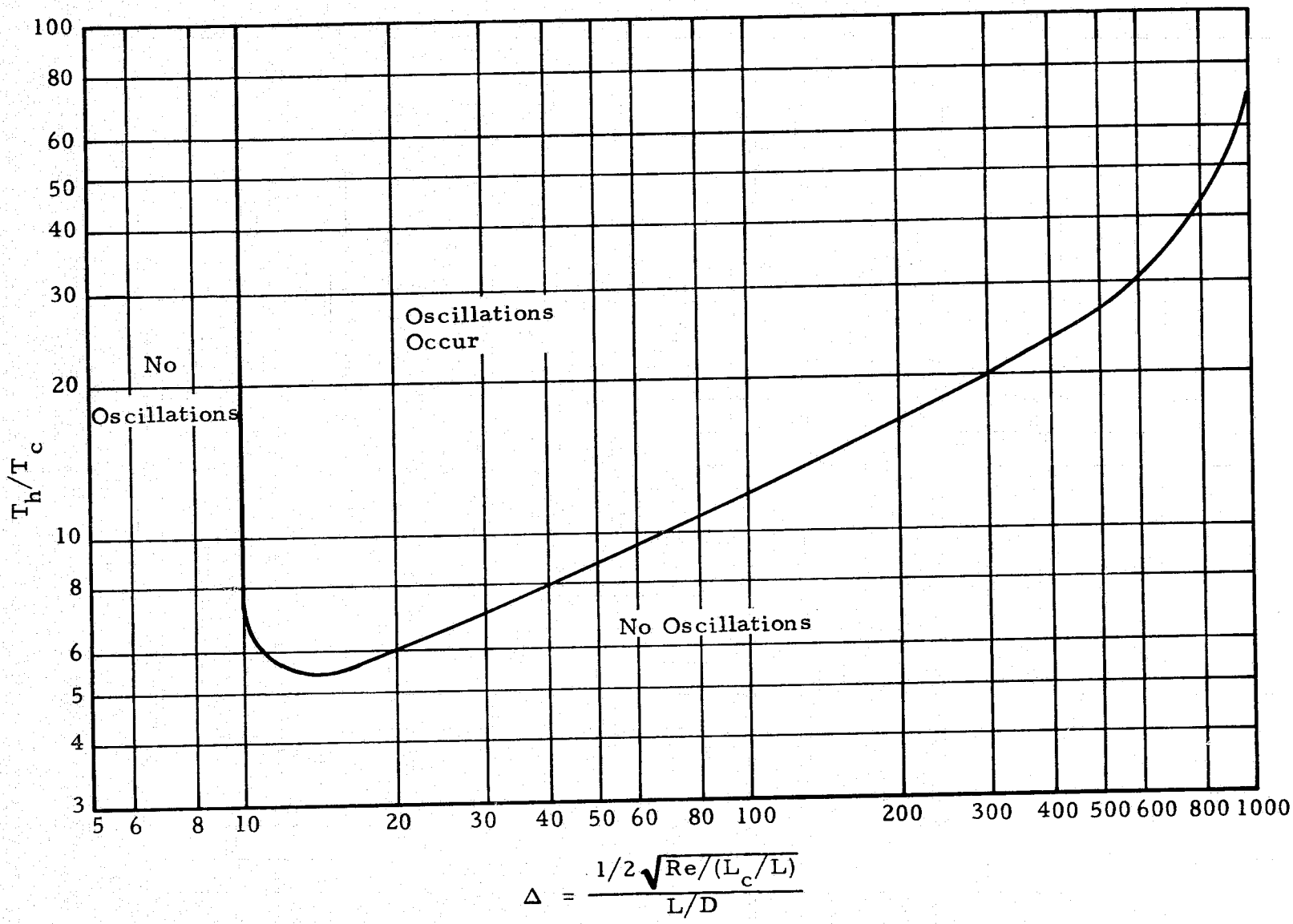

Fig. 13 - Stability Diagram for Helium

as discussed by Rott (Ref. 21). The Reynolds number, Re, is based on the cold end temperature, the tube length and the kinematic viscosity of helium at T_c. For parametric values lying "inside" the curve, oscillations can be expected to occur. No oscillations should occur for T_h/T_c versus Δ lying "outside" the curve. Comparison with other predictions and to experimental data is given in Section 2.4.

For T_h/T_c ratios less than about 5, no oscillations were predicted for any value of Δ. The range of T_h/T_c which can produce oscillations is larger for the larger L/D ratios. As L/D decreases, Δ increases requiring an increase in the T_h/T_c ratio necessary to produce sustained oscillations. For values of Δ below 10, no oscillations were produced for any T_h/T_c ratios. For Δ greater than approximately 1000 no oscillations should exist for practical T_h/T_c ratios.

An example Δ calculation is shown below for the following case.

L	38.85 in.
D	0.259 in.
L_c	19.425 in.
Re	1.1×10^8
T_h/T_c	21.1
Δ	49.4

Using these values of T_h/T_c and Δ, Fig. 13 shows that oscillations can definitely occur in this system. The Lockheed experimental program verified the existence curve for this case, i.e., oscillations did indeed occur.

Figure 14 is a plot of the peak-to-peak pressure amplitude versus L/D for parametric values of L_c/L. A T_h/T_c ratio of 25 was chosen. The pressure amplitude increases with increasing tube L/D for all values of L_c/L and the increase is linear. The increase in P_A with L_c/L is caused by exposing more of the tube to the cold temperature which produces a sharper thermal gradient in the tube itself which in turn increases the amplitude of the

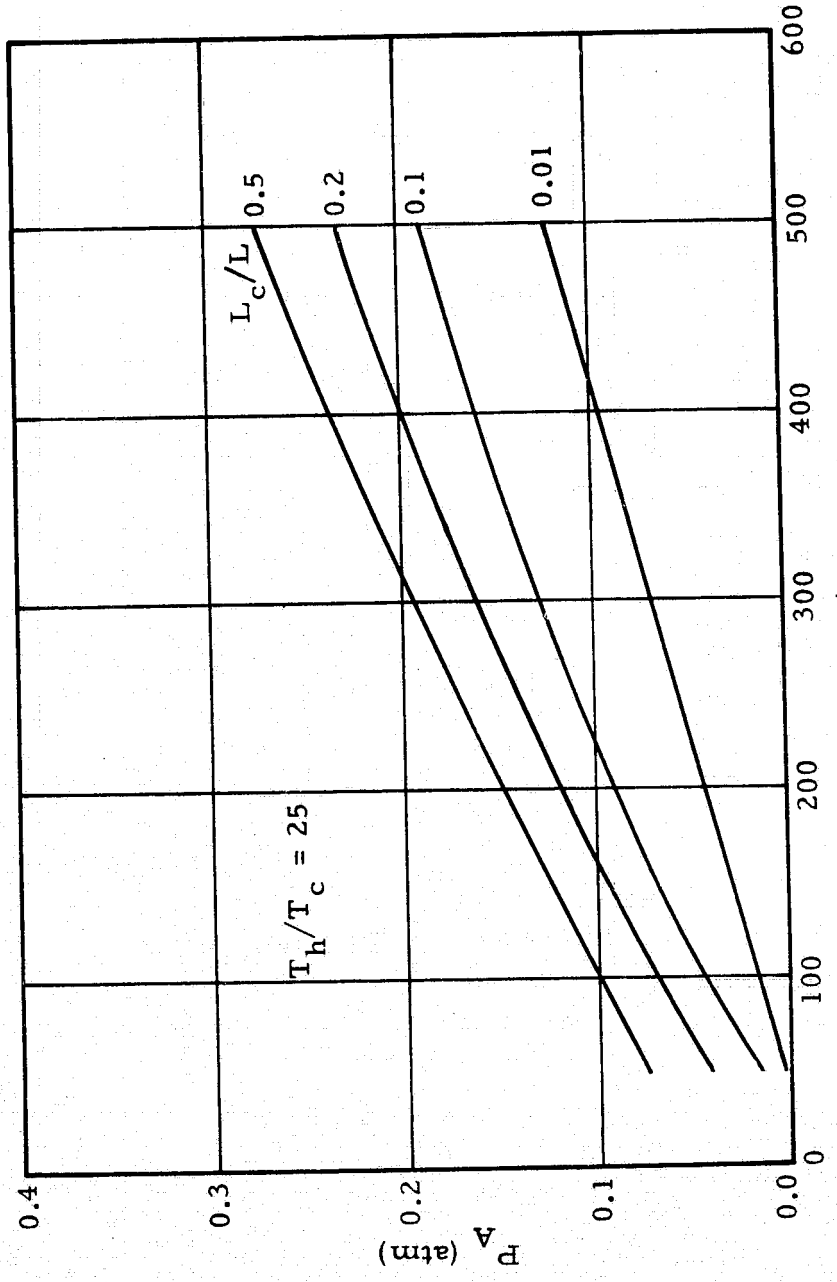

Fig. 14 - Pressure Amplitude vs L/D for Parametric L_c/L

oscillations. The effect of T_h/T_c on the pressure amplitude is shown in Fig. 15. The amplitude decreases with decreasing T_h/T_c for all values of L/D. The amplitude goes to zero at the critical T_h/T_c which for these cases range from approximately 11 for L/D = 100 to approximately 7.5 for L/D = 500. The maximum temperature ratio used in the matrix of cases is 25 which produces an amplitude of approximately 0.19 atm for L/D = 500. A parametric L_c/L = 0.1 shown here is typical of all values in the matrix.

The oscillation frequency is shown in Fig. 16 for the same parametric variations of L/D and L_c/L. The tube diameters were held constant and the length was varied to produce the L/D values shown. The frequency decreases with L/D as would be expected since the longer tubes produce lower frequency oscillation than the shorter ones. The frequency was found to vary little with practical T_h/T_c ratios. The variation of f with L_c/L also behaves as it should, i.e., the frequency decreases with increasing L_c/L for a fixed L/D. This occurs because larger L_c/L values correspond to exposing more of the tube to the cold environment which reduces the average temperature of the gas. The average acoustic velocity in the gas column decreases as the average temperature decreases resulting in a lower frequency oscillation.

The oscillation intensity is defined here as the frequency-amplitude product consistent with Bannister (Ref. 14). A plot of the oscillation intensity is shown in Figure 17 for the same L/D and L_c/L as the previous figures. The intensity values for the L_c/L = 0.01 case always increases with L/D while the L_c/L = 0.1 and L_c/L = 0.2 cases rise initially and then decrease. The L_c/L = 0.5 case is monotonically decreasing with L/D, and is a direct result of the definition of intensity used here. The pressure amplitude always increases with increasing L/D and the frequency decreases with increasing L/D. The product will then either increase or decrease depending on the slope of the frequency and amplitude variations. If the pressure amplitude increases faster than the frequency decreases, the the intensity will increase (and vice versa).

The magnitude of additional heat leak that can be caused by the oscillations is a primary concern to designers of long term storage vessels.

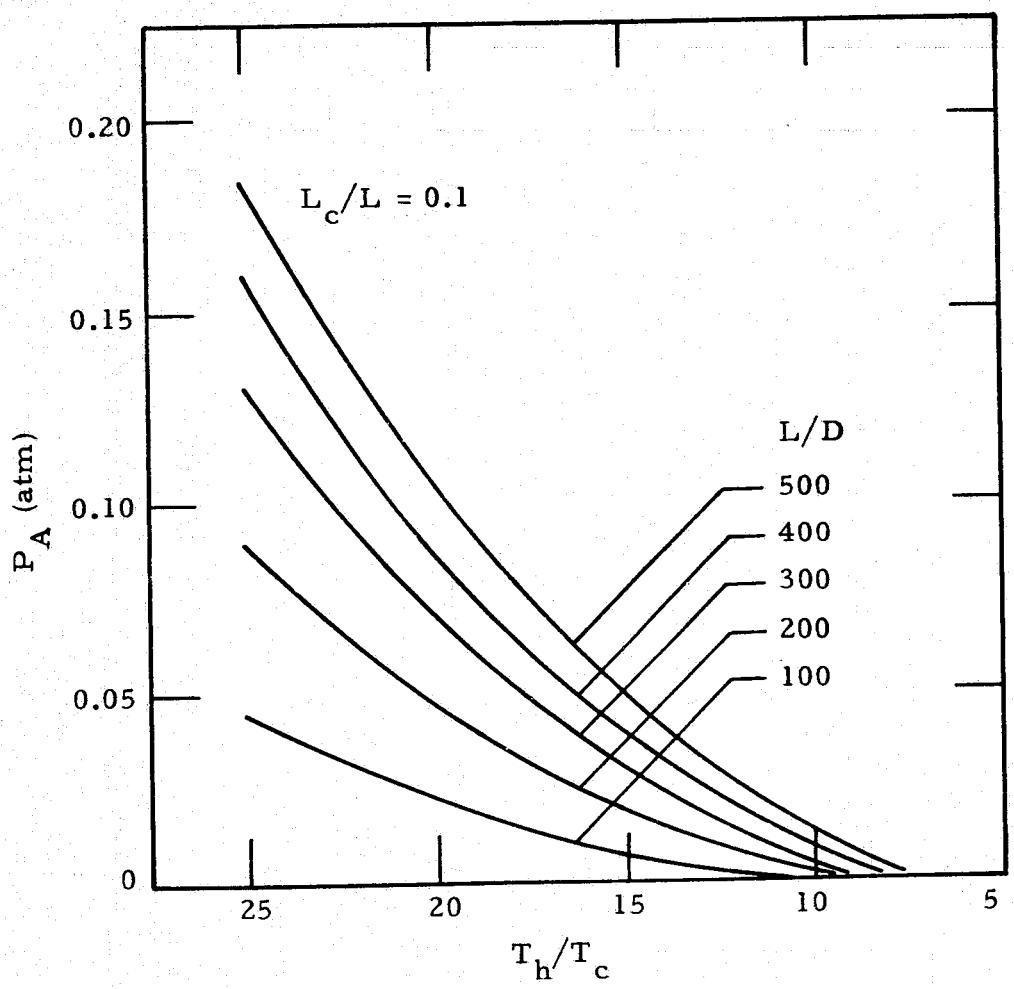

Fig. 15 - Pressure Amplitude vs T_h/T_c Ratio for Parametric L/D

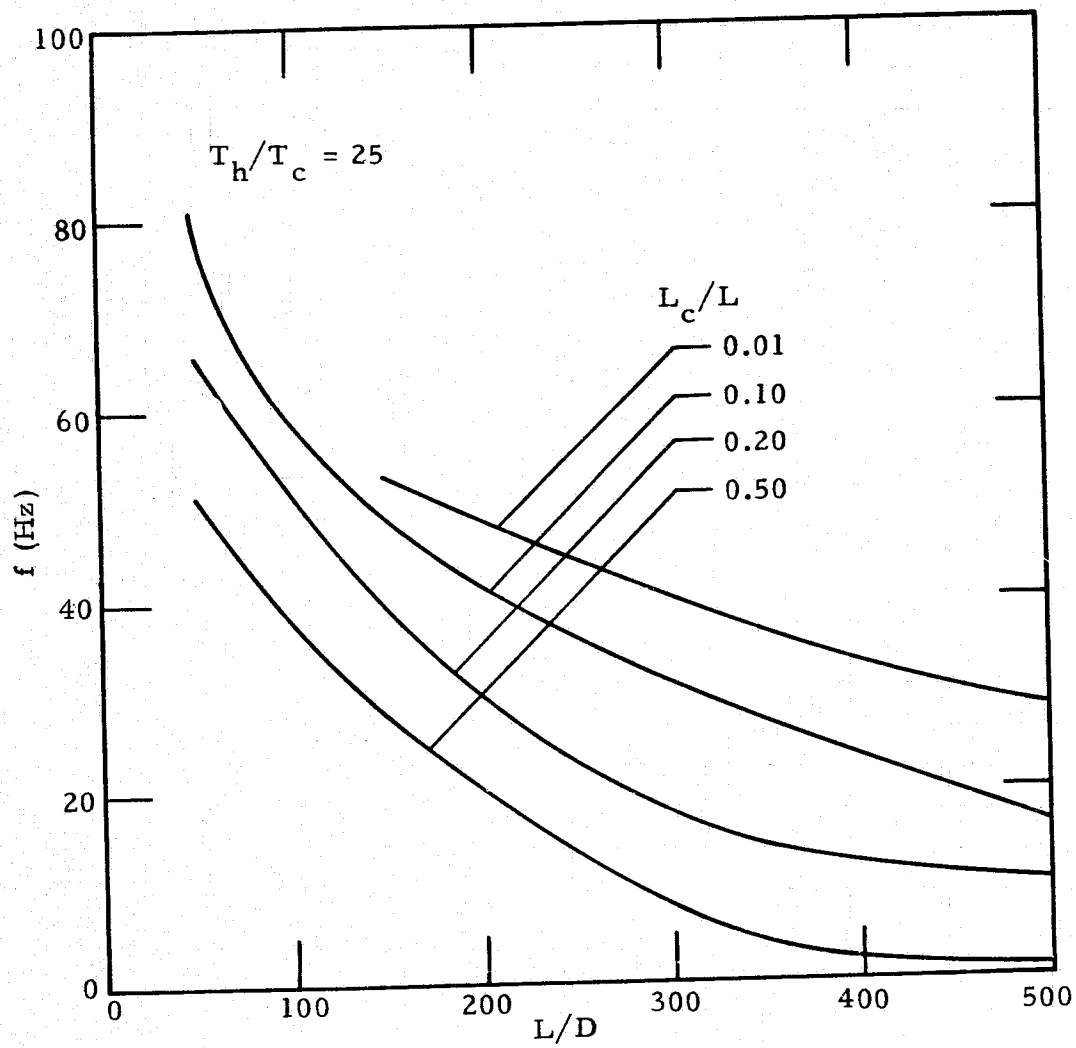

Fig. 16 - Oscillation Frequency vs L/D for Parametric L_c/L

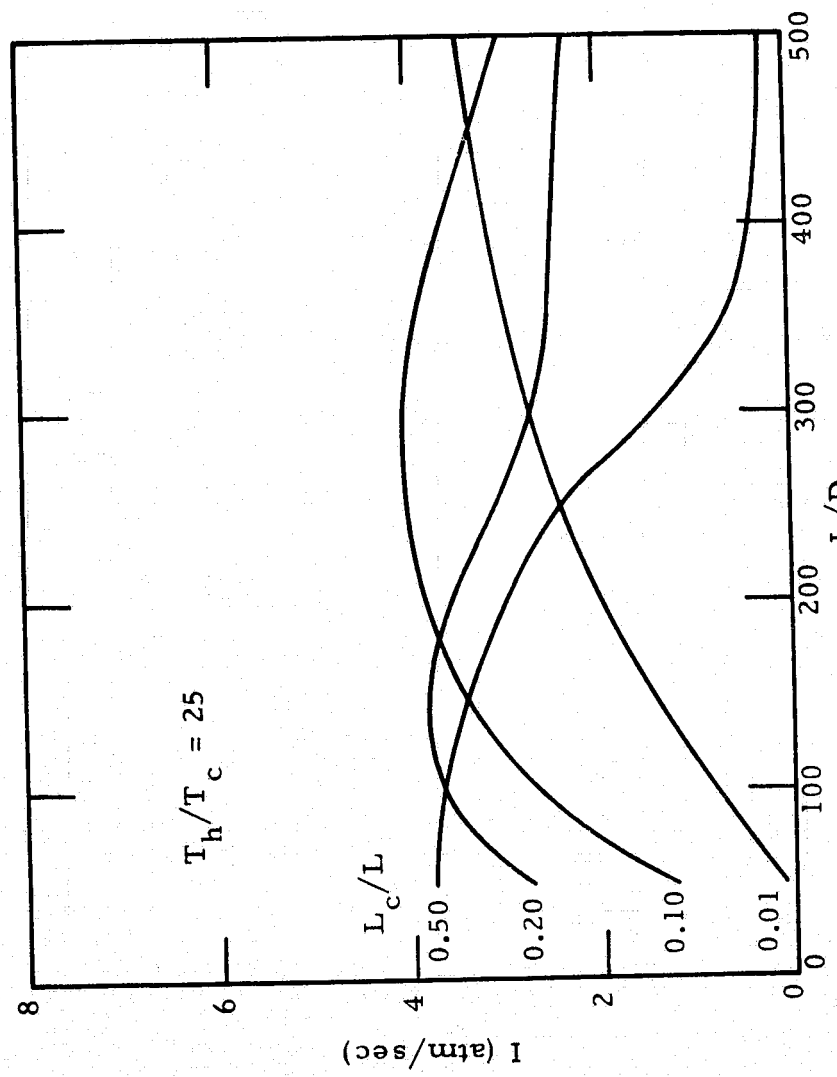

Fig. 17 - Oscillation Intensity ($f \times P_A$) vs L/D for Parametric L_c/L

The mass transfer at the open end of the tube was found to be the controlling mechanism for the increased heat transfer. The TAO program calculates the heat leak at the open end of the tube as discussed in Appendix A.

Figure 18 shows the amount of increased heat transfer versus L/D. The quantity Q is the total heat pumped by the oscillations plus the conduction in the tube wall. The Q_t is simply the conduction heat leak down the tube wall. This figure shows that no additional heat leak is present for L/D less than about 75. If oscillations exist at an L/D of 75, the amplitude is so small that the additional heat transfer is negligible.

However, the Q/Q_t ratio rises rapidly when tube L/D's exceed 100 with as much as an order of magnitude increase for L/D = 200 and over two orders of magnitude above L/D = 450. The variation of Q/Q_t with L_c/L shows a reversal trend between L/D = 100 and L/D = 200. For L/D = 100, the Q/Q_t ratio increases with increasing L_c/L. However, for L/D = 200 and above the variation with L_c/L is not linear. This behavior is a direct result of the nonlinear intensity versus L/D seen in Figure 17. For small (100) L/D ratios, the intensity, hence Q/Q_t, increases with increasing L_c/L. For the larger L/D's (500) the intensity, hence Q/Q_t, decreases with increasing L_c/L. For intermediate L/D values, the Q/Q_t ratio follows the intensity variation in Fig. 17. These calculations are compared to experimental data in Section 2.4.

Figure 19 is a cross plot of the Q/Q_t ratio versus pressure amplitude for $L_c/L = 0.1$. The curve is typical for all parametric values of L_c/L in the matrix. The increase in Q/Q_t with increasing amplitude is due to the larger amount of mass pumped out of the tube by the larger amplitude pressure waves. The effect of T_h/T_c on Q/Q_t can be seen by comparing Figures 15 and 19. As the T_h/T_c ratio is decreased, the amplitude and hence Q/Q_t, is also decreased.

In summary, the parametric study has provided insight into complex thermal acoustic oscillations phenomena. Briefly stated, four significant

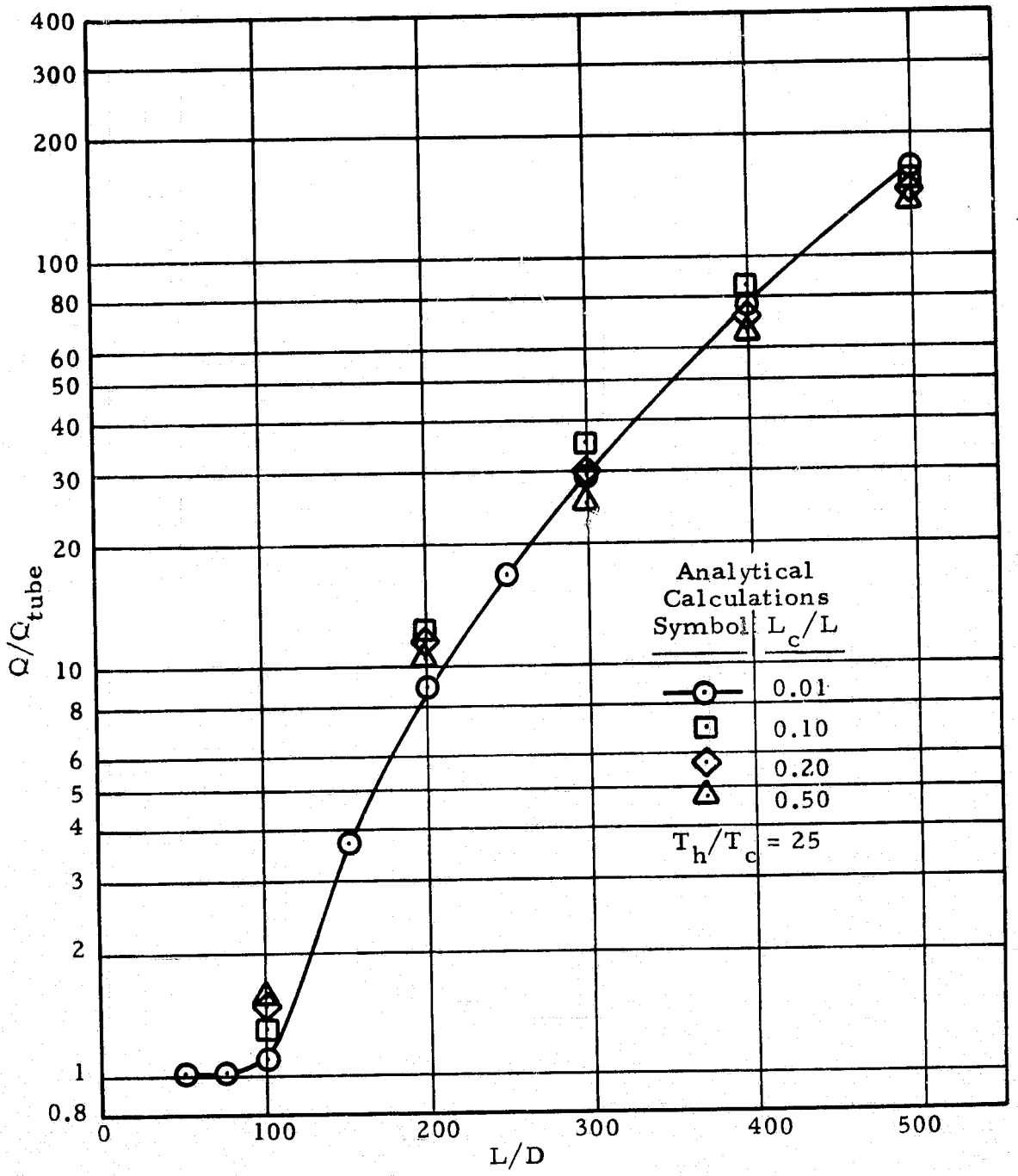

Fig. 18 - Ratio of Total Heat Leak (with Oscillations) to Normal Conduction Heat Leak vs L/D for Parametric L_c/L

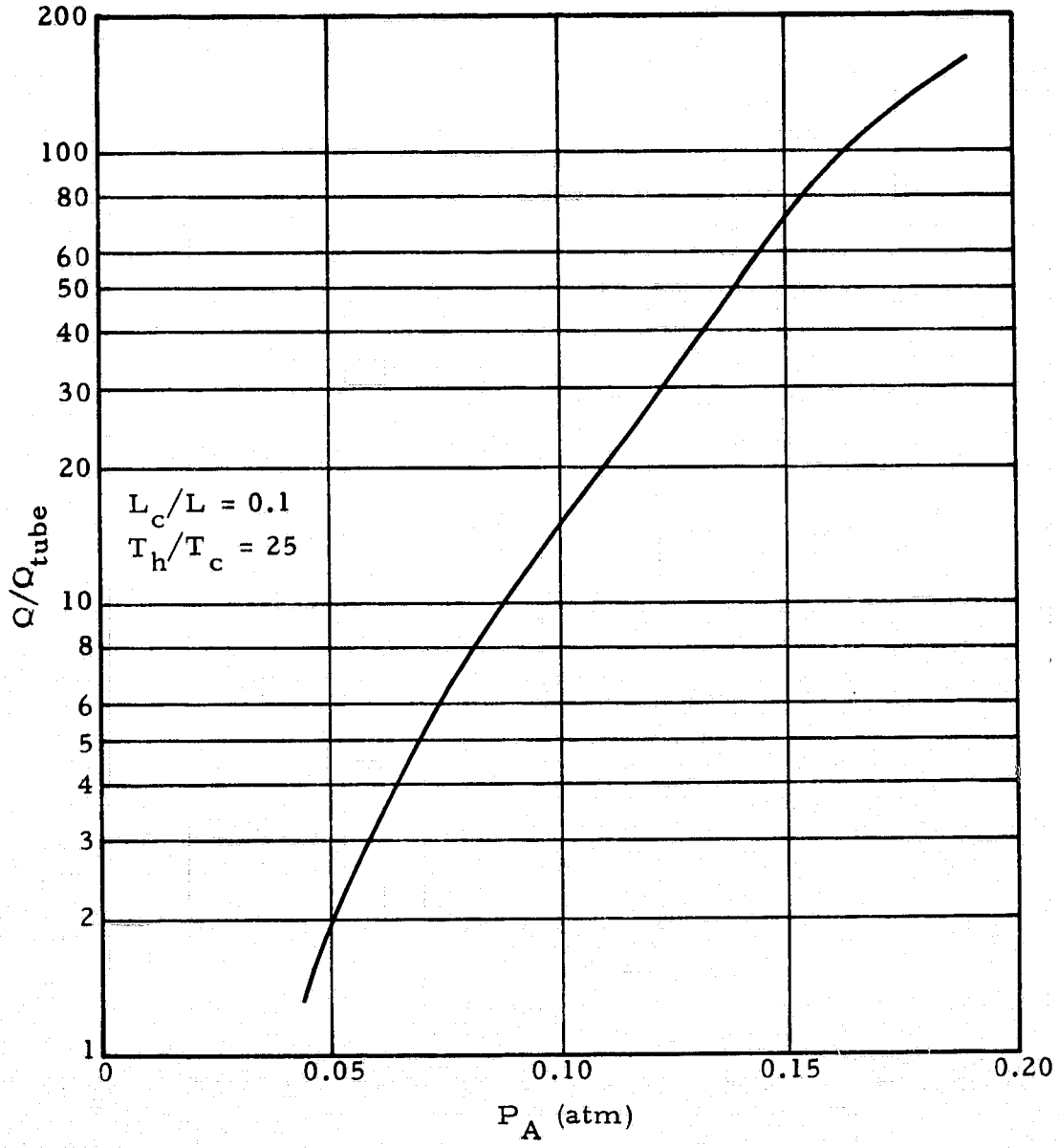

Fig. 19 - Ratio of Total Heat Leak (with Oscillation) to Normal Conduction Heat Leak vs Pressure Amplitude

factors were found that influence thermal acoustic oscillations. They are:

- L/D — Length to diameter ratio of tube
- T_h/T_c — Ratio of hot end temperature to cold end temperature
- L_c/L — Length of tube exposed to cold environment ratioed to total tube length
- Re — The acoustic Reynolds number of the gas at an average temperature.

In addition, the curves should be useful in analyzing configurations for the possibility of oscillations occurring and of their characteristics.

2.3 EXPERIMENTAL VERIFICATION PROGRAM

The experimental verification program objective was to establish the validity and accuracy of the theoretical predictions of the oscillation frequencies, amplitudes and intensities (frequency times amplitude). The resultant effects of those parameters on the total heat leak to a very low temperature environment such as a liquid helium container was also of importance during this portion of the program.

Because of the critical nature of the measurement of the frequency and amplitude of the occurring oscillations, a precision instrument which had been calibrated using secondary standards was used. A description of the characteristics of this instrument, a Piezotron dynamic pressure transducer manufactured by Sunstrand Data Control, Inc., is included in the following subsection.

2.3.1 Description of Test Hardware

Shown in Figure 20 is a schematic of the test arrangement for the measurement of the frequency and amplitude of the oscillations which occur in the tubes.

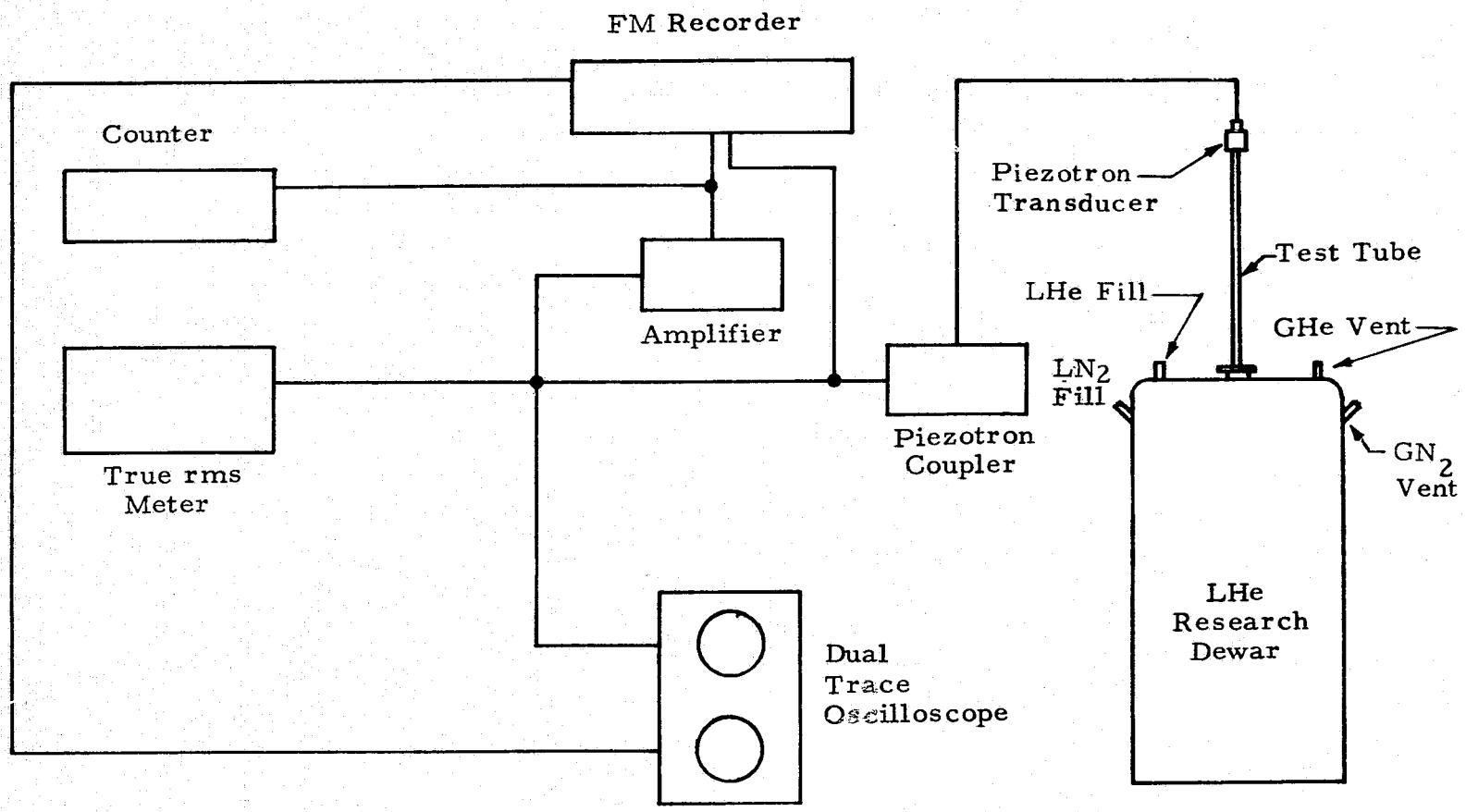

Fig. 20 - Schematic of TAO Test Hardware

The most critical component of the test system was the Kistler Model 206 "Piezotron" pressure transducer supplied by Sundstrand Data Control, Inc. This transducer is a dynamic pressure sensor with a high sensitivity; nominally in the 1400 to 1800 mV/kg/cm^2 range (100 to 125 mV/psi). Prior to using the transducers, calibrations were performed by Sundstrand using traceable secondary standards for the following parameters:

- Pressure Range — 5.62 kg/cm^2
- Resolution — 5.62 x 10^{-5} kg/cm^2
- Sensitivity — 1715 mV/kg/cm^2
- Linearity — $\pm$ 1% full scale
- Rise Time — 3 μsec
- Low Frequency Time Constant — 2.5 sec
- Full Scale Output Voltage — 8.0 V
- Low Frequency Response — 0.05 Hz
- High Frequency Response — 20 kHz

For optimum operation of the Piezotron pressure transducer in this program, Sundstrand recommended the use of a modified ballistic mount. A schematic of this mounting system is shown in Figure 21. The clearance shown in Figure 21 around the base of the transducer, and the entrance section from the tube opening to the sensing face of the transducer are the critical points of this mount. The clearance around the circumference of the transducer is 0.015 cm and the opening to the diaphragm is 0.225 cm diameter x 0.225 cm deep. This mount design minimized pressure transducer volume and satisfied the basic criteria of TAO testing that the volume of the pressure measurement system should not represent a significant part of the total volume of the tube being tested. The total vacant volume of the transducer mount system was only 0.0459 cm^3 (0.0028 in^3) whereas the minimum volume tube tested was 8.47 cm^3 (0.517 in^3). The transducer mount volume represented a maximum of only about 0.5% of the total. The reason that this volume must be very small is to prevent the possibility of this

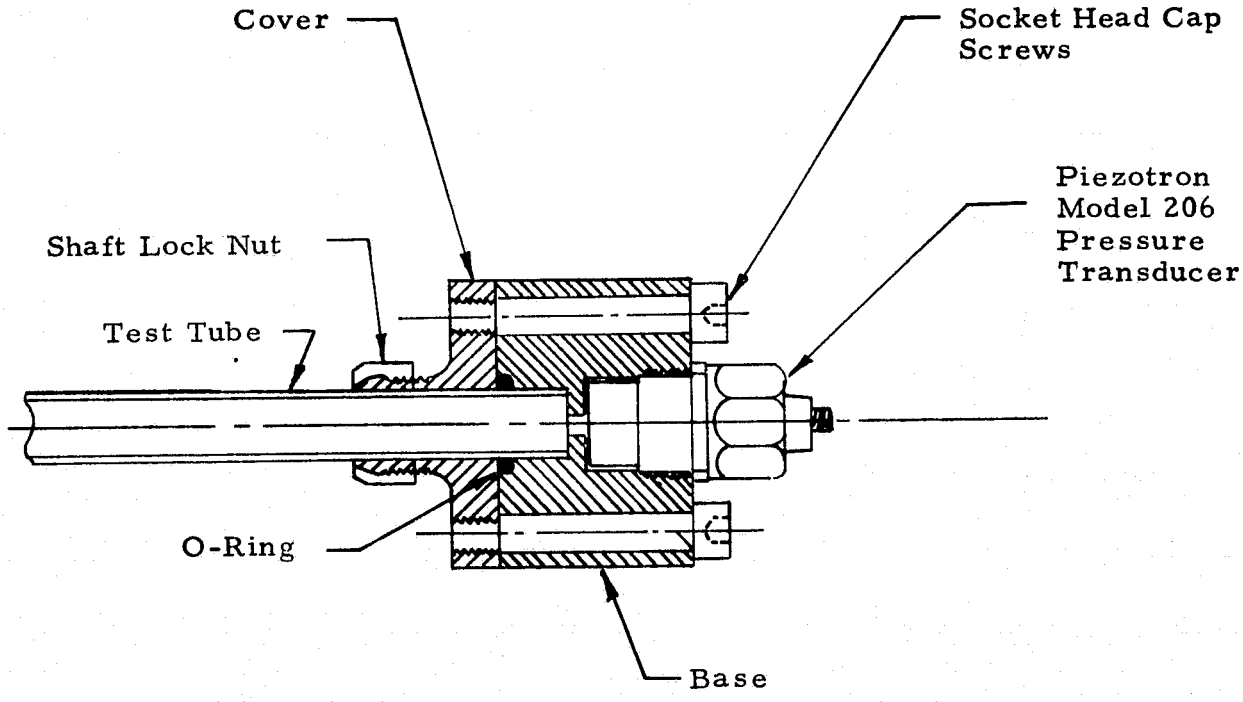

Fig. 21 - Schematic of Modified Ballistic Mount for Piezotron Model 206 Pressure Transducer

"extra" volume acting as a Helmholtz resonator with characteristics that could dampen the oscillations. The literature reviewed early in the program indicated that a tuned Helmholtz resonator could effectively stop all oscillations. This condition was undesirable for these tests.

A schematic of the research dewar used for these tests is shown in Figure 22. The LHe dewar was procured from Cryogenic Associates, Inc. The boiloff loss of LHe under conditions of no external heat sources (tube, liquid level detector, lead wires, etc.) is 0.27 liters/hr and LN_2 loss of 0.15 liters/hr. The dewar, with the neckplug installed, had a LHe capacity of 28 liters. The dewar was filled from commercial 100 liter dewars of LHe through a standard vacuum jacket helium transfer line.

The lower half of the internal (LHe) compartment of the dewar was constructed of aluminum with the upper half being made of low conductivity phenolic. The bi-material section was joined with an epoxy-type material rated for LHe temperature.

The LHe dewar used was designed for minimum no-load boiloff rates. This characteristic permitted accurate measurement of the thermal acoustic oscillations effects since the total heating rate was primarily caused by thermal acoustic oscillations. The boil-off due to conduction only (no oscillations present) was small in most cases. The oscillations were started by lowering the tube further into the dewar until oscillations would occur. Following the oscillation frequency and amplitude measurement tests, the dewar static loss of LHe was far in excess of the rated 0.27 liters/hour. Cryogenic Associates personnel were consulted and concluded that permeation of GHe through the inner tank wall to the vacuum jacket increased the pressure in the superinsulation and decreased the insulation characteristics of this system. Consequently the original test dewar was no longer used in the program and additional heat leak measurements were conducted using a commercial LHe dewar. This approach limited these measurements to one tube o.d. size (0.953 cm or 0.375 in.), but both aluminum and stainless steel

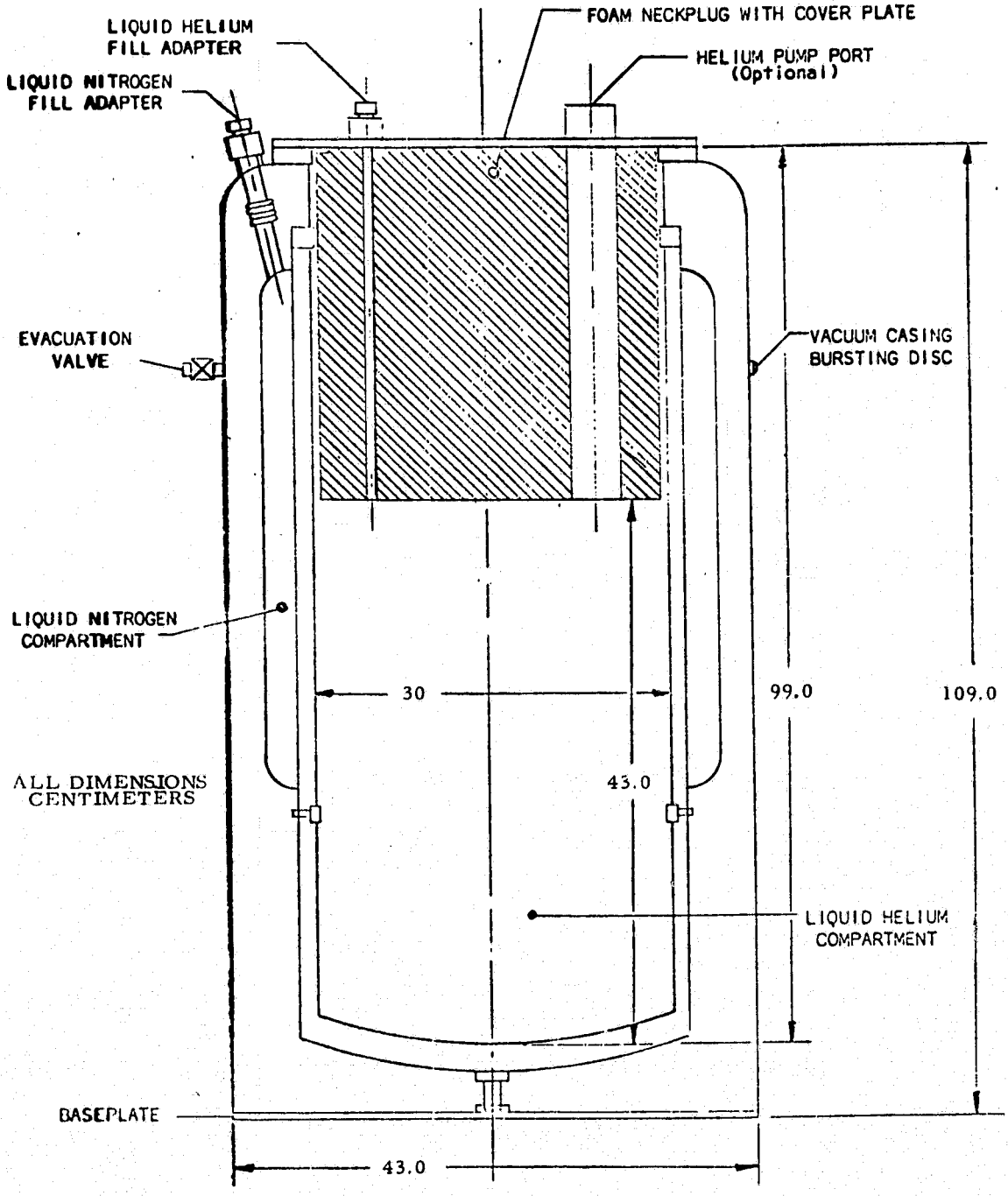

Fig. 22 - Research LHe Dewar

tubes were tested for this effect. This will be discussed later in more detail in section 2.5.

In reviewing the schematic of the test hardward in Fig. 20, the signal from the Piezotron couples (with a gain ratio of 10:1) was connected to several components. They include: (1) one trace input of a dual trace oscilloscope; (2) a McIntosh audio amplifier which was calibrated for a 10:1 gain on the signal; (3) a true rms meter; and (4) an Ampex FM recorder. From the McIntosh amplifier, the signal was input into: (1) a second channel of the FM recorder, and (2) a frequency meter, or counter. The output signal from the FM recorder was input to the second trace of the dual trace oscilloscope. Although the dual trace oscilloscope appears on the schematic as two separate traces, in reality this unit was a single cathode ray tube (CRT) unit with dual trace capability. This allowed an overlay of the signals being obtained from both the unamplified source (Piezotron coupler) and the amplified source being input to the recorder. The recorder had a playback capability on the record mode (with a time lag in terms of milliseconds). By adjusting the "sync" feature of the oscilloscope and maintaining a 10:1 ratio on the scales of the two traces, the two signals could be overlayed on the CRT with extreme accuracy. These signals were for monitoring purposes and were never used for data acquisition.

All data for reduction purposes were obtained from the counter (frequency meter) and the true rms meter. The counter required a signal input of 10 mV to trigger it, which required that this signal be input from the McIntosh amplifier. This meant that the minimum raw data signal which could trigger the counter was only one millivolt, thus allowing an oscillation indication to be detected on this meter prior to being able to view it on the oscilloscope. This additional capability allowed both lower signal detection and higher accuracy level than using the oscilloscope alone.

Although, as mentioned earlier, the counter used in the system required at 10 mV input to trigger the unit, the 1 mV signal level fed to the McIntosh

amplifier was actually so low that the intensity of the oscillations at this level are of almost no consequence. The reason for ensuring that signal levels this low were detected was to enable the investigators to determine more accurately the time of initiation of the oscillations. This capability proved to be of benefit when variations from the previously documented results of Bannister were observed, such as: (1) oscillations occurring at distances of the open end of the tube greater than 15 cm above the liquid level, and (2) amplitudes of the oscillations being a relatively strong function of this distance while the frequency was weakly dependent. The latter (frequency and amplitude dependence on distance above liquid level) was not anticipated from early theoretical prediction.

The tubes tested during this program are shown in Table 1. As indicated, both stainless steel (type 304 CRES) and aluminum (6061-T6) were tested. Only stainless steel was tested for the length-to-diameter ratio of 1000 since for this case no conditions were predicted to exist for oscillations to occur from the analytical results. All tubes tested were seamless units. This type tubing has smooth interior surfaces and are generally more concentric than rolled tubes.

2.3.2 Experimental Results

The results of the experimental program showed that variations in the primary parameters not readily apparent from previous documentation were present in these tests. These include a distance from the liquid level dependence of both frequency and amplitude of the thermally driven oscillations. The frequency dependence was weak compared to the amplitude dependence. A 10 to 20% variation of frequency was typical, while a variation in excess of 100% of the minimum amplitude was not unusual.

The ratio of total tube heat leak to conduction heat leak is obviously dependent upon the conduction heat leak, which is a function of the tube length, cross section area and length between hot and cold temperature

Table 1

TUBES TESTED FOR THERMAL ACOUSTIC OSCILLATIONS

Inside Diameter (cm)	Wall Thickness (cm)	Outside Diameter (cm)	Length (cm)	L/I.D. —
Stainless Steel (Type 304 CRES)				
0.221	0.048	0.317	221	1000
0.658	0.147	0.952	197	300
0.658	0.147	0.952	99	150
0.658	0.147	0.952	66	100
Aluminum (6061-T6)				
0.658	0.147	0.952	132	200
0.658	0.147	0.952	99	150
0.658	0.147	0.952	66	100

boundaries. The net heat leak caused by the oscillations were of comparible magnitude when comparing the stainless steel and aluminum 0.952 cm o.d. tubes, but the conduction of heat through the aluminum tube is about an order of magnitude larger than the stainless steel. This was a dominant factor in determining the total heat leak. Both tubes were 0.147 cm wall thickness.

- Oscillation Intensity Measurements

As pointed out in the discussion of the analytical model used for prediction of the oscillation onset criteria, the ratio T_h/T_c is of primary importance in predicting the intensity of the oscillations. For purposes of determining the values of T_h and T_c, a copper constantan thermocouple was used to measure T_h and a temperature-dependent resistor (cryoresistor) was used to determine T_c. The cryoresistor was calibrated by NASA-MSFC prior to testing. The calibration curve for this unit is shown in Fig. 23. Because of the 45.7 cm long neckplug in the research dewar, the actual test set-up appeared as shown in Fig. 24. Since it was desirable that the capability exist to completely remove the tube being tested, the cryoresistor was mounted on the edge of the aluminum guide plate on the bottom of the phenolic mount which held the foam neckplug in place. The value of T_c was thus assumed to be the mean difference between that measured by the cryoresistor and the value for LHe ($4.2^{\circ}K$). The analytical predictions are based on a mean value of the temperature of that portion of the tube exposed to the GHe environment. The measured T_h was taken at the mid-point of the portion of the tube exposed to ambient conditions. This temperature measurement was made with a copper-constantan thermocouple soldered to an adjustable clamp which forced the thermocouple bead onto the tube surface. Except for those cases where the temperature of the exposed part of the tube was intentionally heated or cooled, the typical measurement was within a few degrees of ambient at all times. This would indicate that even in the oscillatory mode, the gas interchange was not modifying the temperature of the gas in the tube enough to overcome the conduction to the gas from the tube.

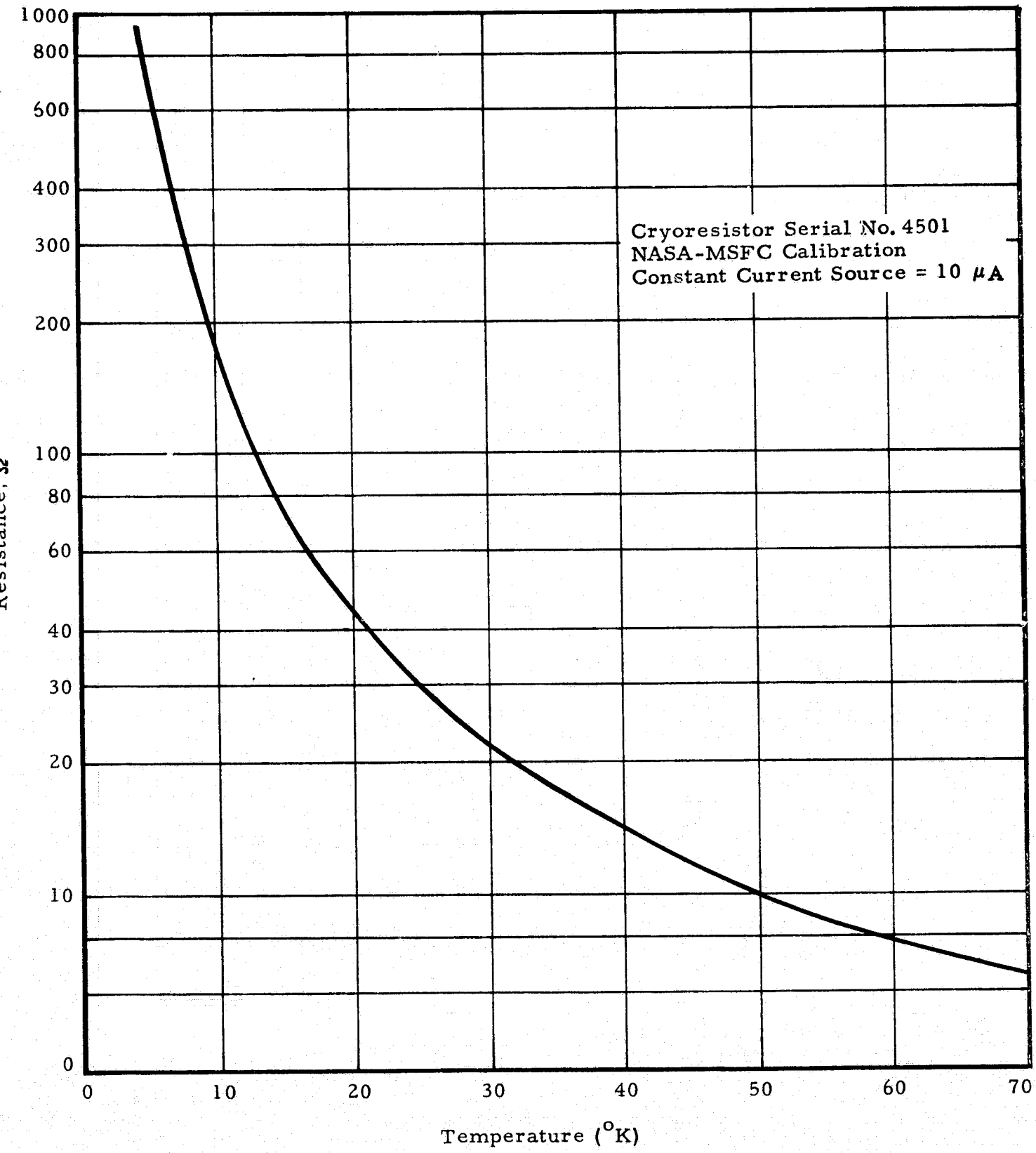

Fig. 23 - Calibration Curve of Resistance vs Temperature for Cryoresistor

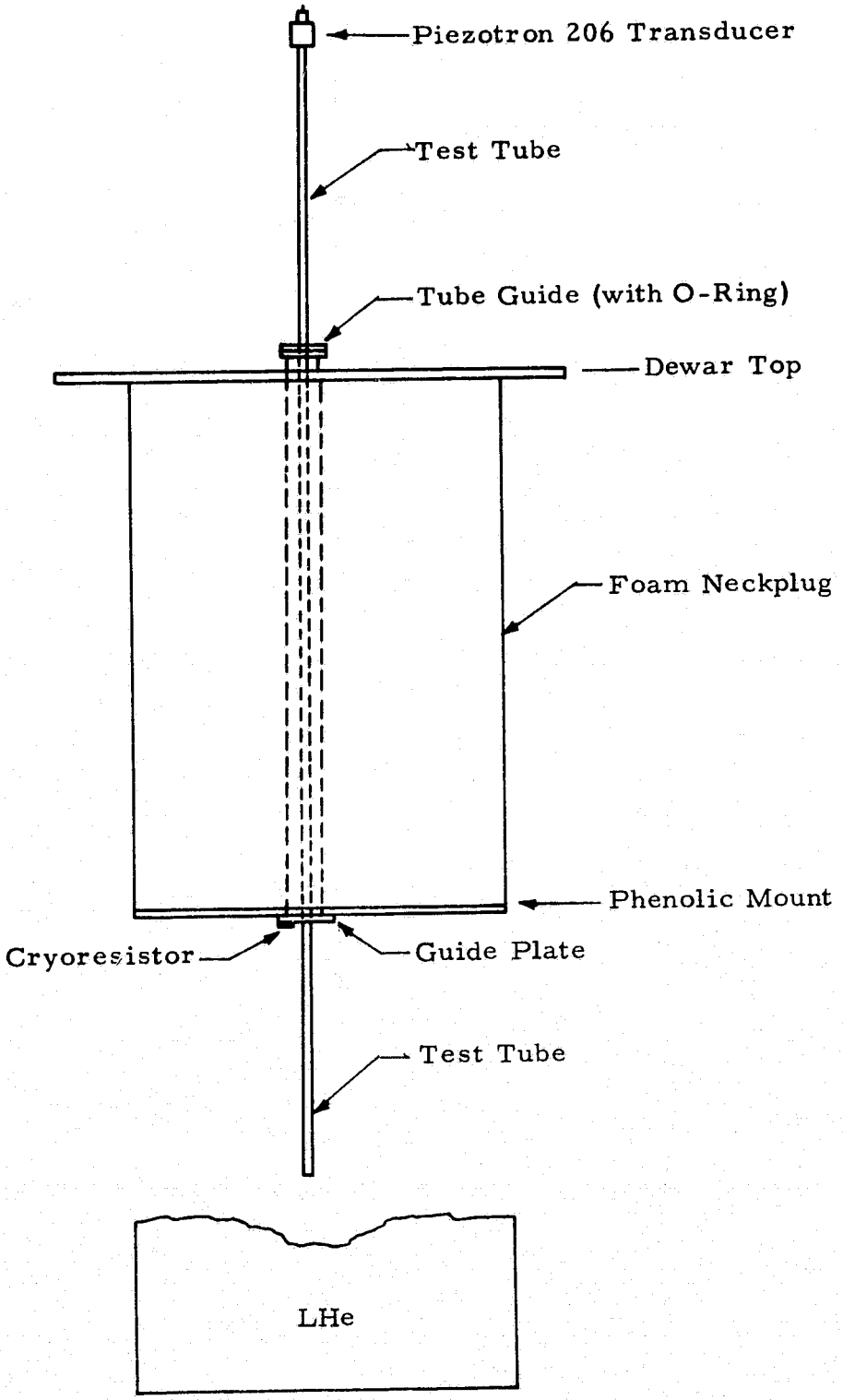

Fig. 24 - Schematic of Test Tube/Foam Plug Configuration

Results of the oscillation intensity tests are shown in Tables 2a through 2h. These tabulated results are shown in Fig. 25 as a function of the L_c/L parameter. In this case, as in the analytical predictions, L_c is that portion of the tube actually extending into the helium cavity below the neckplug and L is the total tube length. The forms of the curves faired through the experimental data in Fig. 25 do not tend toward any apparent systematic variation either as a function of L_c/L or the tube material. These type results were not unexpected. The strong frequency and amplitude dependencies as a function of ullage volume, distance below the neckplug and distance above the LHe surface cannot be explained at this time.

For example, examination of Table 2h reveals an interesting and unexplained phenomenon. During the initial portion of testing, the intensity is seen to increase by a factor of 3 as the L_c/L ratio is increased from 0 to 0.154. While retaining the tube at the $L_c/L = 0.154$ position (15.2 cm), the Piezotron transducer was removed to allow venting of gaseous helium through the tube. During the process there was no insulation to retain the tube in the cold condition. Also during the venting process the oscillations were initially audible while standing several meters away. As the tube cooled, the oscillations diminished in amplitude until they were no longer audible and a continuous stream of very cold vapor could be seen being emitted from the tube. While oscillating in the audible range the pulses of cold gas were discrete and visible. When the transducer mount was replaced on the tube, the oscillations stopped. None were expected at this low T_h/T_c ratio. When the average temperature of the exposed portion of the tube approached ambient conditions, oscillations were expected to be self-initiated. This never occurred. Attempts to force the oscillations to start by using both external heat (to raise the T_h/T_c ratio) and mechanical perturbations were unsuccessful.

At this point the quantity of liquid helium had dropped to approximately 12 liters which corresponds to about 44% of the dewar capacity. In one of J.D. Bannister's studies, he had indicated there were times when his experiment dewar had to be approximately 75% full (the total capacity is unknown)

Table 2a

OSCILLATION INTENSITY TEST RESULTS

Material	=	304 CRES stainless steel
L/D	=	1000
Inside Diameter	=	0.221 cm
Wall Thickness	=	0.048 cm

L_c (cm)	T_c (^oK)	T_h (^oK)	f (Hz)	amp (kg/cm^2)	I ($Hz\text{-}kg/cm^2$)
0.0	13.6	294	No oscillations		
2.5	13.6	294	No oscillations		
5.1	13.6	293	No oscillations		
7.6	13.6	293	No oscillations		
12.7	13.6	290	No oscillations		
Attempts to thermally or mechanically induce oscillations unsuccessful.					
Following data after ~ 4 hours equilibrium					
0	13.6	297	No oscillations		
15.2	13.6	297	No oscillations		
10.2	13.6	297	No oscillations		
12.7	13.6	296	No oscillations		
22.8*	13.6	290	18	0.0208	0.364

*Open end immersed in liquid.

L_c = length of tube exposed to helium reservoir

T_c = temperature at bottom of neckplug

T_h = temperature at mid-point of exposed tube

f = frequency of oscillations

amp = peak-to-peak value of pressure oscillations

I = intensity of oscillations (f x amp)

Table 2b

OSCILLATION INTENSITY TEST RESULTS

Material = 304 CRES stainless steel
L/D = 300
i. d. = 0.658 cm
Wall Thickness = 0.147 cm

L_c (cm)	T_c (^oK)	T_h (^oK)	f (Hz)	amp (kg/cm^2)	I (Hz - kg/cm^2)
0	13.6	296	30	.0784	2.35
Elapsed time ~ 1 hour 45 minutes					
0	13.6	296	29	.0861	2.50
7.62	13.6	296	26	.1177	3.06
15.2	13.6	298	25	.202	5.05
25.4	13.6	298	23	.269	6.18
30.5	13.6	298	21	.291	6.12
40.6*	13.6	298	10	.255	2.55
33.0	13.6	297	21	.291	6.12
15.2	13.6	297	25	.179	4.46

*Open end immersed in liquid.

L_c = length of tube exposed to helium reservoir
T_c = temperature at bottom of neckplug
T_h = temperature at mid-point of exposed tube
f = frequency of oscillations
amp = peak-to-peak value of pressure oscillations
I = intensity of oscillations (f x amp)

Table 2c

OSCILLATION INTENSITY TEST RESULTS

Material = 304 CRES stainless steel
L/D = 150
i.d. = 0.658 cm
Wall Thickness = 0.147 cm

L_c (cm)	T_c (^oK)	T_h (^oK)	f (Hz)	amp (kg/cm^2)	I ($Hz\text{-}kg/cm^2$)
0	13.6	296	43	0.1028	4.42
5.1	13.6	296	38	.1310	4.98
10.2	13.6	297	35	.1608	5.62
15.2	13.6	297	33	.1690	5.58
20.3	13.6	297	31	.1773	5.50
25.4	13.6	296	30	.1392	4.18
30.5*	13.6	296	23	.0268	0.62
15.2	13.6	298	35	.184	6.44
15.2	13.6	284	35	.177	6.21

*Open end immersed in liquid.

L_c = length of tube exposed to helium reservoir
T_c = temperature at bottom of neckplug
T_h = temperature at mid-point of exposed tube
f = frequency of oscillations
amp = peak-to-peak value of pressure oscillations
I = intensity of oscillations (f x amp)

Table 2d

OSCILLATION INTENSITY TEST RESULTS

Material = 6061-T6 aluminum
L/D = 200
i. d. = 0.658 cm
Wall Thickness = 0.147 cm

L_c (cm)	T_c (^oK)	T_h (^oK)	f (Hz)	amp (kg/cm^2)	I ($Hz\text{-}kg/cm^2$)
0	13.6	294	45	.0646	2.91
0	13.6	292	42	.0703	2.95
0	13.6	292	40	.0762	3.05
5.1	13.6	291	36	.1292	4.66
5.1	13.6	291	36	.1292	4.66
10.2	13.6	289	33	.2022	6.68
15.2	13.6	288	30	.1857	5.57
15.2	13.6	287	30	.1857	5.57
20.3	13.6	287	28	.1841	5.16
25.4*	13.6	290	16	.1011	1.62
25.4*	13.6	288	16	.0962	1.54
5.1	13.6	288	36	.1659	5.97
5.1	13.6	288	35	.1728	6.05

*Open end immersed in liquid

L_c = length of tube exposed to helium reservoir
T_c = temperature at bottom of neckplug
T_h = temperature at mid-point of exposed tube
f = frequency of oscillations
amp = peak-to-peak value of pressure oscillations
I = intensity of oscillations (f x amp)

Table 2e

OSCILLATION INTENSITY TEST RESULTS

Material = 6061-T6 aluminum
L/D = 150
i. d. = 0.658 cm
Wall Thickness = 0.147 cm

L_c (cm)	T_c (^oK)	T_h (^oK)	f (Hz)	amp (kg/cm^2)	I ($Hz\text{-}kg/cm^2$)
0	13.6	285	57	.0568	3.24
2.5	13.6	288	53	.0599	3.18
2.5	13.6	287	52	.0564	2.93
7.6	13.6	287	45	.1112	5.00
7.6	13.6	284	43	.1299	5.59
12.7	13.6	280	38	.1891	7.19
17.8	13.6	278	35	.2086	7.31
17.8	13.6	281	35	.2077	7.27
22.8*	13.6	278	29	.0398	1.15

*Open end immersed in liquid

L_c = length of tube exposed to helium reservoir
T_c = temperature at bottom of neckplug
T_h = temperature at mid-point of exposed tube
f = frequency of oscillations
amp = peak-to-peak value of pressure oscillations
I = intensity of oscillations (f x amp)

Table 2f

OSCILLATION INTENSITY TEST RESULTS

Material = 6061-T6 aluminum
L/D = 100
i. d. = 0.658 cm
Wall Thickness = 0.147 cm

L_c (cm)	T_c (^oK)	T_h (^oK)	f (Hz)	amp (kg/cm^2)	I ($Hz\text{-}kg/cm^2$)
0	13.6	278	61	.0348	2.12
2.5	13.6	294	61	.0340	2.08
5.1	13.6	305	No oscillations		
7.6	13.6	290	No oscillations		

L_c = length of tube exposed to helium reservoir
T_c = temperature at bottom of neckplug
T_h = temperature at mid-point of exposed tube
f = frequency of oscillations
amp = peak-to-peak value of pressure oscillations
I = intensity of oscillations (f x amp)

Table 2g

OSCILLATION INTENSITY TEST RESULTS

Material = 6061-T6 aluminum
L/D = 150
i. d. = 0.658 cm
Wall Thickness = 0.147 cm

L_c (cm)	T_c (^oK)	T_h (^oK)	f (Hz)	amp (kg/cm^2)	I ($Hz \cdot kg/cm^2$)
2.5	13.6	285	49	.0794	3.89
15.2	13.6	280	38	.2004	7.62
15.2	13.6	271	38	.1891	7.19
15.2*	13.6	181	35	.1106	3.87
15.2*	13.6	138	35	.0431	1.51
15.2*	13.6	105	34	.0365	1.24
15.2*	13.6	83	34	.0232	0.79
15.2*	13.6	81	No oscillations		
15.2	13.6	222	37	.1261	4.66
15.2	13.6	261	38	.1602	6.09
15.2	13.6	268	38	.1856	7.05

*External portion of tube chilled with LN_2 using jacket around tube.

L_c = length of tube exposed to helium reservoir
T_c = temperature at bottom of neckplug
T_h = temperature at mid-point of exposed tube
f = frequency of oscillations
amp = peak-to-peak value of pressure oscillations
I = intensity of oscillations (f x amp)

Table 2h

OSCILLATION INTENSITY REST RESULTS

Material = 6061-T6 aluminum
L/D = 150
i. d. = 0.658 cm
Wall Thickness = 0.147 cm

L_c (cm)	T_c (^oK)	T_h (^oK)	f (Hz)	amp (kg/cm^2)	I (Hz-kg/cm^2)
0.0	13.6	289	52	.0544	2.83
0.0	13.6	286	50	.0629	3.14
7.6	13.6	286	42	.1468	6.16
15.2	13.6	280	37	.2022	7.49
15.2	13.6	275	37	.1940	7.18
GHe vented through tube prior to following readings					
15.2	13.6	181	No Oscillations		
15.2	13.6	211	No Oscillations		
15.2	13.6	238	No Oscillations		
15.2	13.6	257	No Oscillations		
15.2	13.6	273	No Oscillations		
15.2	13.6	278	No Oscillations		
Refilled dewar with LHe prior to following readings					
0.0	13.6	292	59	.0332	1.96
0.0	13.6	288	57	.0357	2.04
0.0	13.6	284	56	.0363	2.03
0.0	13.6	284	55	.0370	2.03
15.2	13.6	283	38	.1458	5.54
Elapsed time = 50 minutes					
15.2	13.6	279	38	.1360	5.17
Elapsed time = 110 minutes					
15.2	13.6	279	38	.1458	5.54
Elapsed time = 165 minutes					
15.2	13.6	279	38	.1524	5.80
Elapsed time = 190 minutes					
15.2	13.6	279	37	.1584	5.86
Elapsed time = 230 minutes					
15.2	13.6	279	37	.1690	6.25
Elapsed time = 280 minutes					
15.2	13.6	278	36	.1740	6.26

L_c = length of tube exposed to helium reservoir
T_c = temperature at bottom of neck plug
T_h = temperature at mid-point of exposed tube
f = frequency of oscillations
amp = peak-to-peak value of pressure oscillations
I = intensity of oscillations (f x amp)

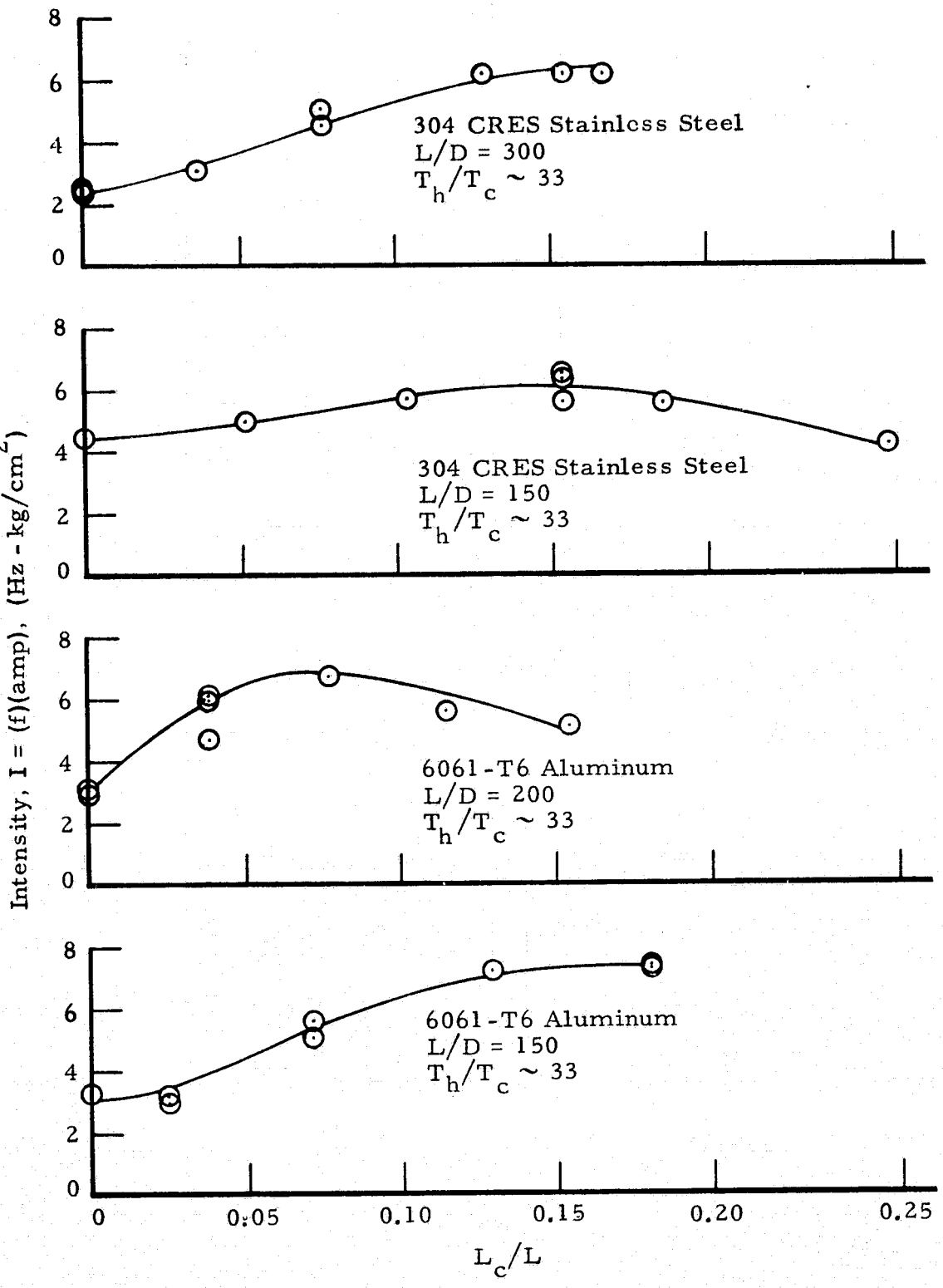

Fig. 25 - Experimental Measurements of Oscillation Intensity as a Function of L_c/L

in order to obtain oscillations. To see if this was a possible "tuned volume" effect where a minimum ullage volume is required to have the oscillations exist, liquid helium was added until the 75% full condition was attained. During the refill process the oscillations were self initiated. The dewar then contained approximately 40% more LHe than when the initial values shown in Table 2h were measured (75% full versus 52%). There is a maximum difference of 39% in the intensity between the last data point prior to venting the helium and the data point identified as occurring 50 minutes following the refill process.

Following the refill, an attempt was made to confirmed this "tuned volume" postulated by allowing the oscillations to continue until the liquid level dropped below that when the GHe was vented. When the conditions existed where no oscillations could be forced to occur, the liquid level was at the 44% full point. Following an elapsed time of 4 hours 40 minutes, the liquid level had dropped to 38%, the oscillations were still occurring, and had not reached the maximum value obtained earlier in terms of amplitude (and thus intensity). This occurrence neither proved nor disproved the ullage volume effect as being a damping device. The only conclusion which could be reached from this test was that the variables involved in the initiation and sustaining of the oscillations is still not clearly understood and that they are not repeatable to the point where one can duplicate the conditions and obtain exactly the same data consistently.

The variation in intensity shown in Table 2h over the 280 minute period contains an unexplained variation. The values of L_c, T_c, T_h and frequency are essentially constant during the entire period while the pressure amplitude is increasing and the liquid level dropping. The phenomenon of an increasing intensity for an increasing distance between the open end of the tube and the liquid level is exactly opposite of what is found in other cases of changing the separation distance by moving the tube as observed by Bannister (Ref. 14). The difference in these results must be a case of the changing L_c value being an overriding function. The analytical model developed for this study does not include this distance function.

- Boiloff Rate Measurements

As was discussed earlier, the research dewar used for the portion of the tests in which measurement of the oscillation frequencies and amplitudes were made could not be used for the measurement of the increased boiloff rates caused by the oscillations. The static loss of LHe in the research dewar was in excess of the value which could be measured with a flowmeter calibrated to 6000 sccm. The calibration curve for the flowmeter used is shown in Figure 26.

The test hardware was arranged to permit use of the commercial dewars in which the LHe was received. These dewars will accept a standard 0.953 cm (3/8 in.) o.d. tube. The liquid access valve allowed a vertical insertion of the tube in the same way used on the research dewar. The dewar vent valve routed the boiloff to the flowrate measurement system. A schematic of this portion of the total system is shown in Fig. 27. The pressure oscillation frequency and amplitudes were measured and monitored in the same manner as described in the previous section.

Prior to inserting one of the test tubes in the helium dewar the internal pressure was released and the dewar allowed to thermally equilibrate during an over-night period. Although the dewars are pressurized only about 20% above atmospheric, the sensible heat stored at this pressure would have affected the test results. The tests also would have been impossible to run at this pressure level for the test arrangement as shown in Fig. 27 since there was no pressure control device used in the system.

Following the equilibration period, the test tube was inserted in the liquid withdrawal opening on the commercial dewar. This is a valved fitting made to accept a standard 0.952 cm LHe transfer tube. With the compression O-ring fitting which is common on these dewars the tube

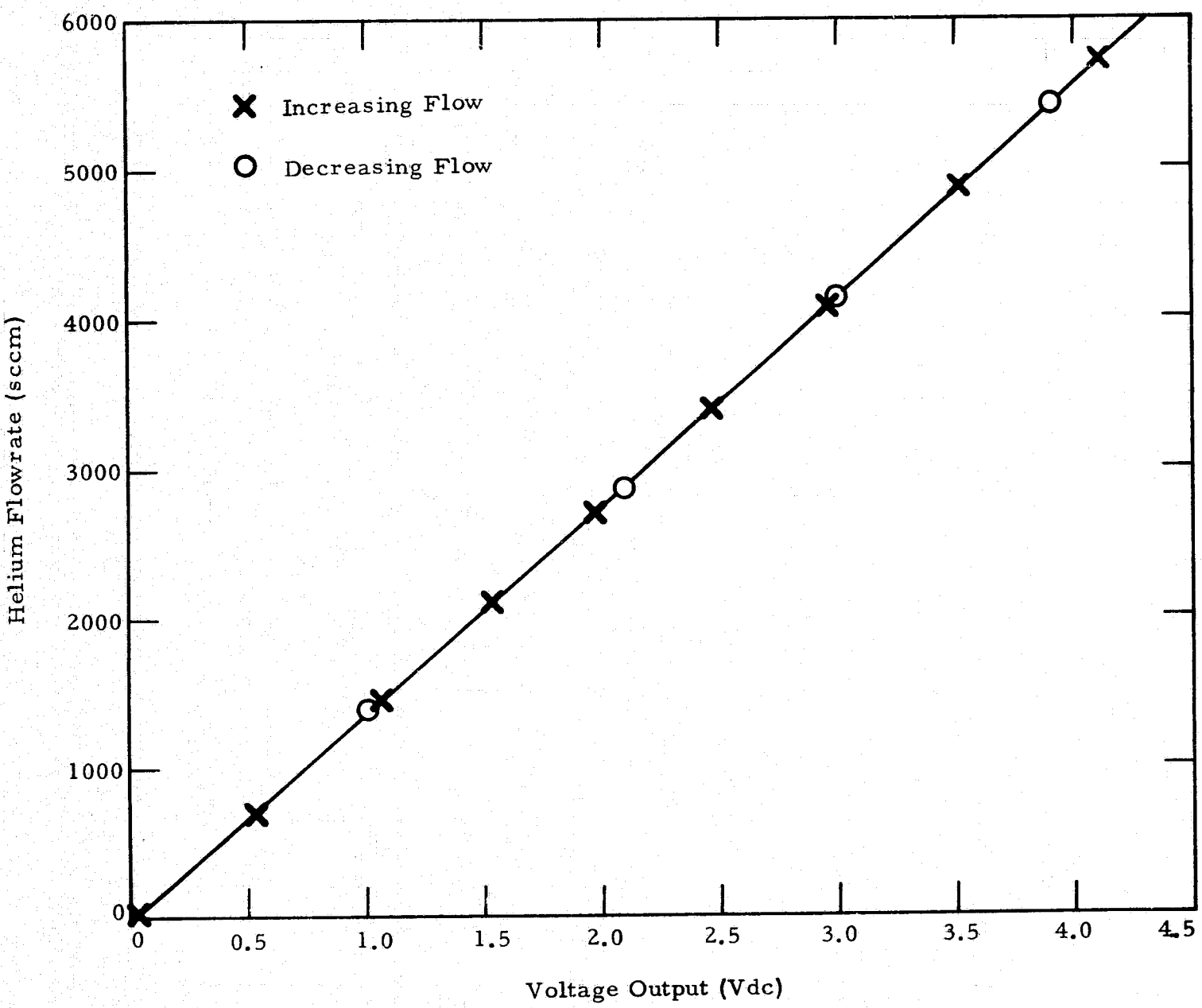

Fig. 26 - Calibration Curve for Hastings-Raydist Flowmeter Used for Measurement of Boiloff Rates

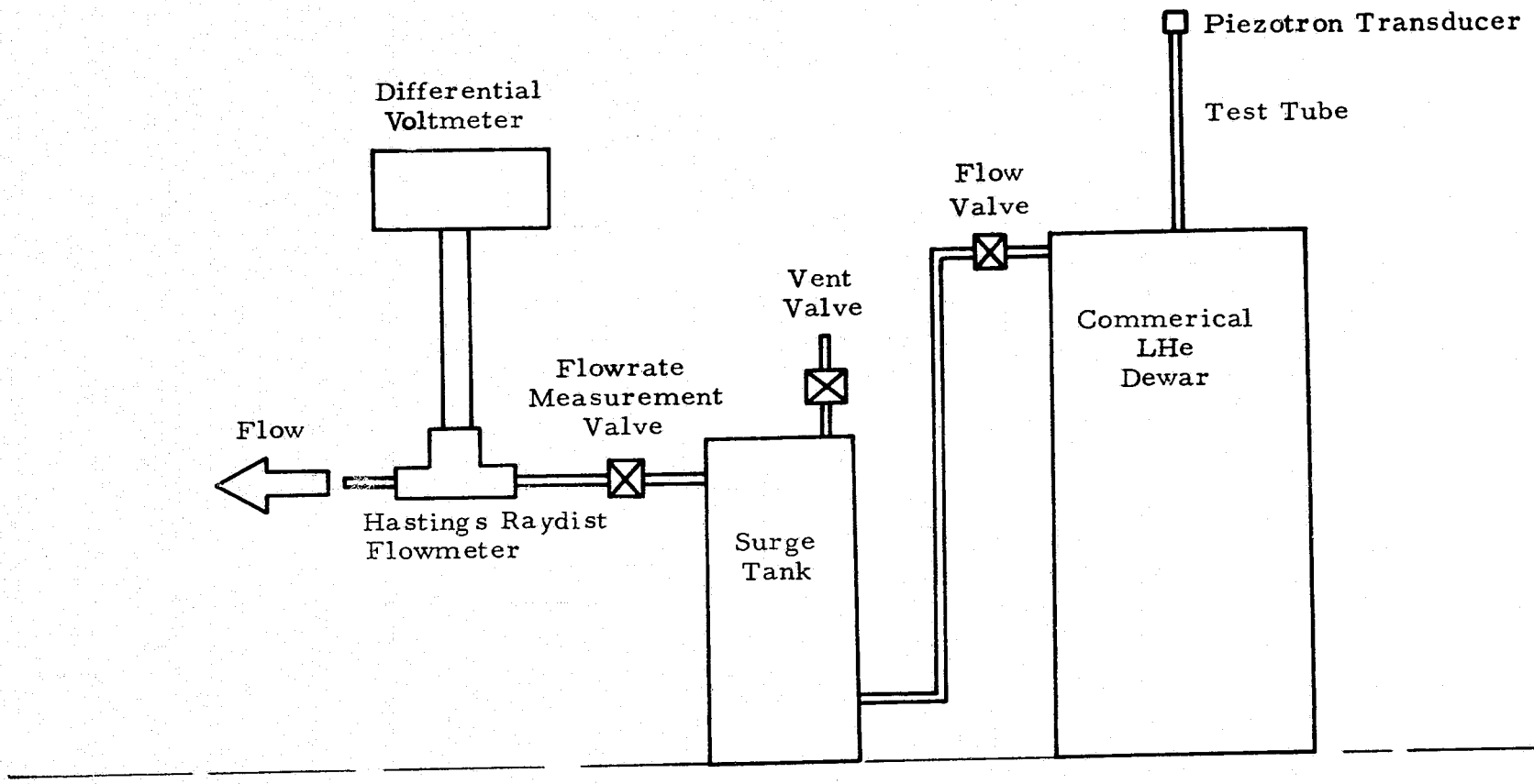

Fig. 27 - Schematic of Flow System for Measuring Boiloff Due to Oscillations

could be inserted any distance desired and held in place by tightening this fitting by hand. The entire system was allowed to equilibrate with the tube inserted the maximum distance possible without oscillations occurring. After equilibrium had been reached (usually another over-night period) the boiloff due to the conductive heat leak in addition to the static loss was measured. Since the static loss had previously been measured, the difference between these two measurements was the net heat leak due to conduction down the tube and into the helium cavity. The results of these measurements are tabulated in Tables 3a and 3b. The tests were conducted using two different commercial dewars which resulted in two different static loss measurements.

Probably the most significant finding which can be seen from these two tables is that the maximum net boiloff rates for both the stainless steel and aluminum tubes are essentially the same. However, the conduction portion of the total for the aluminum tube is between one and two orders of magnitude greater than the stainless steel tube. Because of this, the ratio of the heat transferred with and without oscillations for the aluminum tube was never in excess of 1.5 while that for the stainless steel tube approached a factor of 100.

In previous investigations where extremely large (approaching 1000) heat transfer ratios were projected, the results were based on extremely thin wall tubes. These tube wall thicknesses were generally an order of magnitude less than the ones used during these tests. The tubes used in the present tests, however, were more representative of flight type units.

From the results of these measurements, the test results would indicate that the net heat transfer to the liquid cryogen is probably a heat transfer difference rather than a straightforward ratio of the conduction term and oscillation-plus-conduction terms. This logic is based on the

Table 3a

TEST DATA OF OSCILLATION INTENSITY EFFECT ON HEAT TRANSFER FOR STAINLESS STEEL TUBE

L_h (cm)	L_c (cm)	f (Hz)	amp (kg/cm^2)	I ($Hz\text{-}kg/cm^2$)	Net Boiloff (sccm)	$\frac{Q_{tot,\ osc}}{Q_{tube,\ cond}}$
83.9	63.3	0	0	0	35	0
68.6	78.6	24	.0102	0.244	73	2.08
63.5	83.7	21	.0162	0.340	89	2.54
55.9	91.3	18	.0213	0.384	104	2.97
50.8	96.4	14	.1651	2.312	3076	87.9
50.8	96.4	14	.1535	2.148	2936	83.8
50.8	96.4	14	.1371	1.920	2256	64.4
50.8	96.4	14	.1304	1.827	1924	55.0
78.7	68.5	42	.0261	1.096	385	11.0
73.6	73.6	39	.0529	2.062	706	20.2

0.658 cm i.d. Type 304 CRES Stainless Steel Tube

L/D = 225

Static Boiloff Rate of LHe Dewar = 129 sccm

Static Boiloff with Tube/No Oscillations = 164 sccm

Table 3b

TEST DATA OF OSCILLATION INTENSITY EFFECT ON HEAT TRANSFER FOR ALUMINUM TUBE

L_h (cm)	L_c (cm)	f (Hz)	amp (kg/cm^2)	I ($Hz\text{-}kg/cm^2$)	Net Boiloff (sccm)	$\frac{Q_{tot,\ osc}}{Q_{tube,\ cond}}$
61.0	71.1	0	0	0	2315	0
47.6	84.5	29	.0206	.597	2585	1.117
40.7	91.4	21	.0677	1.422	2770	1.197
30.5	101.6	17	.1040	1.768	3225	1.394
30.5	101.6	17	.0894	1.520	3125	1.352
30.5	101.6	17	.0793	1.349	3025	1.308
15.2	116.9	17	.0462	.785	2405	1.040
30.5	101.6	18	.0711	1.280	2515	1.087
40.7	91.4	21	.0676	1.420	2545	1.102

0.658 cm i.d., Type 6061-T6 Aluminum Tube

L/D = 200

Static Boiloff Rate of LHe Dewar = 455 sccm

Static Boiloff with Tube/No Oscillations = 2770 sccm

fact that although the intensities of the oscillations for the stainless steel and aluminum tubes were of comparable magnitude, the ratio of Q/Q_t (heat transfer with conduction and oscillations/heat transfer due to conduction only) were between one and two orders of magnitude different, with the higher conductivity aluminum tube displaying a much smaller heat transfer ratio. Regardless of this ratio being much smaller, the net heat leaks (for the combined conduction and oscillation contribution) were very nearly the same value.

2.4 ANALYTICAL COMPARISONS WITH PREVIOUS INVESTIGATIONS

This subsection presents a comparison of Lockheed's analytical calculations with theoretical and experimental results reported in the literature. The purpose of the comparisons is to:

- Provide a validity check on the TAO computer program
- Substantiate the model assumptions
- Gain further insight into the mechanisms producing the oscillations, and
- Illustrate the potential influence of the oscillations on cryogenic storage vessels.

Comparison of the analytical calculations with results of previous investigations must be made with caution. The overall complexity of the TAO problem, the assumptions made in analytical models, and the inherent differences in experimental programs can lead to invalid comparisons. The present analytical calculations are compared with results of two previous studies: the theoretical analysis of Rott (Ref. 21), and the experimental data of Bannister (Ref. 14).

Figure 28 is a comparison of the stability diagram for helium (Fig. 13) with results presented by Rott (Ref. 21). Rott's calculations are based on a second order linear theory and the present calculations use a full nonlinear numerical method approach. The agreement for some ranges

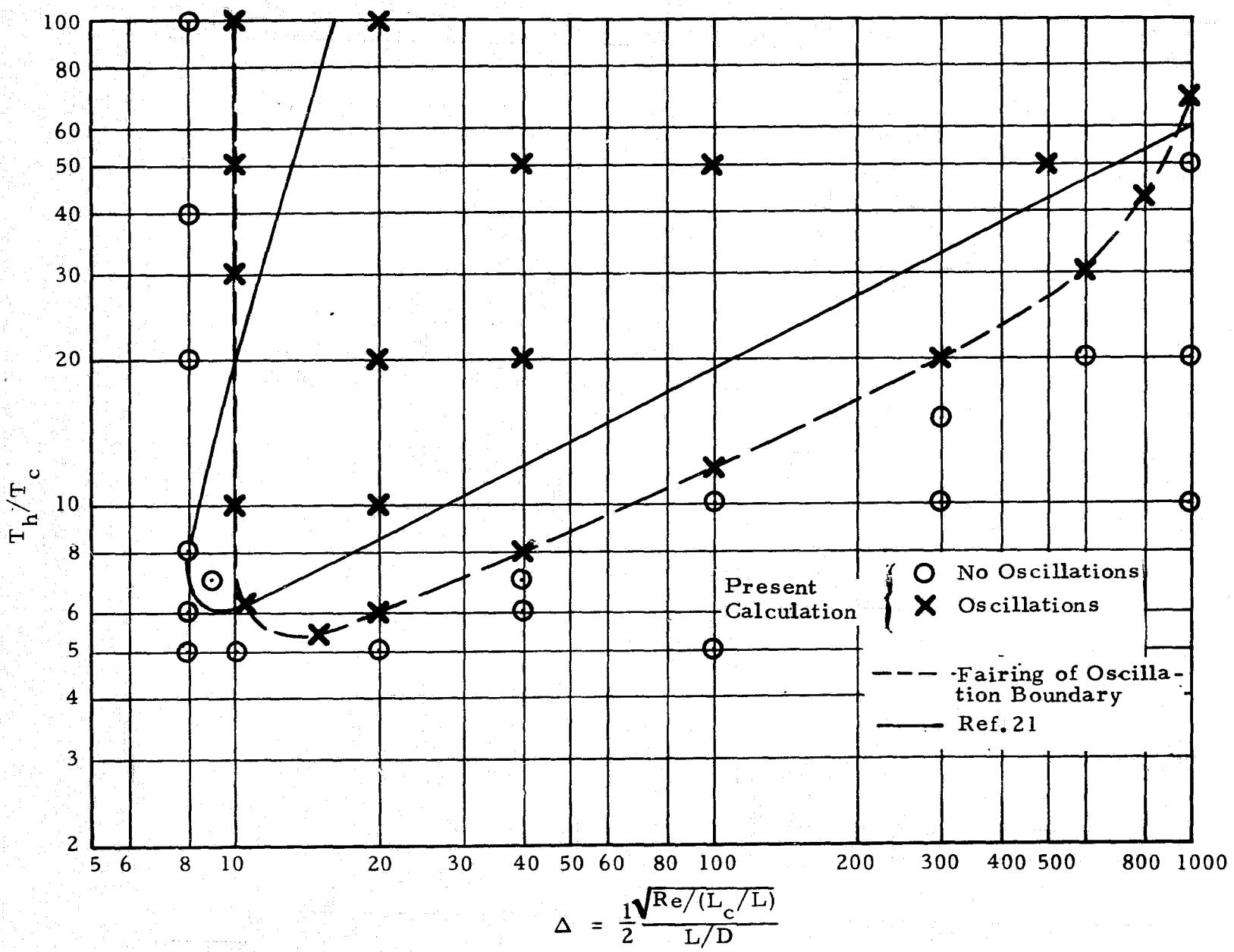

Fig. 28 - Comparison of Present Analytical Calculations with Theory of Rott (Ref. 21) for Helium Stability Diagram

of the parameters T_h/T_c and Δ, is good, but the shape of the curve is different for low values of Δ. Rott's curve bends back for $\Delta \sim 10$ at large T_h/T_c while the present analysis shows a straight line. Also the range of T_h/T_c which can produce oscillations is larger than Rott's predictions for larger values of Δ. It is difficult to determine which shape is most nearly correct. Rott's linear theory may be invalid for some ranges of the Δ parameter, but the current analysis may also be borderline for large L/D ratios (small Δ values). Large L/D ratios, in practice, probably occur due to small diameter tubes. The assumption of viscous Navier-Stokes flow in very narrow tubes is questionable. However, the general agreement between the two predictions does tend to validate the range of parameters where oscillations can be expected. To use the curves the following procedure should be followed. (1) the T_h should be calculated using room temperature where a relative large amount of tube is exposed to ambient conditions; otherwise T_h is best chosen as 290°K. (2) T_c should be chosen as an average of LHe temperature and 13°K. (3) L_c/L should be calculated using the actual length of tube exposed to cold environment. (4) Acoustic Reynolds number should be based on the acoustic velocity, density and viscosity of the gas at an average temperature between T_c and T_h and the length L of the tube. (5) The L/D should be determined from the total tube length and the inside diameter.

Figure 29 compares pressure amplitudes vs L/D with experimental data of Bannister (Ref. 14). These data were not taken with experimental conditions similar to those of the present study. However, a qualitative comparison should be useful for illustration. The present analysis prediction of P_A is shown for $L_c/L = 0.01$ and $T_h/T_c = 25$. The data points of Bannister correspond to different reported test cases. It is not clear from Bannister's paper exactly what each test case consisted of, or what L_c/L and T_h/T_c ratios were used. LMSC's present calculations are all higher than the data he reports. Private communications with Bannister have indicated that his amplitude data may be somewhat low due to experimental problems. LMSC's calculations also indicate that this may be true. The quantitative difference between the LMSC calculations and the previously reported experimental measurements is of the order of 50%.

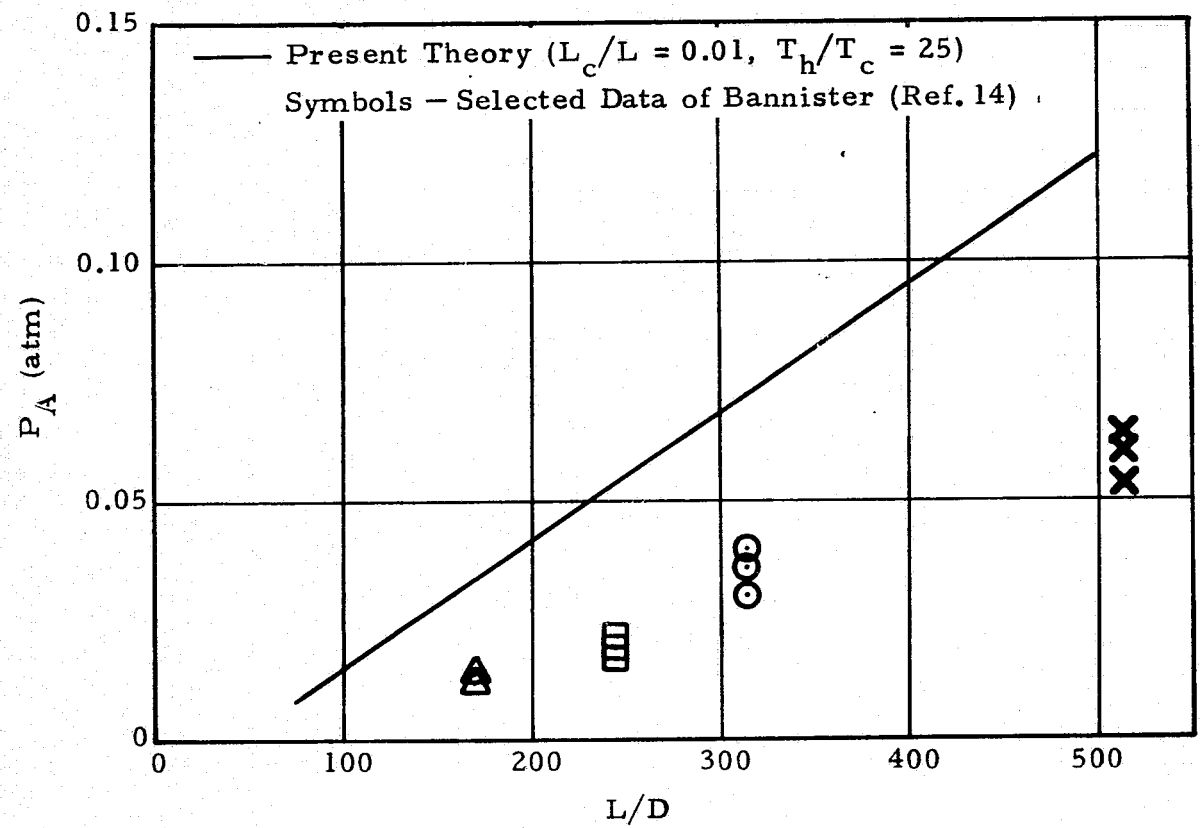

Fig. 29 - Comparison of Pressure Amplitude with Data of Bannister (Ref. 14)

Bannister presents his heat transfer data as a plot of heat pumping rate versus oscillation intensity. These data were replotted as Q/Q_t versus L/D using the tube material properties corresponding to Bannisters specifications. Comparison with the present predictions is given in Fig. 30. The circles are the various data points reported by Bannister. Again the exact test conditions which produce the spread is not known. The dots and the solid line are the present calculations for a tube with perfectly insulating boundaries. The other symbols are for calculations made with varying amounts of the tube exposed to hot and cold temperatures. The percent hot/cold shown in the legend, i.e., 30% hot, 10% cold, indicates that 30% of the tube is exposed to room temperature, 10% is exposed to the cold temperature, and the middle 60% is insulated. This set of boundary values was used instead of the L_c/L concept in order to more correctly simulate the experimental apparatus.

The difference between the LMSC model and Bannister's experiments is less than 30% for all points. The calculations shown by the solid line are between Bannisters ' data points for the mid-range L/D ratios. The predictions are higher than his data for L/D between 100 and 200 and for L/D of approximately 500. The effect of the "percent exposed" parameters is to increase the Q/Q_t above the solid line predictions which correspond to zero percent and indicates that an insulated tube will transfer less heat due to thermal acoustic oscillations. However, the difference in relative heat transfer is small. The inclusion in the model of the proximity of the tube to the liquid surface can be an important factor in obtaining a more favorable comparison of analytical and experimental heat transfer rates.

2.5 COMPARISON OF LMSC THEORY AND EXPERIMENT

This section presents a comparison of the theoretical predictions and experimental data taken in this study. The comparisons cover three major categories: (1) existence of oscillations; (2) wave characteristics; and (3) effects on net heat leak. The comparisons are given in Figs. 31 through 37 which contain the information shown on the next page of text.

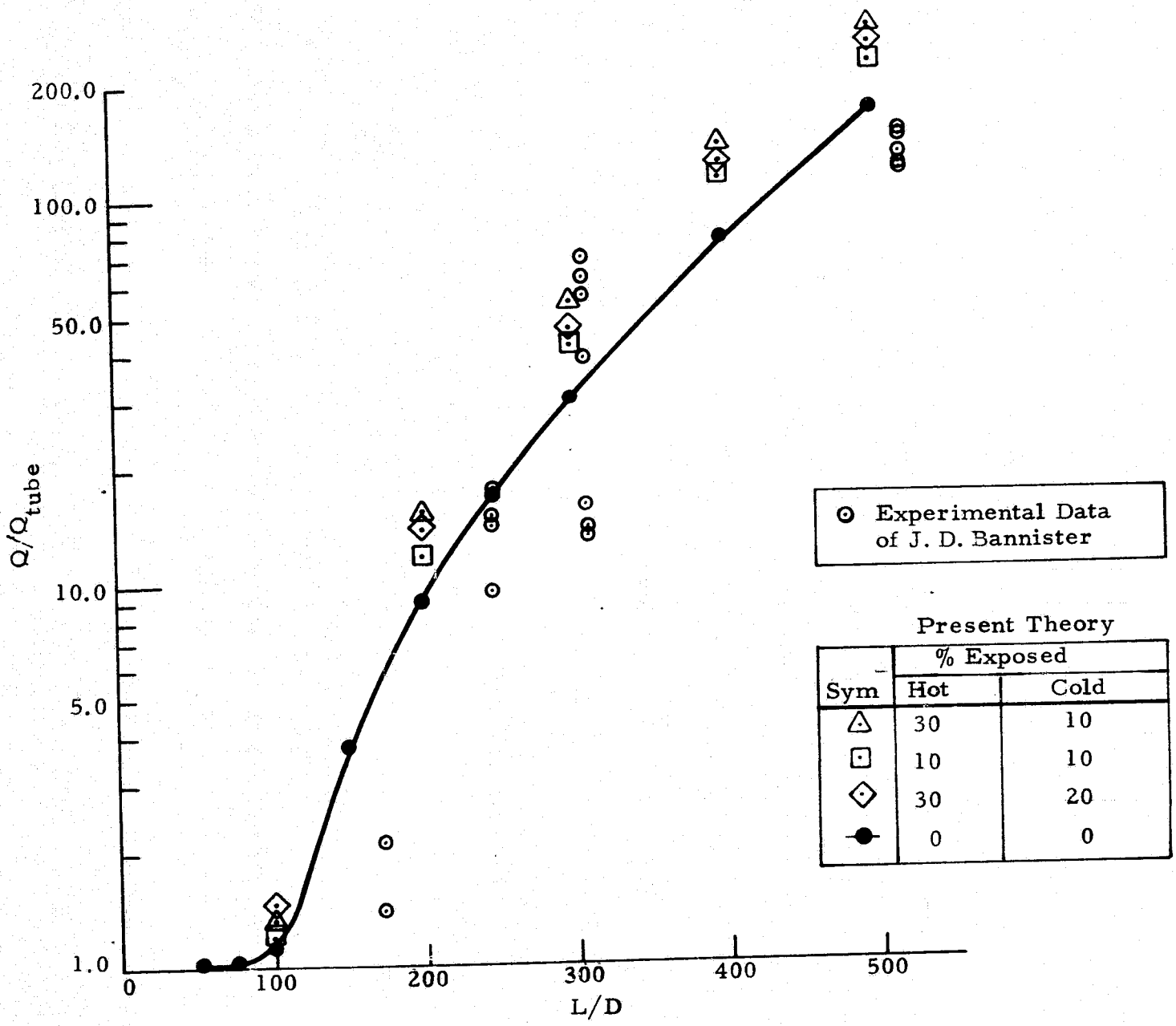

Fig. 30 - Comparison of Present Analytical Calculations with Experimental Data of Bannister (Ref. 14) for Heat Rate vs L/D

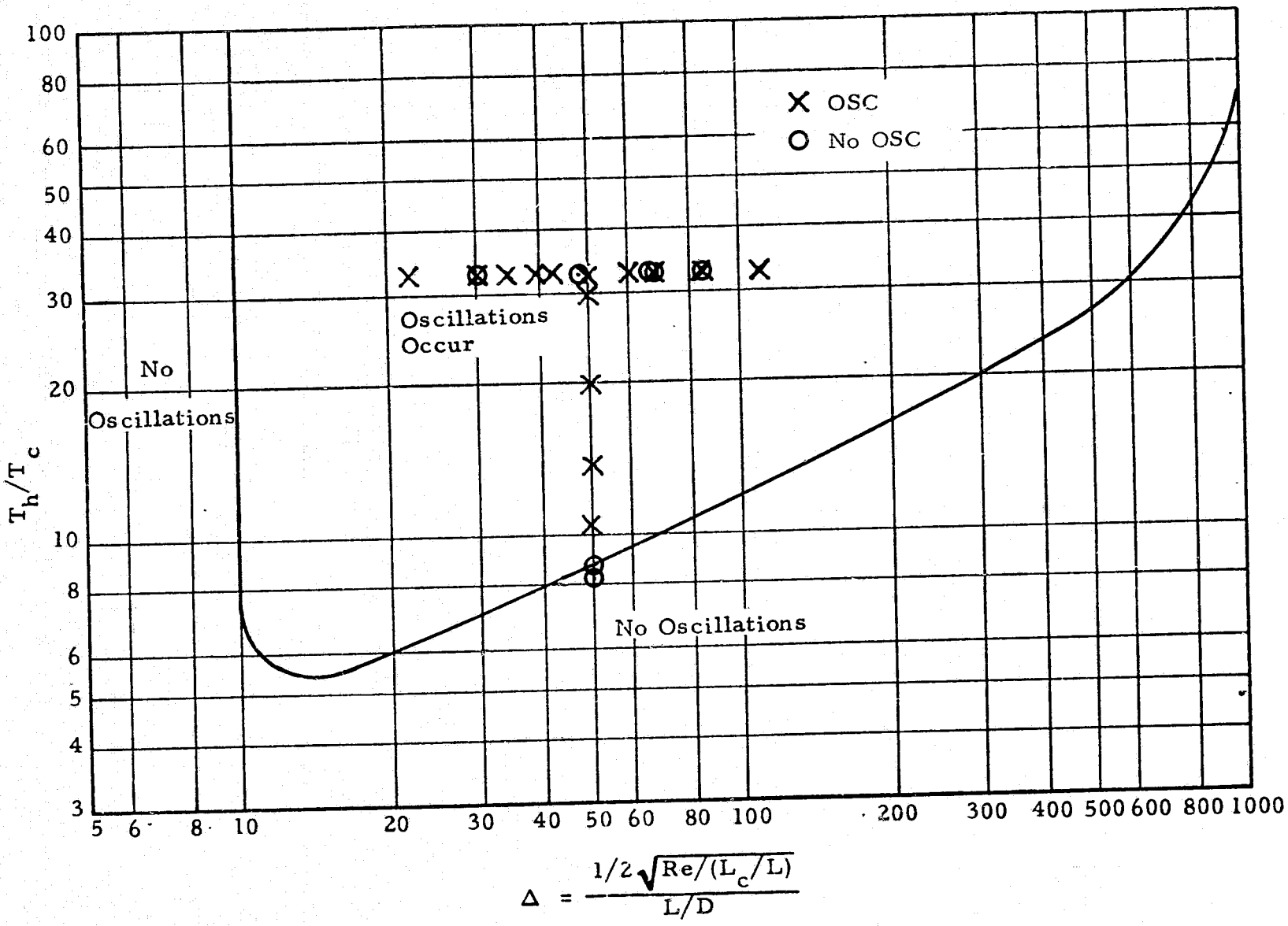

Fig. 31 - Stability Diagram for Helium

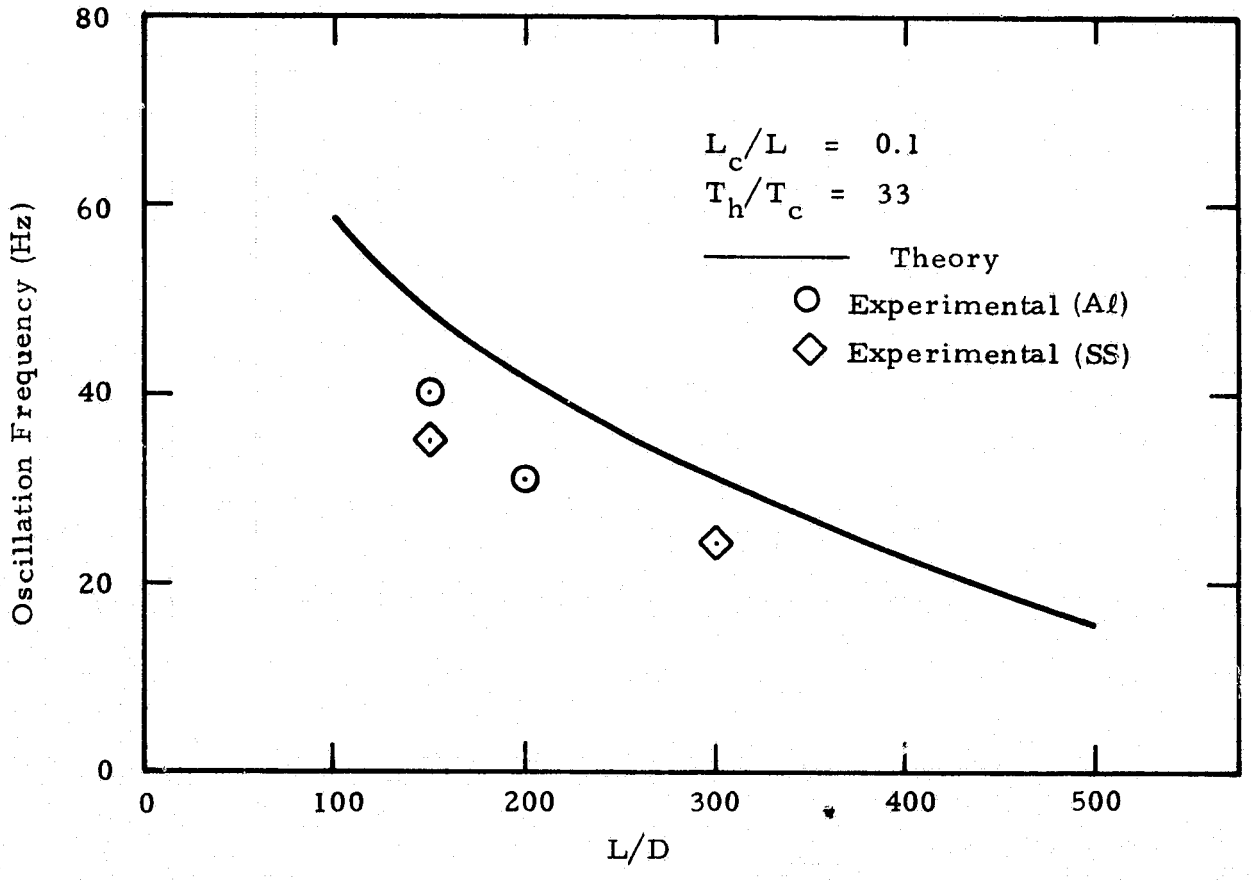

Fig. 32 - Comparison of Analytical and Experimental Oscillation Frequencies as a Function of Tube L/D for Constant L_c/L and T_h/T_c

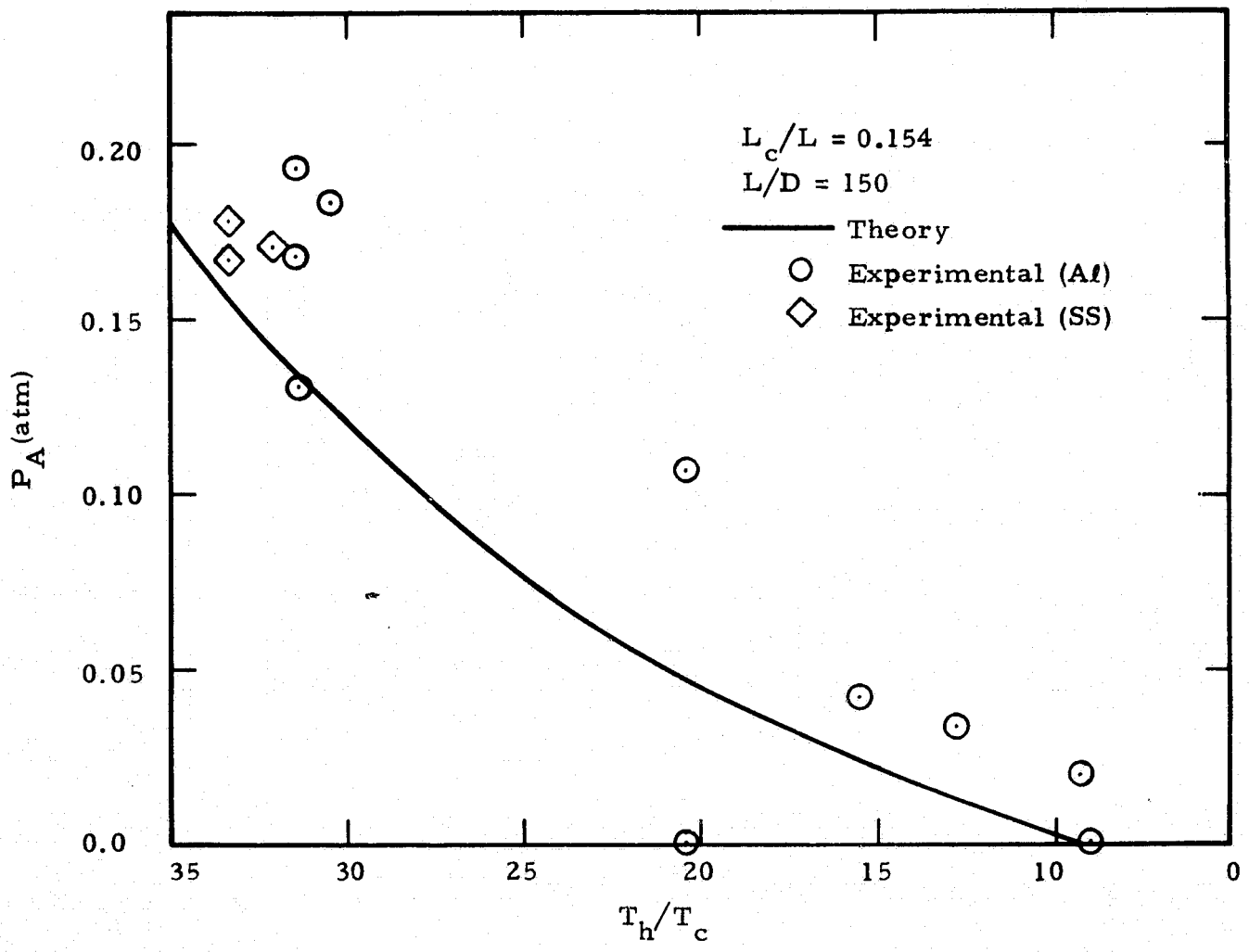

Fig. 33 - Comparison of Analytical and Experimental Peak-to-Peak Pressure Amplitudes for Constant L_c/L and L/D for Parametric T_h/T_c

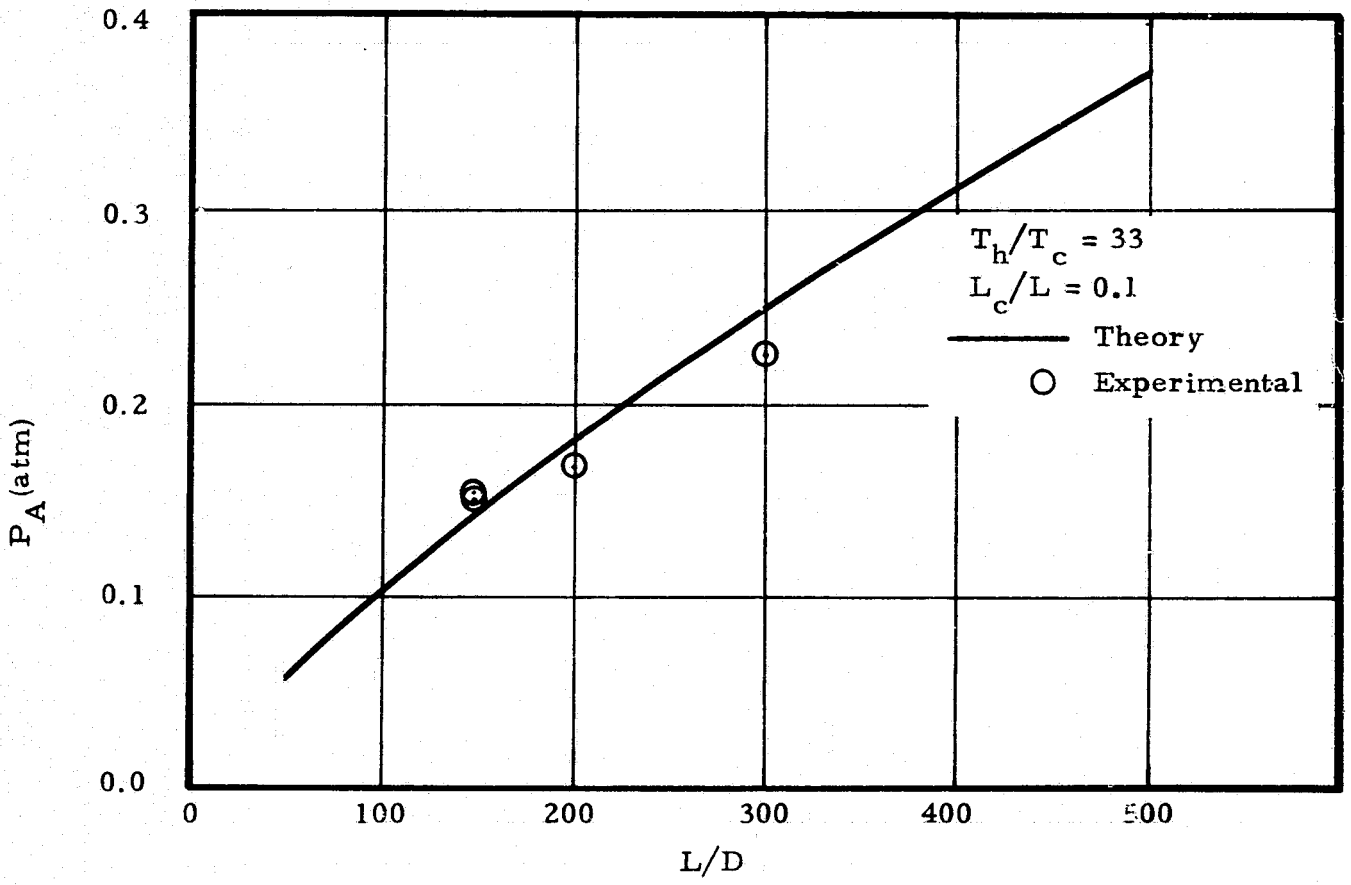

Fig. 34 - Comparison of Analytical and Experimental Peak-to-Peak Pressure Amplitudes for Constant L_c/L and T_h/T_c for Parametric Length/Inside Diameter Ratio

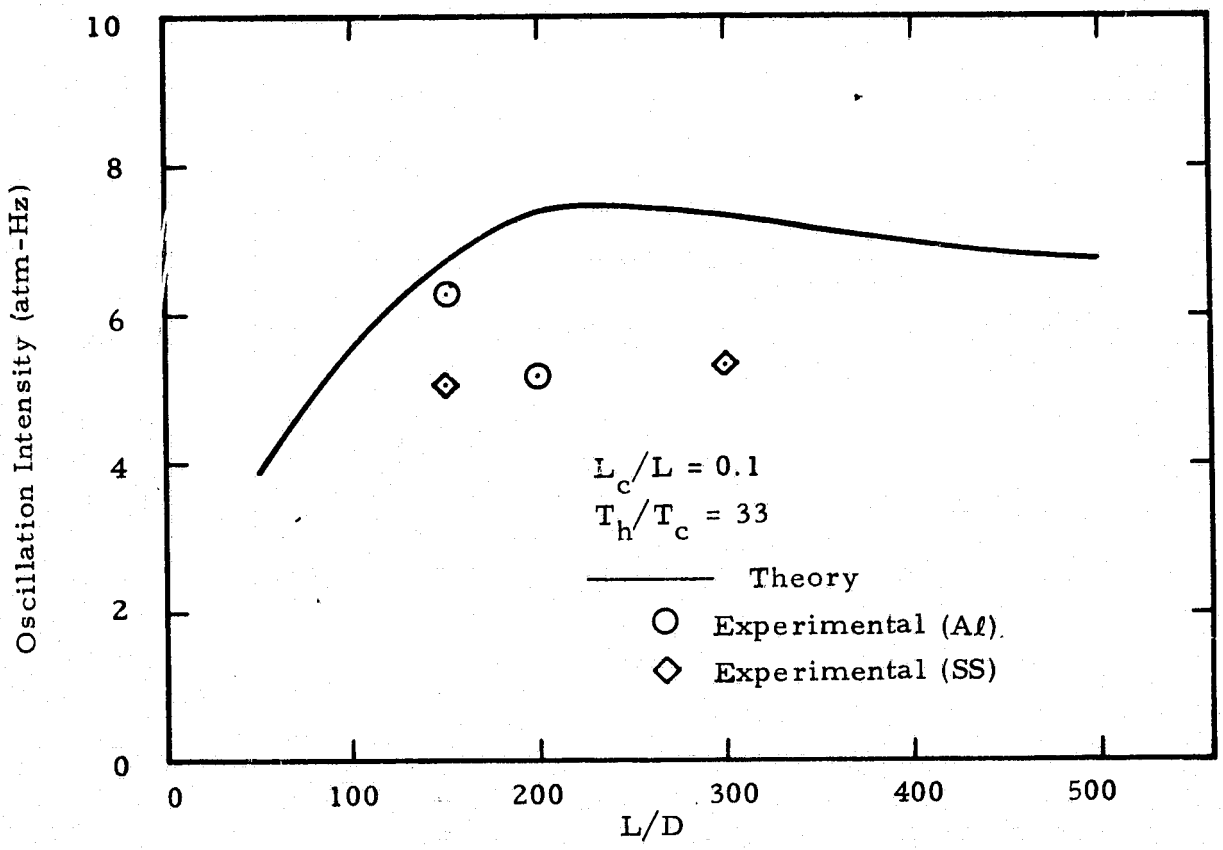

Fig. 35 - Comparison of Analytical and Experimental Oscillation Intensities as a Function of Tube L/D for Constant L_c/L and T_h/T_c

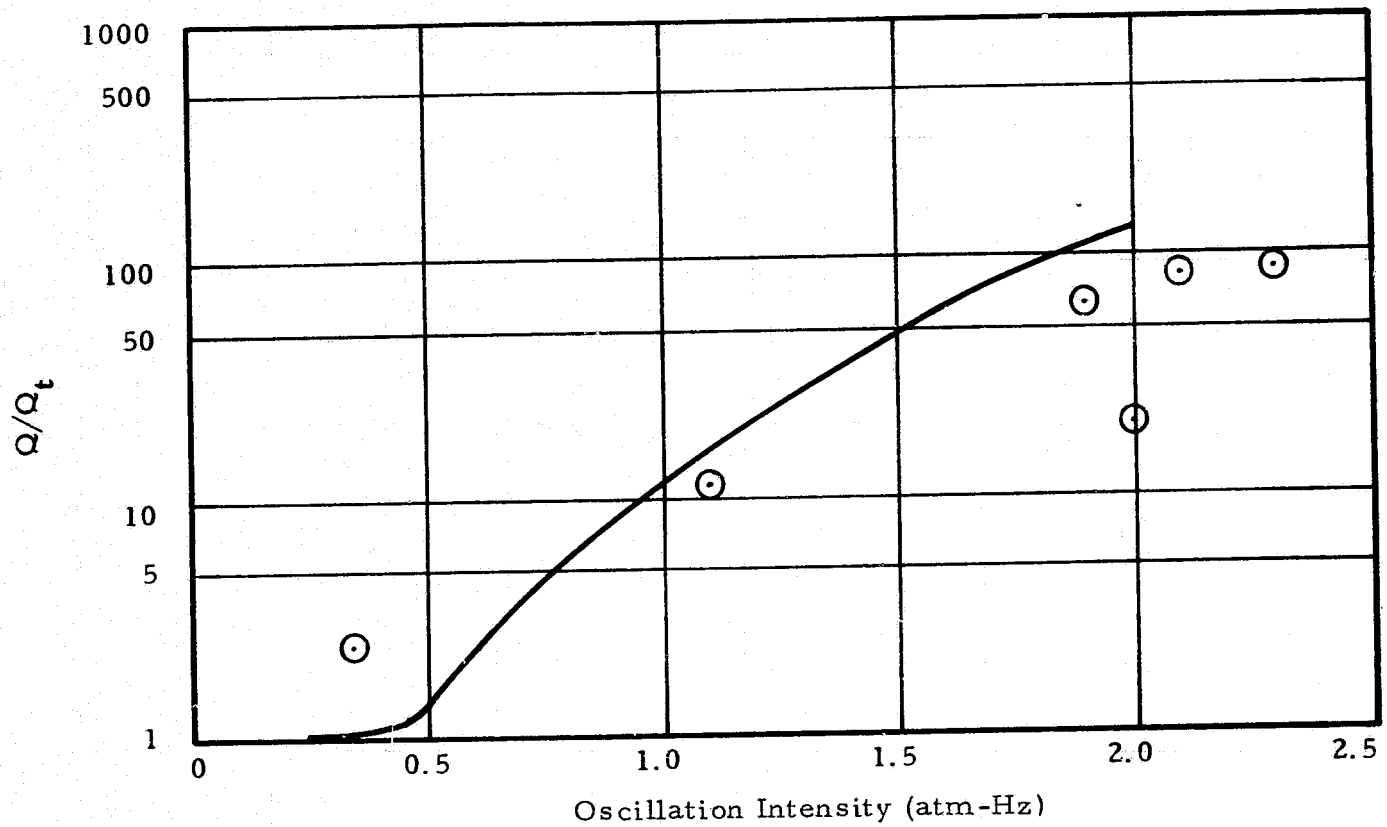

Fig. 36 - Ratio of Total Heat Leak (with Oscillations) to Normal Conduction Heat Leak versus Oscillation Intensity

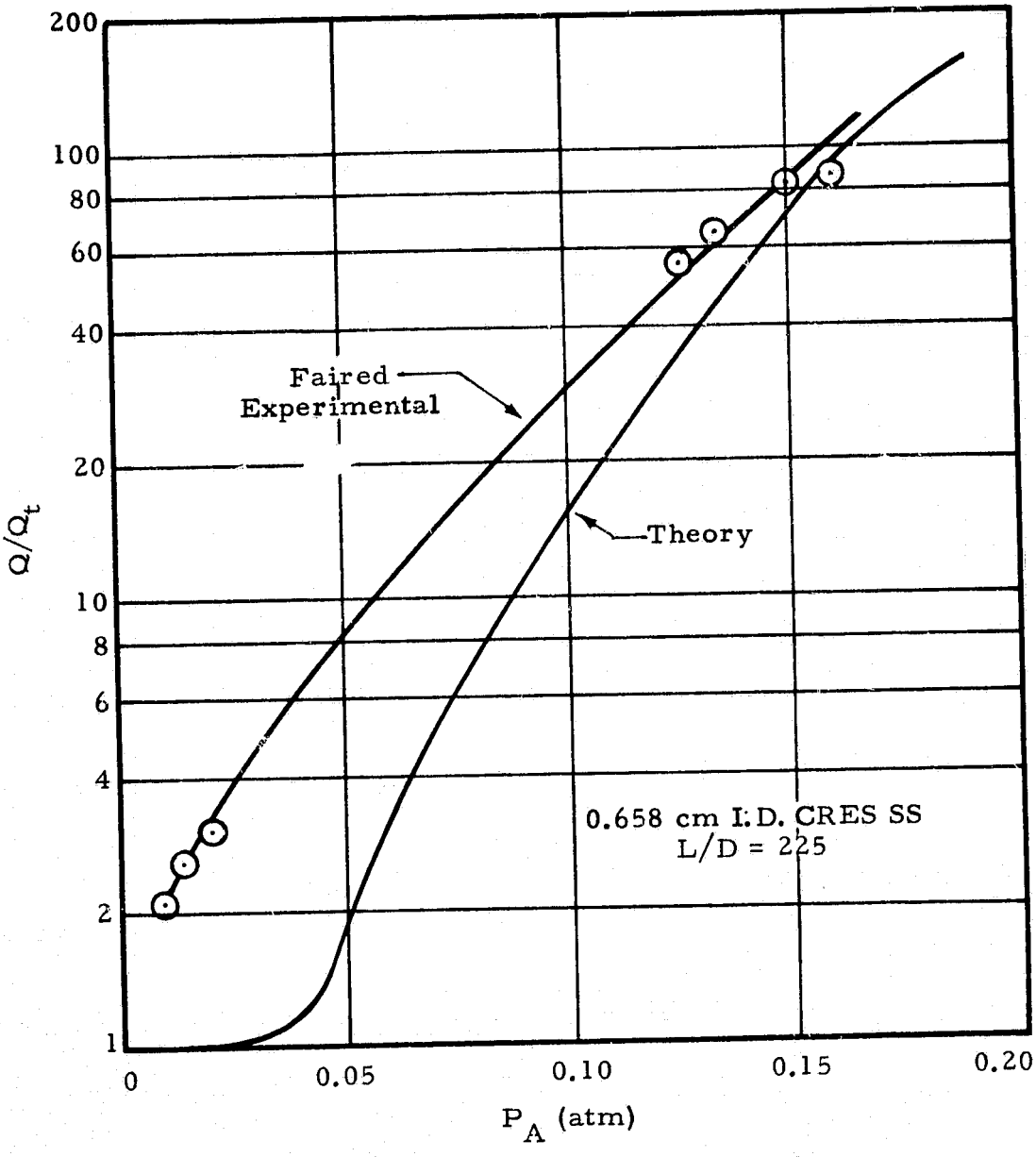

Fig. 37 - Ratio of Total Heat Leak (with oscillations) to Normal Conduction Heat Leak versus Pressure Amplitude

- Existence of oscillations, T_h/T_c versus Δ (Fig. 31)
- Oscillation frequency versus L/D, (Fig. 32)
- Pressure amplitude versus T_h/T_c, (Fig. 33)
- Pressure amplitude versus L/D, (Fig. 34)
- Oscillation intensity versus L/D, (Fig. 35)
- Heat transfer ratio versus oscillation intensity, (Fig. 36)
- Heat transfer ratio versus pressure amplitude, (Fig. 37)

Most of the cases shown consist of comparing the data with theoretical predictions for the exact conditions of the experiment. However, in order to compare some of the parameters, independent of the many others, the experimental data were cross plotted and interpolations were made. For example, the L_c/L ratio and the L/D ratio were simultaneously varied in some of the experiments. A meaningful parametric comparison can be made only by fixing one ratio and varying the other. This technique does not introduce appreciable error into the data. Attempts to introduce "error bands" on the experimental measurements were not successful. The careful calibration of all the instruments should, however, render the data virtually free of this type of error. Bands on the other experimental errors could not be accurately obtained.

Figure 31 is a plot of the temperature ratio, T_h/T_c versus the Δ parameter. The solid line curve represents the theoretical stability diagram for helium as discussed in Section 2.2. The symbols are representative experimental cases shown for comparison. Any case which lies "inside" the curve should produce sustained oscillations according to the theory. The experimental data points shown by the ✕ symbols did produce oscillations, and the ⊙ symbol cases did not sustain the wave motion. A complete set of experimental points to verify the stability curve was not obtained; however, the data which were obtained show several facts and trends.

The case $\Delta = 50$ for varying T_h/T_c shows that the oscillations cease to exist for T_h/T_c ratios less than 10, while the theory predicts about 9 for this

critical ratio. The 10% agreement of this data point is well within any error bands of theory or data. This close agreement suggests that the theoretical curve can be used with reasonable confidence for extrapolating cases which have not been verified experimentally.

Most of the data were taken with $T_h/T_c \sim 33$. The remaining points on the curve of Fig. 31 are for constant T_h/T_c with varying Δ. The range of L/D values shown cover 100 to 1000. All these cases shown should produce sustained oscillations according to the theory. All of the cases for L/D = 150, 200 300 did indeed oscillate as predicted. However, the extreme limits, L/D = 100, L/D = 1000 did not behave as predicted. These tubes produce sustained oscillations for some of the L_c/L ratios, but did not oscillate at all for others. This experimental behavior is as yet unexplained. This comparison does show reasonable agreement for most of the data taken.

Figure 32 is a plot of the oscillation frequency versus length/diameter ratio for constant T_h/T_c and L_c/L ratios. The theory consistently predicts higher frequencies than shown by the data. The largest difference occurs for L/D = 150 with the difference decreasing for the larger L/D ratios. The theory predicts about 48 Hz for L/D = 150 while the measurements give ~40 Hz for aluminum tubes and 35 Hz for the stainless tubes. The reason for the predictions being higher than the data is due to presence of the liquid helium in the experiments, while the theory does not model the liquid region. The proximity of the tube to the liquid surface has a marked effect on the frequency. Moving the tube closer to the liquid surface decreases the frequency. This most likely accounts for the discrepancies in Fig. 32. Due to the complexity of the experimental apparatus, and instrumentation, no attempt is made to place error bands on the measured data. Such bands would contain more error than the data itself.

A comparison of peak-to-peak pressure amplitude versus the temperature ratio T_h/T_c is given in Fig. 33. For this comparison the L/D and L_c/L ratios were held constant to study the effects of T_h/T_c on amplitude. The data points

essentially band the theoretical curve with two points falling below and most of the data falling above it. The amplitude increases as the tube is moved closer to the liquid surface. The theory then underpredicts the pressure amplitude since the liquid/vapor interface is not in the analytical model. The agreement between theory and experiment appears to be better for pressure amplitude than for oscillation frequency. Both theory and experiment predict shutdown of oscillations ($P_A \sim 0$) for T_h/T_c just below 10.

Figure 34 compares pressure amplitude for varying length-to-diameter ratio for fixed $T_h/T_c \approx 33$. The data points band the theoretical predictions with the experiment showing slightly larger amplitudes for lower L/D values and slightly smaller amplitudes for larger L/D values. The agreement of these parameters is better than that shown in the previous figure (Fig. 33). The apparent reason for the better agreement is that the L_c/L ratio is 0.1 for Fig. 34 and 0.154 for Fig. 33. This means that the tube was farther from the liquid surface for the cases shown in Fig. 34. The theory should thus be better as the tube gets farther from the liquid surface. This accounts for the better agreement shown in Fig. 34.

The oscillation intensity (P_A x f) as a function of length/diameter ratio is shown in Fig. 35. The curve shows that the theory consistently predicts larger intensities than the measured data. This is a direct result of the frequency prediction shown in Fig. 32. The amplitude predictions were close to the data while the frequency predictions were consistently high. The intensity, which is defined here is the amplitude-frequency product, is thus consistently higher than the data. For L/D = 300, the data show $I \approx 4.8$ while the theory predicts $I \approx 7$. The predictions appear to be better for the aluminum tubes than for the stainless steel tubes.

A comparison of heat transfer ratio versus oscillation intensity is given in Fig. 36. The parameter Q/Q_t is defined as the ratio of the total heat leak to the pure conduction (no oscillation) heat leak. The theoretical predictions are lower than the data for small intensities and higher than the data fo large

intensities. However, the data points do band the theory and indicate quantitative agreement. The heat transfer is increased by an order of magnitude for intensities ~1.0 (atm-Hz) and by two orders of magnitude at $I \approx 2.0$. The agreement shown in Fig. 36 lends validity to its use in predicting heat transfer due to thermal acoustic oscillations. If the oscillation intensity is known (i.e., from measurements), then the effect on the net heat leak can be accurately determined from this curve, without having to measure boiloff rates.

Figure 37 compares the Q/Q_t ratio as a function of pressure amplitude for a fixed L/D. The agreement is much better for larger amplitudes (>0.10) than for smaller amplitudes (<0.05). The theory most likely underpredicts the heat transfer for small amplitude oscillations because of the approximate sine wave boundary condition.

Section 3
CONCLUSIONS

The conclusions reached from this study are now summarized in three categories: (1) thermal acoustic oscillations phenomena including a summary of the implications for cryogenic storage systems, (2) experimental anomalies and (3) analytical methods.

3.1 THERMAL ACOUSTIC OSCILLATIONS PHENOMENA

- A literature review has revealed that thermal acoustic oscillations are a common occurrence in liquid helium storage systems. Most investigators have discovered very large additional heat leaks because of oscillations.
- The present study has shown by analysis and experiment that the oscillations do occur and can be sustained for long periods of time.
- Thermal acoustic oscillations can potentially occur in any cryogenic system which contains a tube penetration.
- The oscillations can be initiated purely by thermal means, i.e., expansion of gas in a tube heated on one end and having an open end exposed to a very cold environment.
- The stability of oscillations has been shown to be a function of the length/diameter ratio of the tube, the temperature ratio of warm end to cold end, the length of tube exposed to the cold environment, the proximity of the tube to the liquid surface and perhaps external disturbances.
- o A stability diagram was derived for use in estimating the existence of oscillations in LHe apparatus. The analytical model can be used to construct similar diagrams for other cryogens.
- Thermal acoustic oscillations produce large heat leaks to stored cryogens. Analysis and experiment have shown that as much as two orders of magnitude increase in heat transfer can occur if oscillations are present.
- The frequency of the oscillations studied range from ~2 Hz for large L/D ratios to ~60 Hz for mid-range ($L/D \approx 100$) to as large as 100 Hz for shorter tubes.

- A warm-end to cold-end temperature ratio $T_h/T_c \sim 10$ is required to sustain oscillation in tubes with small L/D ratios. Longer tubes will oscillate with T_h/T_c as low as ~6.
- Pressure amplitudes (peak-to-peak) of ~0.4 atm were obtained for large L/D tubes (~500) while $P_A \sim 0.1$ are measured for smaller L/D (~100). The amplitude correlates somewhat linearly with L/D.
- Thermal acoustic oscillations can disturb the liquid cryogen itself by injecting mass causing stirring and apparent "turbulent-like" flow at the vapor/liquid interface.
- The ratio of total heat transfer to pure conduction heat transfer correlates with oscillation intensity. Additional heat leaks 100 times the normal (no oscillation) values can occur for intensities of ~2.0 atm-Hz.
- The large heat leak produced by the oscillations could have significant effects on storage of cryogens for space missions such as the Tug. The boiloff rates could be large enough to cut the mission time short or prohibit it altogether.
- The study has identified system parameters which are at the designers disposal for possibly preventing oscillations from occurring:
  a. A T_h/T_c ratio below about 6 should prevent sustained oscillations. This is accomplished most readily by cooling the closed end of the tube.
  b. The L_c/L ratio should be kept small, i.e., minimize the length of tube exposed to the cold environment.
  c. Tubes with small L/D ratios (less than 25 for example) are less likely to induce oscillations.
  d. The open end of the tube should not be placed close to the liquid surface. This will minimize stirring if oscillations do occur.
  e. The oscillations can be damped by occasional venting through a valve, etc., at the closed end of the tube.

3.2 EXPERIMENTAL ANOMALIES

- Certain of the tubes tested could be made to oscillate as predicted, while others (L/D = 100, L/D = 1000) could not. This is as yet unexplained.

- The initiation of the oscillations appears to be a function of the amount of cryogen in the storage vessel. Some tubes would produce oscillations regardless of the percent full of the dewar, while others required at least 50% by volume of liquid helium.
- The internal pressure in the dewar apparently has some influence on sustaining the oscillations. The exact nature of this influence was not defined.
- The heat transfer ratio (Q/Q_t) for the aluminum tubes was found to be much lower than that for the stainless steel tubes. This is a direct result of the much larger (factor of 10) conductivity of aluminum.
- Oscillations could be easily initiated by moving the tubes close to the liquid and then withdrawing them.

3.3 ANALYTICAL METHODS

- An analytical model of thermal acoustic oscillations was developed. An efficient numerical method was devised for solving the nonlinear partial differential equations.
- The nonlinear model, apparently the first successful attempt, allowed a theoretical stability curve to be obtained.
- The TAO/GSA computer program system was developed as a tool for use in understanding and explaining the physical phenomena of thermal acoustic oscillations.
- A parametric analysis revealed the dimensionless groups which govern the oscillations to be:

  T_h/T_c – ratio of warm end temperature to cold end temperature

  L/D – length-to-diameter ratio of tube

  L_c/L – ratio of tube length exposed to cold environment to total length

  Re – acoustic Reynolds number, and

  $\Delta = \dfrac{\frac{1}{2}\sqrt{Re/(L_c/L)}}{L/D}$ – dimensionless parameter correlating the stability of oscillations

- Comparison of analytical prediction to LMSC experimental data and to those data of previous investigations has shown quantitative agreement for most situations.

Section 4
RECOMMENDATIONS

This study was successful in achieving its original objectives. In addition, however, other aspects of the thermal acoustic oscillations phenomena were identified but not quantified. The following summary list contains recommended additions to the study just concluded. These areas should be investigated to further the understanding of the thermal acoustic oscillations phenomena itself and to provide needed additional quantitative data to designers of cryogenic storage systems for space flight. The recommendations are summarized in two categories, (1) analytical methods and (2) experimental program.

4.1 ANALYTICAL METHODS

Task 1: The TAO program does not include the effects of the tube proximity to the liquid surface. The results of the present study have identified this factor as being significant for initiation of oscillations and for characterizing the frequency and amplitude. This task recommends an extension of the existing TAO model to include the variable distance of the open end of the tube from the liquid cryogen. This will be formulated as a boundary condition for the Navier-Stokes equations. A numerical scheme utilizing successive overrelaxation will be developed for converging the solution. This extension to the mathematical model will be added to the TAO computer program.

Task 2: This task proposes to analyze a selected matrix of parametric cases using the revised TAO program. The results obtained will be compared to the previous solutions which neglect the liquid level distance and this effect will be quantified.

Task 3: This task will utilize the additional data obtained from the recommended experimental program given in Section 4.2. The wave characteristics data recorded on FM tape will be converted to digital format. The digitized data will be processed by the General Statistical Analysis (GSA) program to obtain the power spectral density. This approach will allow a detailed examination of the characteristics of the experimentally measured waves. Results of this task, presented as power spectral density plots, will identify the major frequency content of the pressure waves and also the secondary wave forms which have been discovered.

Task 4: This task recommends utilizing the TAO program to analyze systems using cryogens other than liquid helium. A matrix of cases can be processed using nitrogen and hydrogen as the fluids. Results can be compared and contrasted to the helium data.

4.2 EXPERIMENTAL PROGRAM

Task 5: Additional experimental measurements similar to those already obtained are needed to verify the existence diagram. This task recommends obtaining data for varying ratios of the warm end temperature to cold end temperature for parametric values of the Δ parameter. The data can be obtained using the research dewar and the existing tubes. The warm end temperature can be controlled using an LN_2 jacket as was done for the one case studied previously. This task will consist of approximately 25 data points to experimentally define the curve of Fig. 31.

Task 6: The results of selected experimental cases will be recorded via FM tape. The cases to be recorded will be selected to span the range of frequencies from ~1 to 100 Hz. The FM data will be analyzed using the approach described in Task 3.

Task 7: Additional measurements of boiloff rate (hence heat transfer data) need to be obtained for tubes having different wall thicknesses The boiloff data obtained in the current study was limited to one tube diameter. These data will be taken for a range of L/D ratios from 100 to 300 and correlated with theoretical predictions.

Task 8: The study of Bannister, using a glass dewar for visual observation, proved to be invaluable in the present work. In light of the additional knowledge gained in the LMSC study, it is recommended that a similar experiment be conducted. A glass dewar with a tube penetration will be used and the oscillations will be photographed using a shadowgraph technique. Regions of density gradient will be visible as dark and light spots on the movie film. Interaction of the oscillations with the liquid surface can also be seen. This task is a virtual necessity if an understanding of this mechanism is to be obtained.

The task summaries listed here constitute a logical extension to the work just completed. Due to the common occurrence of thermal acoustic oscillations, the large heat leaks they cause and the potential damage to space missions, it is recommended that these tasks be performed. The results will be documented and made available for use in designing around the potentially hazardous environment caused by thermal acoustic oscillations.

Section 5
REFERENCES

1. Sondhauss, C., "Uber die Schallschwingunzen der Luft in erhitzten Glasröhren and in gedeckten Pfeifen von ungleicher Weite," Ann. Phys., Vol. 79, 1850, p. 1.

2. Rayleigh, Lord, "The Explanation of Certain Acoustical Phenomena," Nature, London, Vol. 18, 1878, p. 319.

3. Taconis, K. W. et al., "Measurements Concerning Vapor-Liquid Equilibrium of Solutions of He^3 in He^4 below 2.19°K," Physica; Vol. 15, No. 8-9, 1949, p. 733.

4. Krämers, H. A., "Vibrations of a Gas Column," Physica, Vol. 15, No. 11-12, 1949, p. 971.

5. Wexler, Aaron, "Evaporation Rate of Liquid Helium I," J. Appl. Phys., Vol. 22, No. 12, December 1951.

6. Clement, J. R., and J. Gaffney, "Thermal Oscillations in Low-Temperature Apparatus," Adv. Cryogen. Eng., Vol. 1, 1954, p. 302.

7. Trilling, L., "On Thermally Induced Sound Fields," J. Acoustical Soc. Am., Vol. 27, 1955.

8. Chu, Boa-Teh, "Analysis of a Self-Sustained Thermally Driven Nonlinear Vibration," Phys. Fluids, Vol. 6, No. 11, November 1963.

9. Ditmars, D. A., and G. T. Furukawa, "Detection and Damping of Thermal Acoustic Oscillations in Low-Temperature Measurements," J. Research, NBS, Vol. 69C, No. 1, 1964, p. 35.

10. Feldman, K. T., Jr., "A Study of Heat Generated Pressure Oscillations in a Closed End Pipe," Ph. D. dissertation, University of Missouri, Columbia, February 1966.

11. Feldman, K. T., Jr., "Review of the Literature on Sondhauss Thermoacoustic Phenomena," J. Sound Vib., Vol. 7, 1968, pp. 71-82.

12. Feldman, K. T., Jr., "Review of the Literature on Rijke Thermoacoustic Phenomena," J. Sound Vib., Vol. 7, 1968, pp. 83-89.

13. Feldman, K.T., Jr., and R.L. Carter, "A Study of Heat Driven Pressure Oscillations in a Gas," J. Heat Trans., August 1970, pp. 536-541.

14. Bannister, J.D., "Spontaneous Pressure Oscillations in Tubes Connecting Liquid Helium Reservoirs to 300°K Environments," Bulletin Int. Institute Refrigeration, 1966-5, p. 127.

15. Larkin, B.K., "Heat Flow to a Confined Fluid in Zero Gravity," Progress in Astronautics and Aeronautics, Thermophysics of Spacecraft and Planetary Bodies, ed. by G.B. Heller, Vol. 20, 1967.

16. Thurston, R.S., and J.D. Rogers, "Pressure Oscillations Induced by Forced Convection Heating of Dense Hydrogen," Adv. Cryo. Eng., Vol. 12, Plenum Press, New York, 1967, p. 438.

17. Thullen, P., and J.L. Smith, Jr., "Model for Thermally Sustained Pressure Oscillations Associated with Liquid Helium," Adv. Cryo. Eng., Vol. 13, Plenum Press, New York, 1968, p. 215.

18. Rott, N., "Damped and Thermally Driven Acoustic Oscillations in Wide and Narrow Tubes," ZAMP, Vol. 20, 1969, pp. 230.

19. Mortell, M.P., "Resonant Thermal-Acoustic Oscillations," Int. J. Eng. Sci., Vol. 9, Pergamon Press, Great Britian, 1971, p. 175.

20. Collier, R.S., "Thermally Induced Oscillations in Cryogenic Systems," NBS Report 10749, National Bureau of Standards, Washington, D.C., April 1972.

21. Rott, N., "Thermally Driven Acoustic Oscillations. Part II: Stability Limit for Helium," ZAMP, Vol. 24, 1973, p. 54.

22. Von Hoffmann, T., U. Lienert and H. Quack, "Experiments on Thermally Driven Gas Oscillations," Cryogenics, 1973.

23. Spradley, L.W., "Thermoacoustic Convection of Fluids in Low Gravity," AIAA paper No. 74-76, AIAA 12th Aerospace Sciences Meeting, Washington D.C., January 1974.

24. Seymour, B.R. and M.P. Mortell, "Resonant Acoustic Oscillations with Damping; Small Rate Theory," J. Fluid Mech., Vol. 58, Part 2, 1973, p. 353.

25. Seymour, B.R., and M.P. Mortell, "Nonlinear Resonant Oscillations in Open Tubes," J. Fluid Mech., Vol. 60, Part 4, 1973, p. 733.

26. Hendricks, R.C., R.J. Simoneau and R.V. Smith," Survey of Heat Transfer to Near-Critical Fluids," NASA TMX-52612, 1969.

27. Thuraisamy, V., "Thermodynamic Flow of Super-Critical Oxygen in Zero-Gravity," Bellcomm, TM-72-1022-1, Bellcomm, Inc., Washington, D.C., March 1972.

28. Knudsen, J.R., "The Effects of Viscosity and Heat Conductivity on the Transmission of Plane Sound Waves," J. Acoust. Soc. Am., Vol. 26, 1957.

29. Luikov, A.V., and B.M. Berkovsky, "Thermoconvective Waves," Int. J. Heat Mass Trans., Vol. 13, 1970.

30. Glushkov, I.S., and Y.A. Kareer, "Acoustic Instability in a Non-Adiabatic Gas," Translated from Teplofizika Vysokikh Temperatur, Vol. 8, No. 5, September 1970, p. 957, (Plenum Press, New York).

31. Carrier, G.F., "The Mechanics of the Rijke Tube," Quart. Appl. Math., Vol. XII, No. 4, 1955.

32. Shields, F.D., K.P. Lee and W.J. Wiley, "Numerical Solution for Sound Velocity and Absorption in Cylindrical Tubes," J. Acoust. Soc. Am., Vol. 37, No. 4, 1965, p. 724.

33. Stewart, E., P. Stewart and A. Watson, "Thermo-Acoustic Oscillations in Forced Convection Heat Transfer to Supercritical Pressure Water," Int. J. Heat Mass Trans., Vol. 16, 1973, p. 257.

34. Khalatnikov, I. M., and I. N. Adamenko, "Theory of the Kapitza Temperature Discontinuity at a Solid Body-Liquid Boundary," Soviet Physics JETP, Vol. 36, No. 3, 1973.

35. Norton, M. T., "Frequency of Oscillations in a Dewar Vent Line, Closed on the Warm End," NBS Cryogenic Eng. Lab Note, 1965.

36. Howsen, R. J., "Thermally Sustained Pressure Oscillations in Liquid Helium Apparatus," M. S. thesis, Massachusetts Institute of Technology, Cambridge, May 1968.

37. Brashears, M. R. et al., "Wake Vortex Transport Considerations and Meteorological Data Analysis," LMSC-HREC TR D390424, Lockheed Missiles & Space Company, Huntsville, Ala., November 1974.

Appendix A
MATHEMATICAL FORMULATION OF THE TAO MODEL

Appendix

A.1 MATHEMATICAL MODELING

This mathematical model of thermal acoustic oscillations consists of a set of differential equations and boundary conditions. A model of such a phenomenon must be detailed enough to provide an accurate representation of the physical phenomenon and yet be simple enough that it can be analyzed to yield information about the phenomenon. This combination of requirements cannot be met completely for most real world problems. Some compromise of the two must be used to satisfy, in part, both requirements. The thermal acoustic oscillations problem is a prime example of this type of modeling.

The TAO model used in this work is based on the Navier-Stokes equations for viscous, compressible fluid. These nonlinear differential equations are coupled to the energy equations since the wave motion is induced by thermal effects. This set of coupled nonlinear partial differential equations cannot be solved in analytical "closed form." The approach taken in this analysis is to invoke a numerical method and use a digital computer to obtain solutions.

The purpose of this appendix is to present the details of the mathematical model for the TAO problem. The assumptions which are necessarily made, the governing equations, boundary conditions, the numerical algorithm and the computer program are discussed. The required inputs and the optional outputs are also defined. The General Statistical Analysis Program (GSA) which determines the frequency content of the waves is also discussed.

A.2 EQUATIONS AND BOUNDARY CONDITIONS

The fluid mechanics model begins with the conservation equations of motion, continuity, and energy in Eulerian coordinates. For a viscous, heat conducting Newtonian fluid, these equations are found in standard text books (Refs. A-1 and A-2) in vector form:

Navier-Stokes Equation

$$\rho \frac{D\vec{V}}{Dt} = \vec{F} - \nabla P - \nabla \times [\mu(\nabla \times \vec{V})] + \nabla[(\lambda + 2\mu)\nabla \cdot \vec{V}] \qquad \text{(A-1)}$$

Continuity Equation

$$\frac{D\rho}{Dt} + \rho(\nabla \cdot \vec{V}) = 0 \qquad \text{(A-2)}$$

Energy Equation

$$\rho C_v \frac{DT}{Dt} = \frac{-\beta T}{K}(\nabla \cdot \vec{V}) + \nabla \cdot (k\nabla T) - \nabla \cdot \vec{q}_r + q_e + \phi \qquad \text{(A-3)}$$

Equation of State

$$P = P(\rho, T) \qquad \text{(A-4)}$$

These equations, with appropriate boundary conditions, describe the flow and thermal behavior of the fluid. These are, of course, highly nonlinear and strongly coupled equations such that general solutions are not possible. Appropriate assumptions and simplifications must be made if any solution to the TAO problem is expected.

The geometric configuration and coordinate system used in writing the model equations is given in Fig. A-1. A cylindrical tube with one end closed and the other end open comprises the geometry. The optional case of a tube closed on both ends is included as a subset of the model. A cylindrical

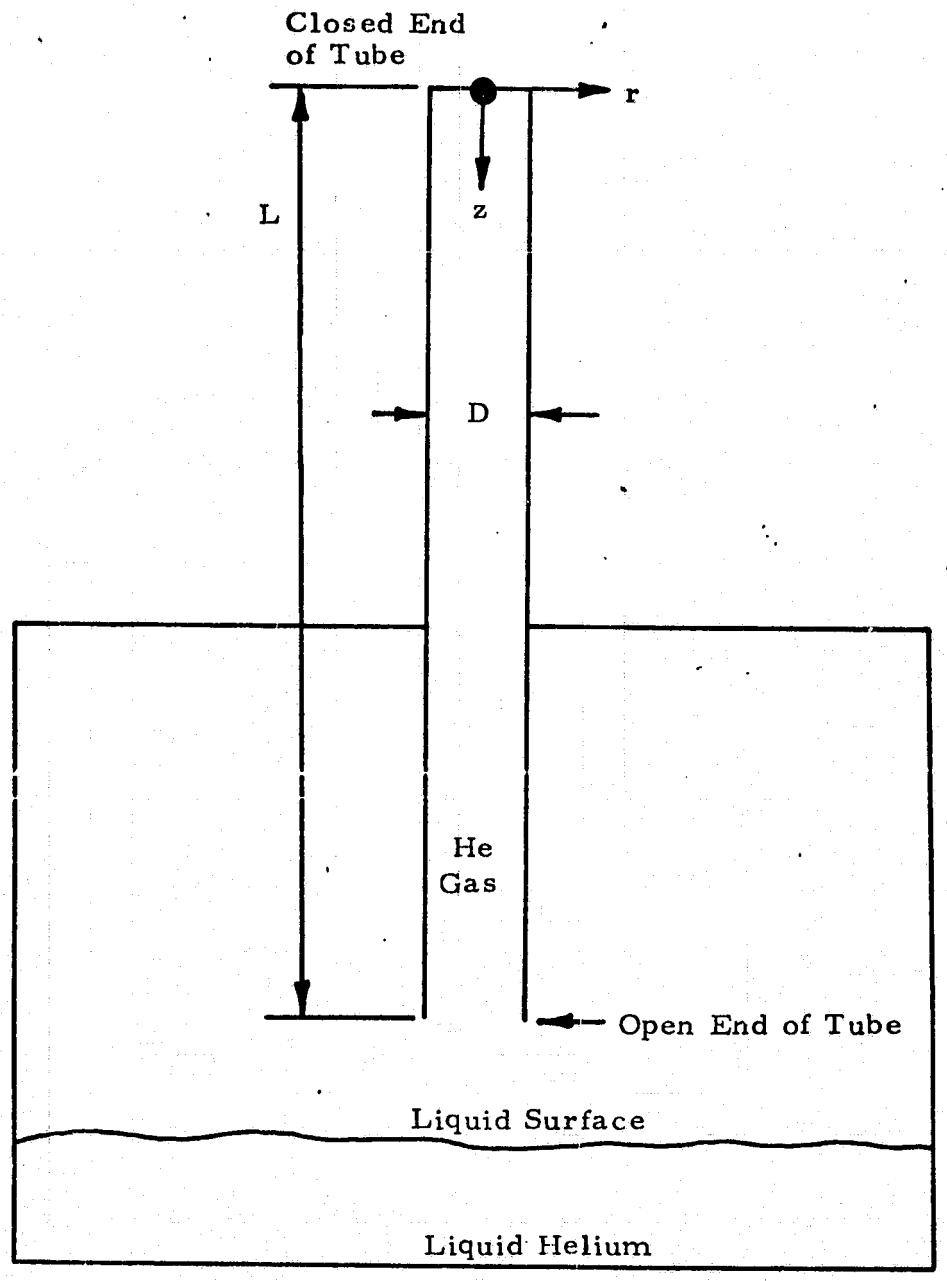

Fig. A-1 - Geometric Configuration and Coordinate System

coordinate system, r, z, is used with the radial coordinate, r, origin at the center of the tube and the axial, z, origin at the closed end. The flow in the tube is chosen to be axisymmetric such that a three-dimensional model is not required. The flow is also assumed to be laminar. This assumption appears to be justified based on past experimental observations.

The model is formulated by considering the flow of a gas in the tube driven by large thermal gradients imposed on the ends of the tube. Interaction of the gas phase with the liquid surface is taken into account in an approximate manner. The liquid region is modeled as a large volume of cold gas (at LHe temperature). An appropriate boundary condition is formulated following this assumption.

The Eulerian formulation of the equations is adopted with the inclusion of a time-dependent term. This approach allows the analysis of the transient as well as the steady state oscillations. The assumptions made in formulating the TAO model are summarized as follows:

- Axisymmetric configuration
- Viscous, compressible, heat conducting fluid
- Laminar flow of a Newtonian fluid
- Stokes viscosity relation is used
- Perfect gas law is invoked with variable compressibility
- No radiation or internal heat sources
- No viscous dissipation of energy
- Gravitational body forces are negligible, and
- Open end of tube is exposed to a large volume of cold gas.

Each of these assumptions has been carefully evaluated and a tradeoff analysis made. The assumptions appear to be well justified within the defined scope of work of this study. The results which have been obtained and compared with experimental data provide the true justification of these assumptions. These comparisons are in the main text of this report.

The Navier-Stokes equation for a Newtonian fluid contain two viscosity coefficients:

μ = shear viscosity or first coefficient
λ = dilatational viscosity or second coefficient

or we may define

$$K = \frac{2\mu + 3\lambda}{3}$$

as a bulk coefficient of viscosity.

The classical Stokes hypothesis yields a relation between the two coefficients

$$\lambda = -2\mu/3$$

A literature survey and a brief analysis have shown that:

(1) for an ideal monatomic gas $K = 0$
(2) for an ideal polyatomic gas $\lambda \sim 0$

Since the present study is directed primarily toward helium (He), the assumption that $\lambda = -2\mu/3$ appears to be justified. The TAO model is derived by applying the assumptions to the full Navier-Stokes equations.

Figure A-2 gives the equations which comprise the mathematical model for thermal acoustic oscillations. These are shown in terms of dimensionless variables which are used in all computation. Figure A-3 summarizes these dimensionless variables and groups. Equation (A-5) represents the conservation of mass in the tube. Equations (A-6) and (A-7) are the radial and axial components of the momentum conservation equations. Equation (A-8) is a mathematical representation of the energy conservation law. The ideal gas law in dimensionless form, (Eq. (A-9)), completes the set of governing equations.

Mass

$$\frac{\partial \rho}{\partial t} + \frac{\xi}{r}\frac{\partial}{\partial r}(r\rho u) + \frac{\partial}{\partial z}(\rho v) = 0 \qquad \text{(A-5)}$$

Radial Momentum

$$\frac{\partial}{\partial t}(\rho u) + \frac{\xi}{r}\frac{\partial}{\partial r}(r\rho u^2) + \frac{\partial}{\partial z}(\rho uv) = -\xi\frac{\partial P}{\partial r} + \frac{\xi^2}{Re}\left(\frac{\partial^2 u}{\partial r^2} + \frac{1}{r}\frac{\partial u}{\partial r} - \frac{u}{r^2} + \frac{1}{\xi^2}\frac{\partial^2 u}{\partial z^2}\right) \qquad \text{(A-6)}$$

Axial Momentum

$$\frac{\partial}{\partial t}(\rho u) + \frac{\xi}{r}\frac{\partial}{\partial r}(r\rho uv) + \frac{\partial}{\partial z}(\rho uv) = -\frac{\partial P}{\partial z} + \frac{\xi^2}{Re}\left[\frac{\partial^2 v}{\partial r^2} + \frac{1}{r}\frac{\partial v}{\partial r} + \frac{1}{\xi^2}\frac{\partial^2 v}{\partial z^2}\right] \qquad \text{(A-7)}$$

Energy

$$\left[\frac{\partial(\rho T)}{\partial t} + \xi\frac{\partial}{\partial r}(\rho uT) + \frac{\partial}{\partial z}(\rho vT)\right] = -(\gamma-1)P\left[\frac{\xi}{r}\frac{\partial}{\partial r}(ru) + \frac{\partial v}{\partial z}\right]$$

$$+ \frac{\gamma}{Re\,Pr}\left[\frac{\xi^2}{r}\frac{\partial T}{\partial r}\left(r\frac{\partial T}{\partial r}\right) + \frac{\partial^2 T}{\partial z^2}\right] \qquad \text{(A-8)}$$

State

$$P = \rho T \qquad \text{(A-9)}$$

Fig. A-2 - Navier-Stokes Equations for Cylinder (Dimensionless Variables)

$$z = z'/L,\ r = r'/R',\ t = t'/L'\sqrt{\frac{\Re T'_o}{m}}$$

$$u = \frac{u'}{\sqrt{\Re T'_o/m}},\ v = \frac{v'}{\sqrt{\Re T'_o/m}},\ \rho = \rho'/\rho'_o$$

$$P = P'/P'_o,\ T = T'/T'_o \qquad \text{(A.10)}$$

$$\xi = 2(L/D),\ \gamma = C'_p/C'_v$$

$$Pr = \frac{\gamma\, C'_v\, \mu'}{k'},\ Re = \frac{\rho'_o L \sqrt{\Re T'_o/m}}{\mu'}$$

(Primes (') indicate variables with physical dimensions. Unprimed variables are dimensionless.)

Fig. A-3 - Dimensionless Groups for Navier-Stokes Equations Used in TAO Model

The mathematical model must contain appropriate boundary conditions in order to represent the physical problem and to allow a solution to be obtained. These are logically organized into: (1) thermal boundary condition; and (2) flow boundary conditions.

Thermal Boundary Conditions

$$
\begin{aligned}
&T(r, z = 0) = T_h \\
&T(r, z = L) = T_c \\
&\frac{\partial T}{\partial r} = 0 \text{ at } r = 0 \\
&\text{or} \begin{cases} \dfrac{\partial T}{\partial r} = q_{loss} \text{ at } r = R \\ T = T_h \text{ at } r = R \end{cases}
\end{aligned}
\qquad \text{(A-11)}
$$

Flow Boundary Conditions

$$
\begin{aligned}
&u = v = 0 \text{ at } z = 0 \\
&u = v = 0 \text{ at } r = R \\
&u = 0 \text{ at } r = 0 \\
&\frac{\partial v}{\partial r} = 0 \text{ at } r = 0 \\
&P_w = \bar{P}_m \left[(1 + A_p \sin(\omega t + \phi) \right] \text{ at } z = L
\end{aligned}
\qquad \text{(A-12)}
$$

The boundary conditions are straightforward except for the pressure at the open end of the tube. The sinusoidal profile with amplitude, A_p, frequency, ω, and phase angle, ϕ, is used. These parameters are used in an iteration process to converge the solution. The A_p, ω and ϕ parameters are obtained by iteration from an initial estimate for the wave characteristics. This iteration is discussed further in Section A.4.

The correct calculation of the heat transfer at the open end of the pipe should include the effects of mass moving in and out of the pipe. This calculation has been incorporated into the TAO program. The heat pumped out by

the oscillations is given by

$$Q_{out} = \int_0^{\tau/2} (\rho v)_w A_g C_p T_m \, d\tau \qquad \text{(A-13)}$$

and the "heat" coming into the tube is

$$\dot{Q}_{in} = \int_{\tau/2}^{\tau} (\rho v)_w A_g C_p T_c \, d\tau \, . \qquad \text{(A-14)}$$

In order to compute the effects of oscillations on the heat transfer, the pure conduction rates are computed and ratios are taken to form the Nusselt number. The conduction rate in the gas column is

$$\dot{Q}_{g,c} = \frac{k_g A_g \Delta T}{L} \qquad \text{(A-15)}$$

and the conduction rate down the tube wall is

$$\dot{Q}_{T,c} = \frac{k_T A_T \Delta T}{L} \, . \qquad \text{(A.16)}$$

The Nusselt number can now be defined as

$$Nu = \frac{1/\tau \left[(Q_{out} + Q_{in}) \right]}{\dot{Q}_{g,c} + \dot{Q}_{T,c}} \qquad \text{(A.17)}$$

These calculations are based on integrating the energy transferred over one complete cycle. This accounts for the hot mass moving out of the pipe and being replaced by cold fluid.

These equations, boundary conditions and heat transfer calculations constitutes the mathematical model for thermal acoustic oscillations.

A.3 NUMERICAL SOLUTION METHOD

The numerical method employed in this analysis is based on explicit finite difference approximations. The use of the unsteady state equations allows a forward-time-marching algorithm to be used since the problem is initial valued in time. Values of the dependent variables are specified at time t_o at a finite number of discrete points on a numerical grid. The differential equations are approximated at these grid points by difference equations. The algorithm used here is based on a combination of techniques presented in the literature plus some new innovations. An excellent review of finite difference approximations for the Navier-Stokes equations is given by Torrance (Ref. A-3). However, these techniques have been applied only to the quasi-incompressible Boussinesq equations. The finite difference approximations used in the present study are patterned after the method of Spradley and Churchill (Ref. A-4). The technique is conditionally stable, free of spatial mesh restriction and is numerically conservative.

A node-centered finite difference grid (shown in Fig. A-4) is used to write the difference equations. All flow variables are evaluated at the center of a cell and differences are taken across a cell using the known values at adjacent cells and/or interpolated values at the boundaries of the cells. The boundary conditions, however, are specified at the walls themselves and not at the center of the cell adjacent to a wall. In writing the difference equations, the subscripts i, j refer to spatial locations on the r, z grid, respectively, and the superscript n denotes time, $n\Delta t$. The grid points are thus defined as

$$r_i = (i - \tfrac{1}{2})\,\Delta r, \quad z_j = (j - \tfrac{1}{2})\,\Delta z \tag{A.18}$$

The grid spacings $\Delta r, \Delta z$ are constant but can be distinct.

Forward time differences are used to approximate the unsteady derivatives (next page of text):

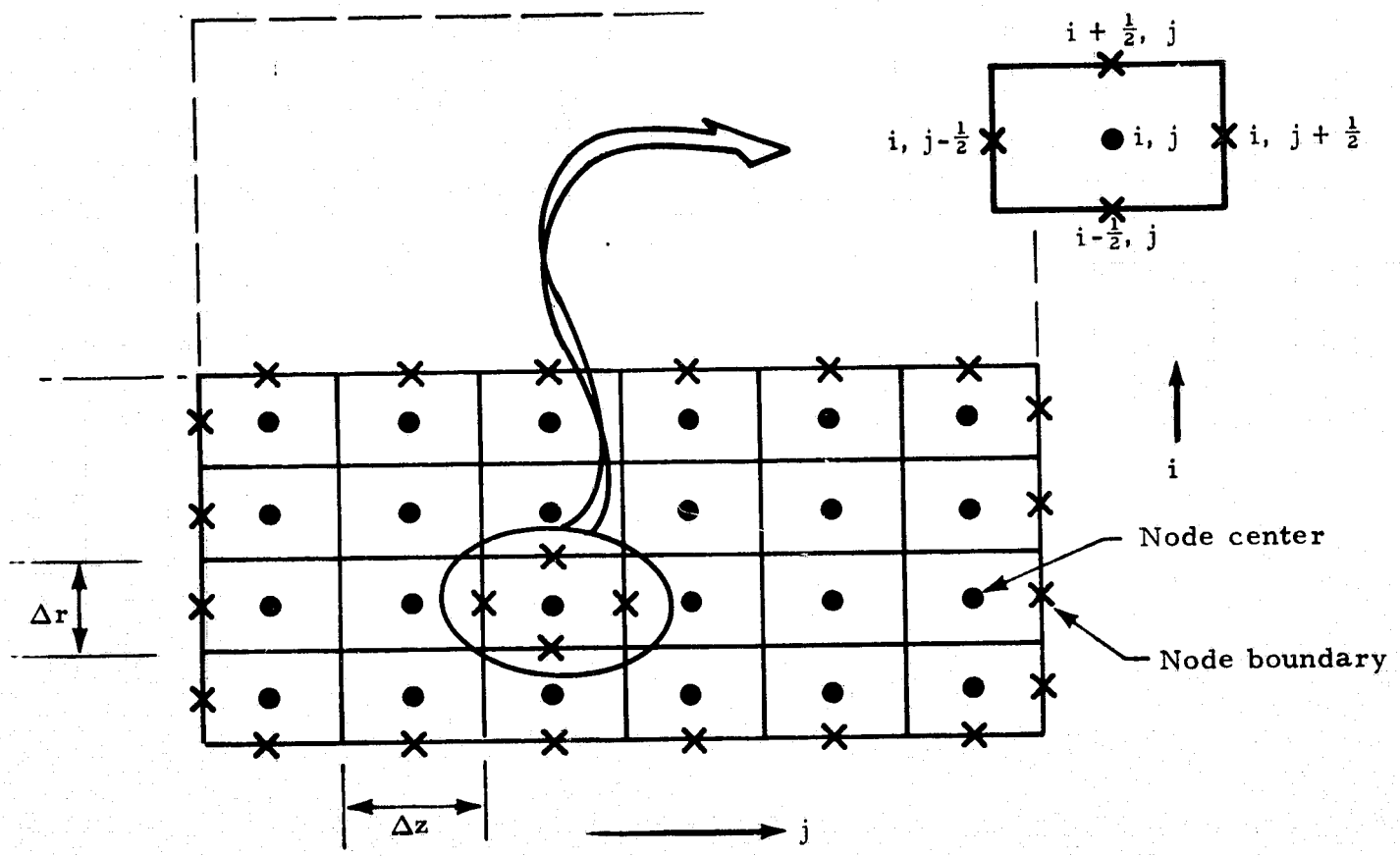

Fig. A-4 - Grid System for Finite Difference Equations

$$\frac{\partial f^{n+1}}{\partial t}_{ij} \approx \frac{f_{ij}^{n+1} - f_{ij}^{n}}{\Delta t} \tag{A.19}$$

where f is any of the flow variables $\rho u, \rho v, \rho, T$. This approach yields a finite difference approximation which is first order in time.

The particular form of the difference operators depends on the type of term to which it is applied. There are basically three types of terms in the governing equations — first order terms, second order terms, and convection terms. Table A-1 summarizes the type of terms and shows the finite difference approximations which are used in this study. Centered differences are used whenever possible but these cannot be applied to the convection terms. A flip flop difference scheme is used for the convection terms in order to preserve numerical stability in the explicit approach. This conservative flip flop method is applied to all the convection terms in the momentum and energy equations. Central differences are used in the continuity equation because the ρu and ρv terms that appear are evaluated at time n+1. This equation is effectively implicit but can be evaluated explicitly since $(\rho u)^{n+1}$, $(\rho v)^{n+1}$ are known and ρ^{n+1} is to be determined. This technique is conditionally stable and conserves mass identically on a numerical grid.

The difference operators for a cell adjacent to a boundary requires a special form. The technique employed here consists of obtaining a value at a cell boundary by averaging over two adjacent cells and then differencing across the cell. For example:

$$\frac{\frac{1}{2}(f_{1j}^{n} + f_{2j}^{n}) - f_{wj}^{n}}{\Delta r} \tag{A.20}$$

is used to compute $\partial f/\partial r$ for the i=1 cells. This form assumes f_{wj}^{n} is a prescribed boundary condition along r=0. This form is thus used for the ρu, ρv and T differences for cells adjacent to solid boundaries. The T differences for cells adjacent to a wall are determined by calculating $(T_{i,2}^{n} - T_{i,1}^{n})/\Delta y$ and then averaging with the known gradient at the wall itself. The pressure differences $\partial P/\partial r$,

Table A-1

FINITE DIFFERENCE APPROXIMATIONS

Type of Term	Differential Form	Finite Differential Approximations
First Order	$\frac{\partial f}{\partial x}$	$(f^n_{i+1,j} - f^n_{i-1,j})/2\,\Delta x)$
Second Order	$\frac{\partial^2 f}{\partial x^2}$	$(f^n_{i+1,j} - 2\,f^n_{i,j} + f^n_{i-1,j})/(\Delta x)^2$
Convection	$\frac{\partial}{\partial x}(uf)$	$\begin{cases} (u^n_{i+\frac{1}{2},j}\, f^n_{i+1,j} - u^n_{i-\frac{1}{2},j}\, f^n_{ij})/\Delta x \text{ if } u^n_{ij} \leq 0 \\ (u^n_{i+\frac{1}{2},j}\, f^n_{i,j} - u^n_{i-\frac{1}{2},j}\, f^n_{i-1,j})/\Delta x \text{ if } u^n_{ij} > 0 \end{cases}$
Notes: $u^n_{i\pm\frac{1}{2},j} = \frac{1}{2}(u^n_{i,j} + u^n_{i\pm1,j})$		

$\partial P/\partial z$ for a cell adjacent to a boundary are obtained by using quadratic extrapolation to obtain the pressure at the boundary and then using central differences to calculate gradients. The pressure at the open end of the tube is calculated explicitly and iterated upon.

This explicit finite difference method for solution of the compressible flow equations is a conditionally stable technique. A restriction is imposed on the size of the time step Δt to insure numerical stability. The criterion for this method was found by numerical experimentation since a rigorous stability analysis for such complex equations is beyond the state of the art. The most restrictive time step was found to be given by the CFL condition, which expressed in the dimensionless variables, is

$$\Delta t < \frac{\Delta}{\sqrt{2\gamma\, T_h}} \tag{A.21}$$

where $\Delta = \min(\Delta r, \Delta z)$, and T_h is the largest temperature in the grid network. This represents basically the time required for a pressure wave to move the distance of one cell width. In real time this corresponds to time steps of the order of 10^{-4} seconds. For problems requiring several seconds of simulation, this is not severely restrictive for third generation computer systems. A time-scaling procedure is used to reduce the computer run time for problems requiring long simulation times such as obtaining steady state solutions.

A scaling procedure developed in Ref. A-5 has been incorporated into the present numerical algorithm to lessen the time step requirement. This procedure is now briefly outlined including its applicability to present problems. The basic problem arises because diffusion processes occur on a time scale much larger than that of acoustic wave motion. The purpose of scaling is to speed up certain of the physical processes occurring in the fluid without disturbing the thermodynamic state of the fluid itself. The following procedure is based on familiar similarity laws of fluid mechanics. The dimensionless groups which apply to the present problem are (next page):

$$\text{Reynolds number, } Re = \frac{\rho L \sqrt{\Re T_o/\dot{m}}}{\mu}$$

$$\text{Prandtl number, } Pr = \mu C_p/k \qquad \text{(A.22)}$$

$$\text{Nusselt number, } Nu = q L/(k\Delta T)$$

$$\text{Mach number, } M = \frac{v}{c}$$

The objective is to increase the real time/computer time ratio by a factor of s such that each time step Δt that is used for computation will correspond to a real time $s\Delta t$. To achieve this objective, we define a flow situation, which is similar, but not perfectly equivalent, to our original problem, by the following transformations:

$$\begin{aligned} t' &= st'_s \\ \mu'_s &= s\mu' \\ k'_s &= sk' \\ q'_s &= sq' \\ v'_s &= sv' \end{aligned} \qquad \text{(A.23)}$$

where the s subscript indicates a flow variable in a new time frame. We then have the thermal conductivity, viscosity, heat input and flow velocity increased by a factor of s. The new time frame t_s in which we compute will now correspond to real time, st. The thermodynamic state of the fluid, temperature, pressure and density, remain unchanged in the new time system. We must now note that each of the dimensionless groups except Mach number are the same in both time frames. We have increased the Mach number by a factor of s since the properties of the fluid which determine the sonic velocity have been preserved. Since the sonic velocity is unchanged, the size of the permissible computation time step Δt_s is unchanged, but the real time Δt is increased. This satisfies the original objective.

The use of the conservation form of the governing equations is essential to the finite difference procedure employed here. The algorithm can be summarized as follows:

- Given conditions at each grid point in time n, the ρu and ρv products are advanced to time n+1 from the momentum equations.
- The ρu, ρv products at time n+1 are used in the continuity equation to obtain the density ρ at time n+1.
- The temperature, T, at n+1 is now calculated from the energy equation using the just computed ρ^{n+1}.
- The pressure, P, at time n+1 is evaluated explicitly from the ideal gas law.
- The process is repeated until $t = t_{max}$ or until a steady state is reached.

A.4 COMPUTER PROGRAM DESCRIPTION

The numerical technique just described was implemented on a digital computer. The program is coded entirely in standard FORTRAN V language. The program has been set-up to run on the Univac 1108 system at NASA-MSFC, but it should execute on any machine having a FORTRAN V compiler, at least 25K of core memory and one tape drive. Limited versions have been executed on the IBM 7094 and EAI 8400.

The program is organized in modular form. A driver program calls a series of subroutines which performs the calculations. Three blocks constitute the main components: input block, compute block, and output block. A diagram of the basic program organization is given as Fig. A-5. Coding of the necessary logic utilizes three "loops" through the program. The outermost loop provides the capability to execute multiple cases in a single run stream. This is used to calculate parametric solutions such as varying the L/D or T_h/T_c, etc. The next loop marches the solution forward in time until a steady state condition is reached. The inner loop is an iteration to converge on the open end boundary value for the oscillating pressure.

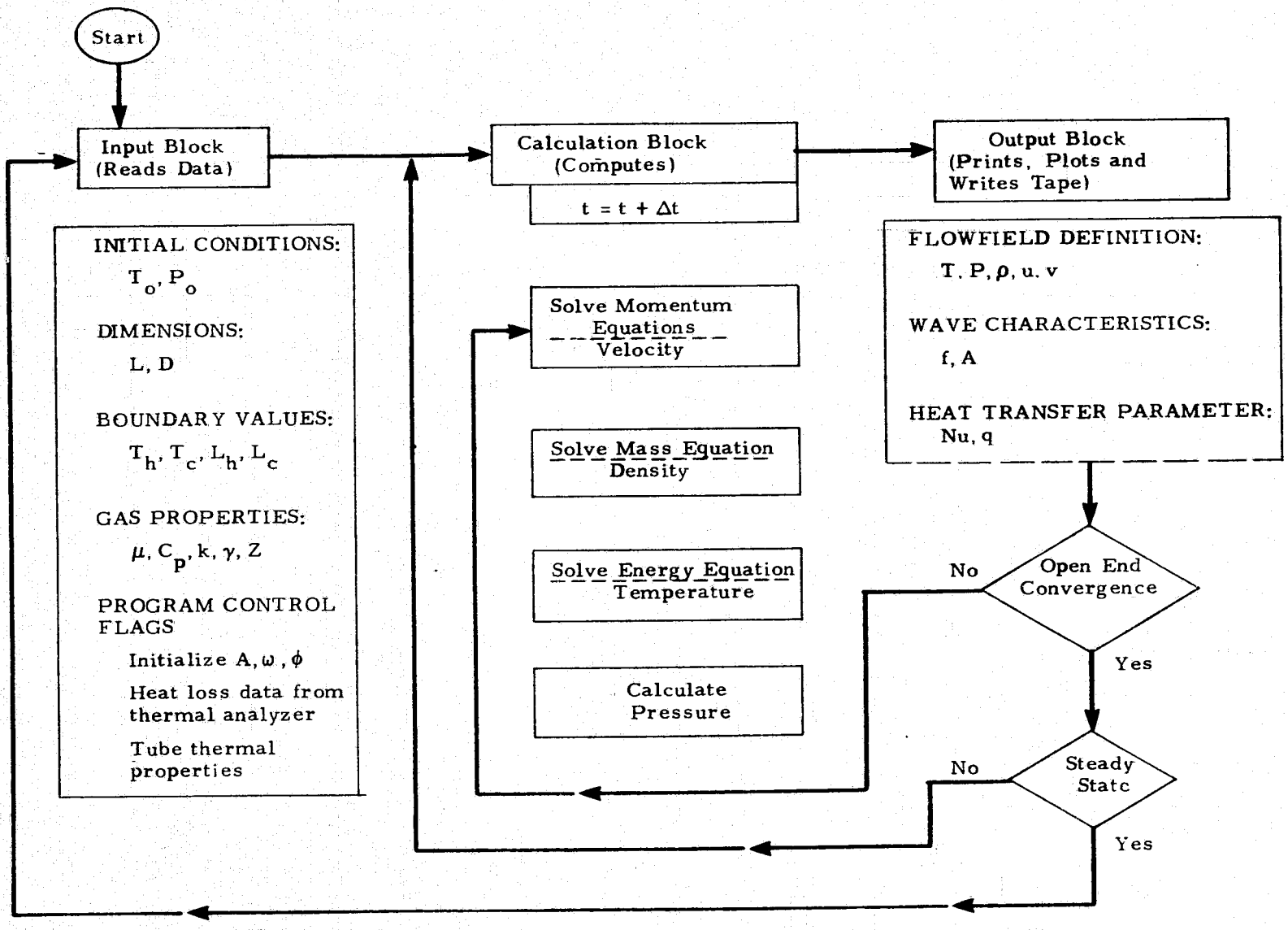

Fig. A-5 - Block Diagram for Thermal Acoustic Oscillations Computer Program (TAO)

A detailed input guide and program listing are not included in this report. The complexity of the TAO problem itself requires an experienced user to properly analyze a configuration. The complexity of finite-difference solutions of the Navier-Stokes equation requires also a special skill. Proper selection of grid size and time-step size is essential for stability of the numerical method. These remarks are made to caution the reader who may get the impression that this computer program will solve all TAO problems by simply inputting punched cards.

The input required is shown in the first block of Fig. A-5. The output consists of printed page format, contour maps and time plots of the flow field. Figure A-6 is a typical output of the pressure oscillations in a closed tube configuration. Figure A-7 is a plot of the temperature oscillations near the open end of the tube with L/D = 100. The plots are produced automatically using the SC 4020 routines.

The TAO program produces an output tape containing the entire flow field. This tape is used for restarting a case and for input to the General Statistical Analysis (GSA) program.

A.5 GENERAL STATISTICAL ANALYSIS PROGRAM (GSA)

One of the main objectives of this study is to determine the frequency characteristics of thermal acoustic oscillations. These could be obtained approximately from the plotted output of the TAO program. However, a more precise approach was taken in this study. A computer program was developed at Lockheed-Huntsville in connection with meteorological studies. This program performs a general statistical analysis of time varying data. The program, termed GSA in this work, is documented in Ref. A-6. A brief description of this program is presented here to illustrate the applicability to the TAO problem and to show the method used to obtain the frequency data which are presented.

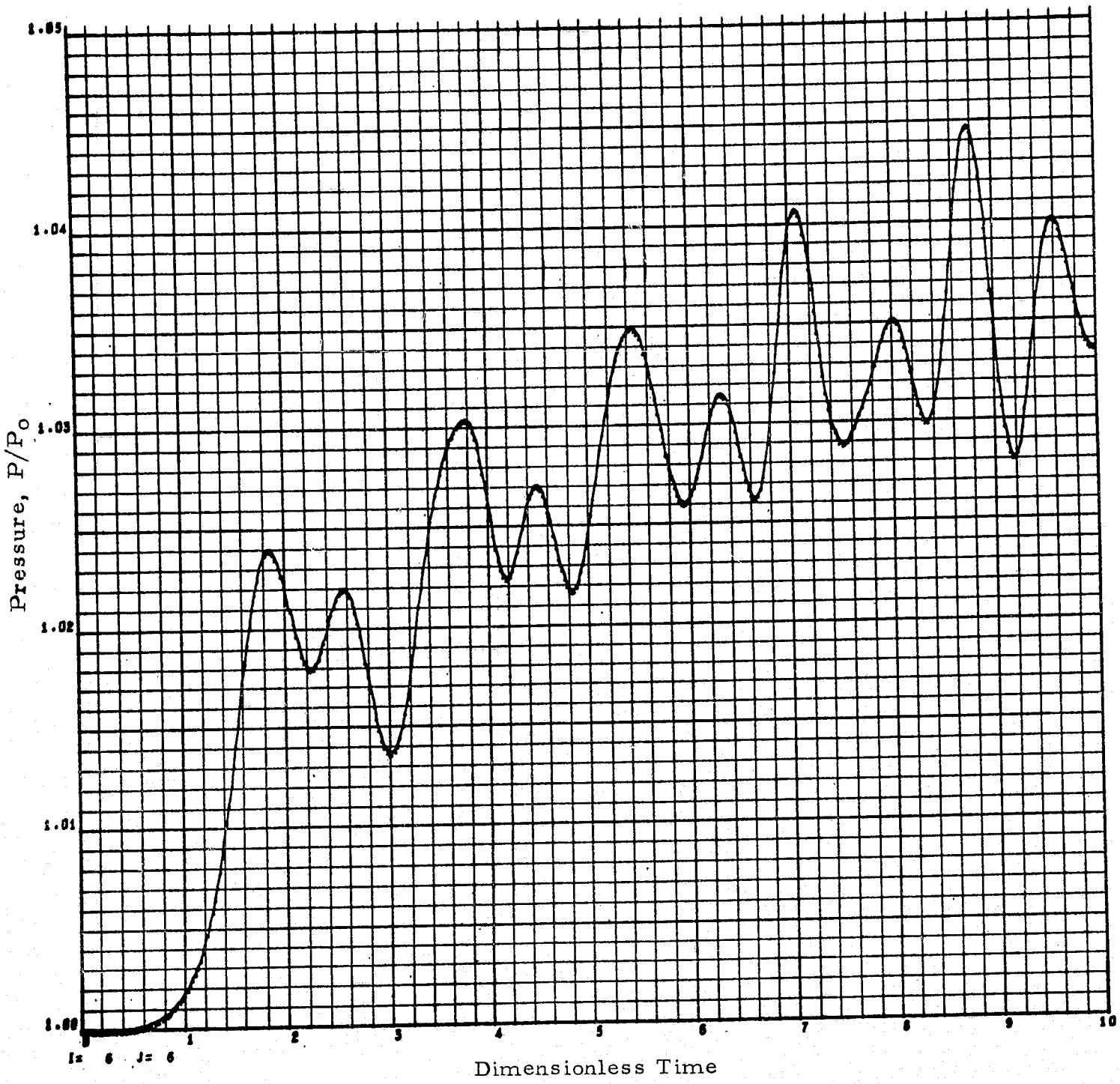

Fig. A-6 - Pressure Profile at 0.25L from Hot End of Closed Tube (Helium, L/D = 15)

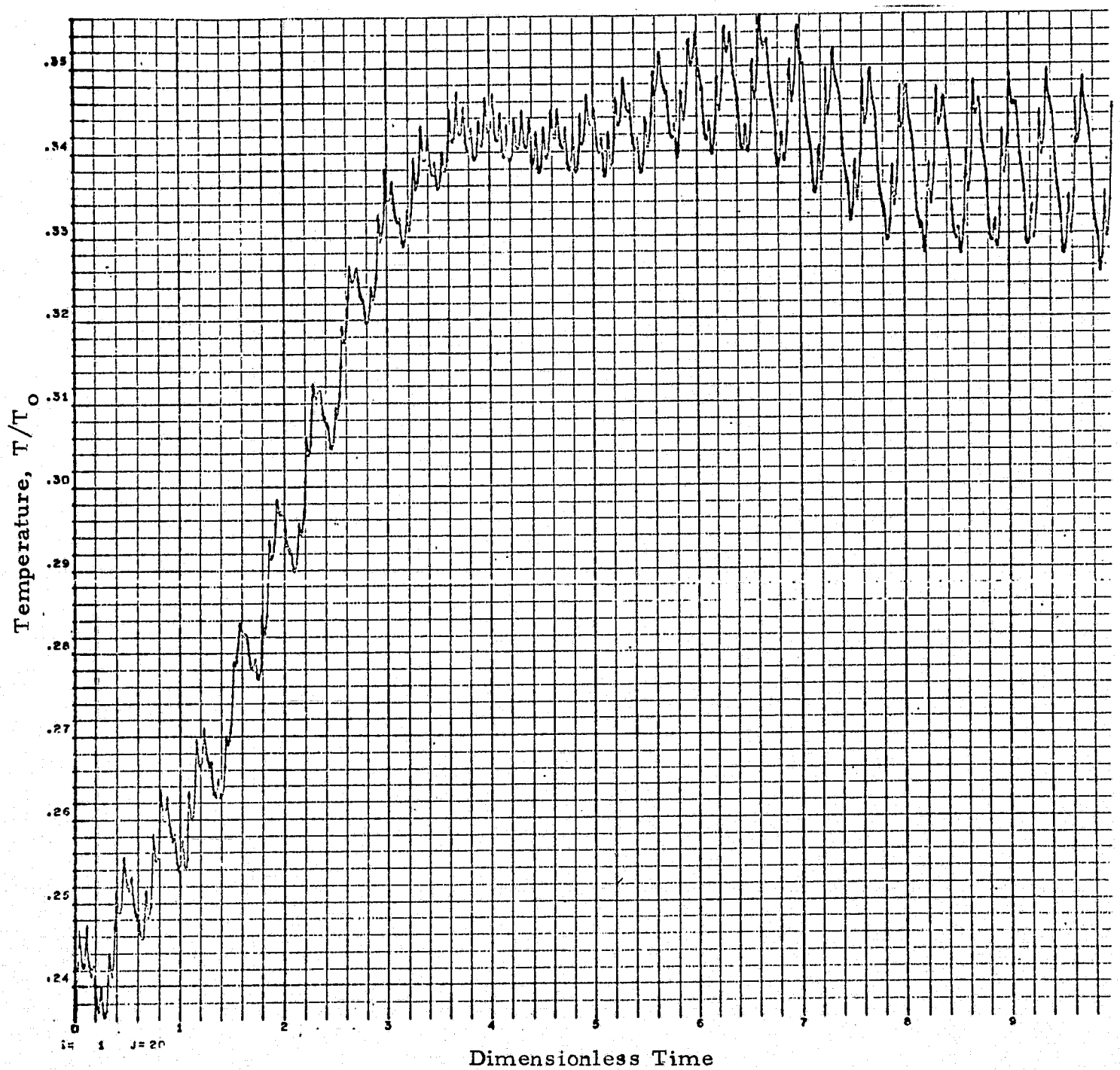

Fig. A-7 - Temperature History at a Point Near the Open End of Tube (L/D = 100)

We start with a time series x(t) having oscillatory properties and being valid a sufficiently long period $0 \leq t \leq T$. The series x(t) may represent the calculated pressure, temperature, density or velocity solutions of the thermal acoustic oscillations computer program. The statistical parameters of x(t), namely, the mean value $\bar{x}$, the variance σ_x^2, the mean square value ψ_x^2, and the standard deviation σ_x, are defined as follows:

$$\begin{aligned} \bar{x} &= 1/T \int_0^T x(t)\, dt \\ \sigma_x^2 &= 1/T \int_0^T \left[x(t) - \bar{x}\right]^2 dt \\ \psi_x^2 &= 1/T \int_0^T x^2(t)\, dt \\ \sigma_x &= \sqrt{\sigma_x^2} \end{aligned} \tag{A.24}$$

The mean value is simply the average of all values within the time interval of $0 \leq t \leq T$. The variance is the mean square value about the mean. The variance is a dynamic or fluctuating component of the time series. It is a measure of the degree of fluctuation. The mean square value represents the general intensity of the time series. It is the average of the squared value of the time history. The standard deviation is simply defined as the positive root of the variance.

By expanding Eq. (A-24), it can be shown that the variance is equal to the mean square value minus the square of the mean value. That is,

$$\sigma_x^2 = \psi_x^2 - \bar{x}^2 \tag{A.25}$$

The auto-correlation function of an oscillatory time series x(t) describes the general dependence of the values of x at one time or the value at another time. An estimate for the auto-correlation between the values of x(t) at times t and $t+\tau$ may be obtained by taking the product of the two

values and averaging over the observation time t. The observation time t is supposed to be sufficiently large to cover many times the periods of the waves contained in x(t). In equation form, the auto-correlation function, $R_x(\tau)$, is defined as

$$R_x(\tau) = \frac{1}{T}\int_0^T x(t)\, x(t+\tau)\, dt \tag{A.26}$$

The quantity $R_x(\tau)$ is always a real-valued even function with a maximum at $\tau = 0$, and may be either positive or negative. In terms of the auto-correlation function, the mean value of x(t) is given by

$$x = \left[R_x(\infty)\right]^{1/2} \tag{A.27}$$

In words, the mean value of x(t) is equal to the positive square root of the auto-correlation as the time displacement becomes very long. Similarly, the mean square value of x(t) is given by

$$\psi_x^2 = R_x(0) \tag{A.28}$$

That is, the mean square value is equal to the auto-correlation at zero time displacement.

The power spectral density function (also called the auto-spectral density function) of x(t) describes the general frequency composition of x(t) in terms of the spectral density of its mean square value. The mean square values of the time series x(t) in a frequency range between f and f + Δf, i.e., x(t, f, Δf), may be obtained by filtering the series with a band-pass filter having sharp cutoff characteristics, and computing the average of the squared output from the filter. This average squared value will approach an exact mean square value as the observation time, t, becomes large. That is, for sufficiently large t,

$$\psi_x^2\,(f, \Delta f) = \frac{1}{T}\int_0^T x^2\,(t, f, \Delta f)\, dt \tag{A.29}$$

where ψ_x^2 (f,Δf) is the mean square value of x in the frequency range from f to f + Δf.

The power spectral density function of x(t) is defined as

$$G_x(f) = \lim_{\Delta f \to 0} \frac{\psi_x^2 (f, \Delta f)}{\Delta f} \tag{A.30}$$

$$= \lim_{\Delta f \to 0} \left[\frac{1}{\Delta f} \cdot \frac{1}{T} \int_0^T x^2(t, f, \Delta f) \right] dt$$

Hence, the power spectral density of x(t) at the frequency f, i.e., $G_x(f)$, is the mean square value of x(t) at f per unit frequency.

An important property of the power spectral density function lies in its relationship to the auto-correlation function, $R_x(t)$. For a set of stationary oscillatory data, the two set statistical functions $G_x(f)$ and $R_x(t)$ are related by a Fourier transform as follows

$$G_x(f) = 2 \int_{-\infty}^{\infty} R_x(t)\, e^{-j2\pi ft} \tag{A.31}$$

$$= 4 \int_0^{\infty} R_x(t) \cos 2\pi ft \, dt$$

where $j = \sqrt{-1}$.

Other statistical properties of x(t), such as mean value and square value, are also related to $G_x(f)$.

This type of approach provides an excellent analysis for the TAO data. Consider a time series as shown in Fig. A-8 (top). This is typical of the

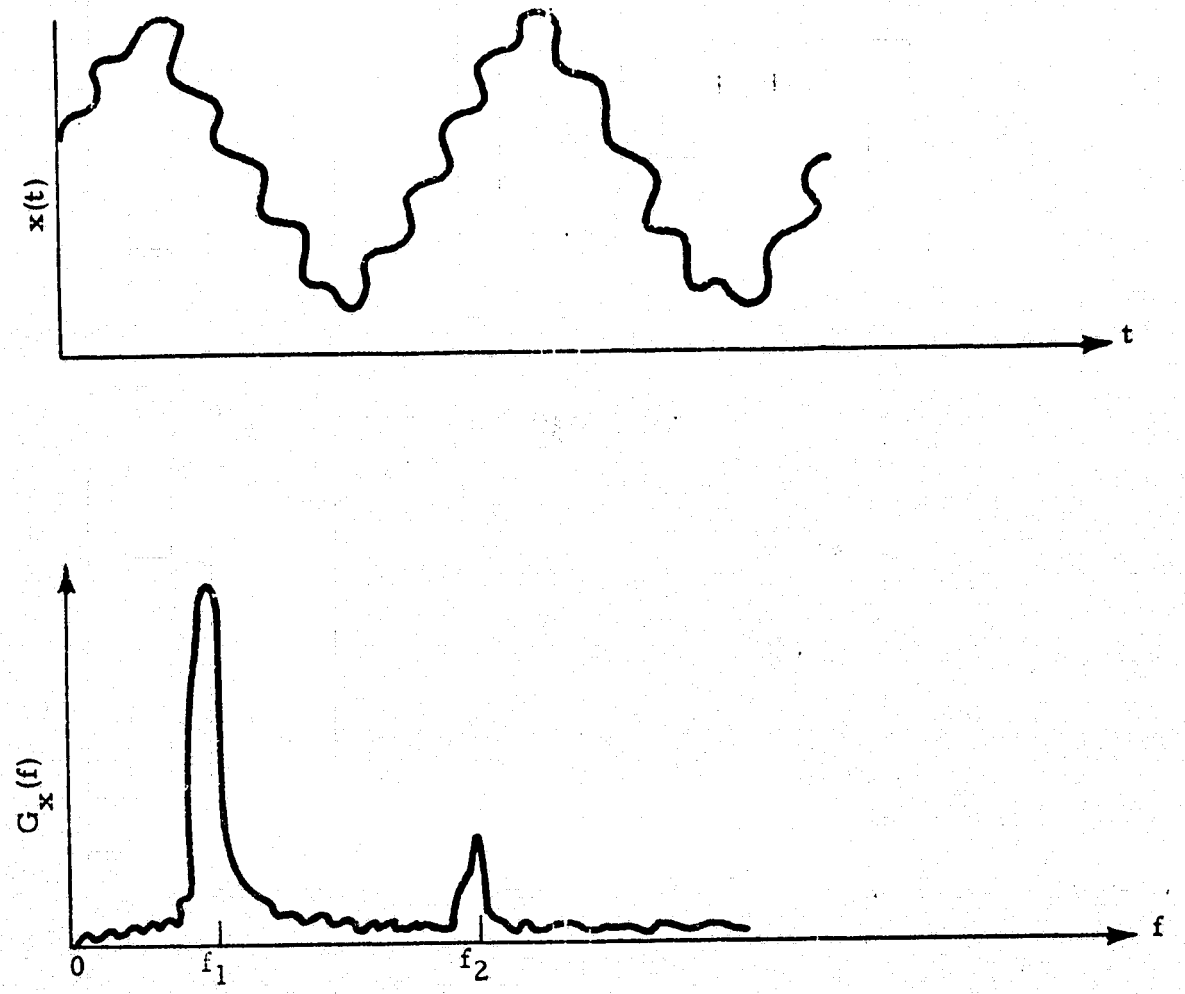

Fig. A-8 - Example of Power Spectral Density for Multiple Frequency Content

pressure wave data in a tube. The power spectral density is shown at the bottom of Fig. A-8. The lower frequency f_1 has a larger energy content than the higher frequency f_2. The calculated TAO waves exhibit this type of character.

Figure A-9 is a summary flow chart of the GSA program. It shows the basic logic of the program and the statistical functions which are computed. The inputs x, y can be any functions of time such as temperature and pressure. These are supplied via magnetic tape from the TAO solutions. The program then calculates mean values, mean squared values, standard deviations and variances. The data are then detrended and tapered to give zero mean value and slope. The Fourier transform of the complex function $z = x + jy$ is now computed using a Fast Fourier Transform (FFT) algorithm. The first calculations are then made for a number of statistical functions as shown on the second column of Fig. A-9.

A.6 REFERENCES

A-1. Aris, R., Vectors, Tensors, and the Basic Equations of Fluid Mechanics, Prentice-Hall, New Jersey, 1962.

A-2. Eskinazi, S., Vector Mechanics of Fluids and Magnetofluids, Academic Press, New York, 1967.

A-3. Torrance, K. E., "Comparison of Finite-Difference Computations of Natural Convection," J. Research, National Bureau of Standards, Vol. 72B, No. 4, October 1968.

A-4. Spradley, L. W., and S. W. Churchill, "Pressure and Buoyancy-Driven Thermal Convection in a Rectangular Enclosure," to appear in J. Fluid Mechanics, 1975.

A-5. Spradley, L. W. et al., "A Numerical Solution for Thermoacoustic Convection of Fluids in Low Gravity," NASA-CR-2269, May 1973.

A-6. Brashears, M. R. et al., "Wake Vortex Transport Considerations and Meteorological Data Analysis," LMSC-HREC TR D390424, Lockheed Missiles & Space Company, Huntsville, Ala., November 1974.

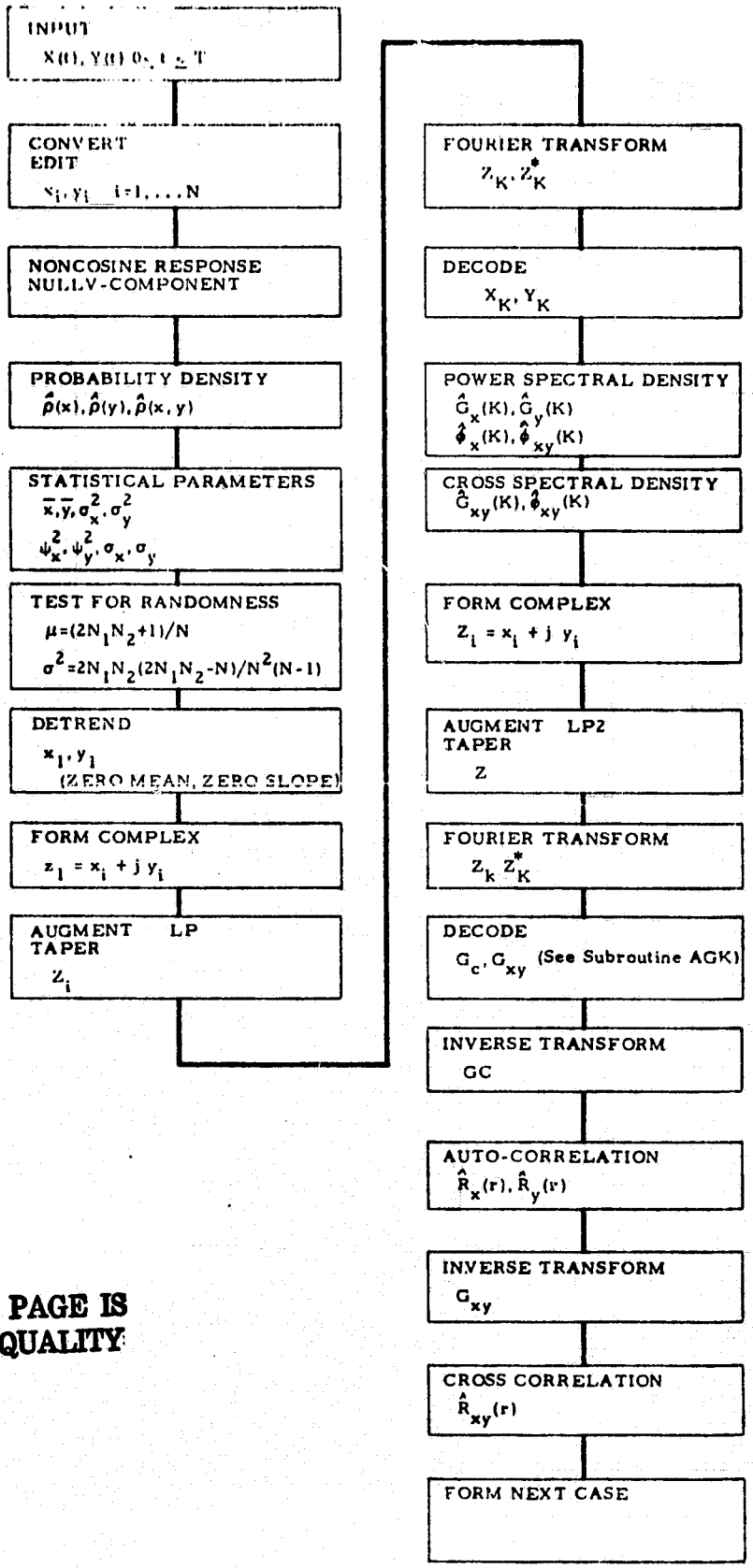

Fig. A-9 - General Statistical Analysis Computer Program Schematic Flow Chart

A.7 APPENDIX A NOMENCLATURE

Thermal Acoustic Oscillations

Symbol	Description
C_p	specific heat at constant pressure
C_v	specific heat at constant volume
D	diameter of tube
$\vec{F}$	body force vector
f	any flow variable
i	node point "i" on finite-difference grid
j	node point "j" on finite-difference grid
k	thermal conductivity
K	coefficient of isothermal compressibility
L	length of tube
m	molecular weight of gas
M	Mach number
n	time point "n" in finite-difference grid
Nu	Nusselt number
P	pressure
Pr	Prandtl number
q	total heat flux
$\vec{q}_r$	radiation heat flux vector
q_e	internal heat generation rate
$\mathfrak{R}$	universal gas constant
Re	acoustic Reynolds number
r	radial coordinate

Symbol	Description
s	time scale factor
t	time
T	temperature
u	velocity component in r-direction
v	velocity component in z-direction
$\overline{V}$	velocity vector
Z	axial coordinate
Greek	
β	coefficient of thermal expansion
γ	ratio of specific heats (C_p/C_v)
ξ	2L/D (aspect ratio)
λ	"second" or bulk coefficient of viscosity
μ	dynamic viscosity
ω	perturbation frequency
ρ	density
ϕ	viscous dissipation function
Subscripts	
o	initial condition or reference value
c	cold condition
h	hot condition
w	wall condition
g	gas
i	space coordinate designation in finite difference grid
m	mean value
out	going out of tube

Symbol	Description
in	coming into tube
T	tube
Superscripts	
n	time coordinate designation in finite-difference grid
'	indicates dimensional quantities
Operators	
$\partial/\partial t$	time partial derivative
$\partial/\partial z$, $\partial/\partial r$	space partial derivative
D/Dt	substantial derivative: $\partial/\partial t + (\bar{V} \cdot \nabla)$
$\cdot$	dot product of vectors
∇	gradient operator
∇	divergence operator
x	cross product of vectors
Statistical Analysis	
$x(t)$, $y(t)$	arbitrary functions of time
x_i, y_i	discrete values of $x(t)$, $y(t)$
$\bar{x}, \bar{y}$	mean values
ψ_x^2, ψ_y^2	mean square values
σ_x, σ_y	standard deviations
σ_x^2, σ_y^2	statistical variance
z_i	complex function $x_i + jy_i$
Z_k	Fourier transform of z
Z_k^*	complex conjugate of Z_k

Symbol	Description
G_x, G_y	power spectral density function
ϕ_x, ϕ_y	phase angle
T	period of oscillations
R_x	auto-correlation function
f	frequency of oscillation
Δf	incremental frequency